

Thermal field methods of the shallow subsurface

Zur Erlangung des akademischen Grades eines
DOKTORS DER NATURWISSENSCHAFTEN
von der Fakultät für
Bauingenieur, Geo- und Umweltwissenschaften

des Karlsruher Instituts für Technologie (KIT)

genehmigte

DISSERTATION

von

Dipl.-Min. Valentin Kurt Wagner

aus Crailsheim

Tag der mündlichen

Prüfung: 17.02.2014

Referent: Jun.-Prof. Dr. habil. Philipp Blum

Korreferent: Prof. Dr. Thomas Kohl

Karlsruhe 2014

Abstract

Temperature is one major physical quantity to characterize the subsurface because the temperature distribution and heat propagation depend on the properties of the subsurface. Therefore, heat can be used as a tracer. Furthermore, the attention on subsurface temperature is rising, because of the increasing popularity of geothermal energy. This additional application area of subsurface temperature and the combined new insights further strengthen the applicability of heat as a subsurface tracer. This thesis further promotes heat as a tracer by evaluating a thermal tracer test and comparing the obtained results to previous studies. Additionally, a new thermal field test for the hydraulic characterization of the subsurface is developed. This new development transfers the classical geothermal field test, the thermal response test (TRT), to a powerful hydrogeological field test, by introducing a new evaluation approach.

The first part of this thesis encloses three separate studies regarding the TRT. The TRT is a field investigation technique to determine heat transport parameters of the subsurface. This is crucial for the planning of shallow geothermal energy systems, and particularly relevant for a proper configuration of borehole heat exchangers (BHE). The TRT estimates the thermal conductivity of the subsurface and the borehole resistance of the BHE. Over a period of several days, the heat carrier fluid is artificially heated at the inlet of the BHE and the thermal response, the temperature evolution at the outlet, is recorded. By calibrating the Kelvin line-source equation, the searched parameters are obtained. The first study analyses the tampering effects of simplifications assumed for the standard TRT evaluation by interpreting numerical generated datasets. The analyzed tampering effects, which are not considered by the Kelvin line-source theory but by the applied numerical model, are the shank spacing of the BHE, the initial non-uniform temperature distribution of the subsurface and variations of thermal dispersivity in the subsurface. This study reveals minor tempering effects for the various shank spacings of the BHE and moderate tampering effects for the initial non-uniform temperature distribution, which slightly exceed a distortion of 10%. However, a significant tampering effect of the varying thermal dispersivities with constant Darcy velocities of 0.1 m day^{-1} is observed, which cause an overestimation between 20% and 190% of the actual thermal conductivity.

The second study picks up this significant tampering influence of groundwater flow on the standard TRT evaluation and develops a new evaluation approach to overcome this limitation. To fulfill this objective, a suitable analytical solution, the moving line source equation, is chosen as the basis of the new evaluation approach. To overcome potential distorting influences of the missing representation of the BHE geometry, the moving line source basis is supplemented by a numerically generated correction term. Using this correction term, it is possible to determine the integral Darcy velocity by a TRT evaluation. This approach is successfully tested on three literature-based TRT datasets.

The third study offers the objective to establish the TRT as a geothermal field test in the application area of hydrogeological field test, such as the pumping test. This study benefits from the fact that the thermal properties of an aquifer are not as variable as the hydraulic ones, especially the hydraulic conductivity. Therefore it is possible to determine a hydraulic conductivity range with the new TRT evaluation approach, based on the assumption of realistic ranges for the thermal conductivity, the volumetric heat capacity, the thermal dispersivity and the thermal borehole resistance. The suggested hydraulic characterization method is successfully tested on a large scale geothermal laboratory experiment and a commercially performed TRT. Additionally, this successful evaluation represents a validation of the new TRT evaluation developed in the second study.

The fourth study examines a thermal tracer test (TTT). During this TTT 16 m³ of 22°C hot water are injected into a porous aquifer and the heat propagation is monitored by a down gradient well transect of five separate observation wells. The explored Lauswiesen test site is located near Tübingen, Germany. Based on the knowledge from previous studies, a numerical model is generated to obtain artificial results, which accord to an ideal heat transport behavior. From the measured and simulated thermal breakthrough curves the peak arrival time and the peak temperature are determined and comprehensively compared. Based on this comparison, the primarily responsible heat transport processes are identified. These are the layered structure of the aquifer, vertical and horizontal orientated preferential flow paths, and an induced transient hydraulic head change during the injection of the tracer. The results of the TTT are confirmed by comprehensively comparing them to the results of direct push injection logging measurements.

Kurzfassung

Die Temperatur ist eine der bedeutendsten physikalischen Größen um den Untergrund zu charakterisieren, da die Temperaturverteilung und der Wärmetransport von den Eigenschaften des Untergrundes abhängen. Daher kann Wärme als Tracer eingesetzt werden. Des Weiteren steigt die Aufmerksamkeit für die Temperatur des Untergrundes durch die steigende Popularität der geothermischen Energie. Dieses zusätzliche Anwendungsfeld für Untergrundtemperaturen und der damit verbundene Erkenntnisgewinn, verstärkt die Anwendbarkeit von Wärme als Tracer. Diese Arbeit treibt den Einsatz von Wärme als Tracer voran, indem ein thermischer Tracertest ausgewertet wird und die erzielten Resultate mit früheren Studien verglichen werden. Zusätzlich wird ein neuer thermischer Feldversuch für die hydraulische Charakterisierung des Untergrundes entwickelt. Diese Neuentwicklung überführt den klassischen geothermischen Feldversuch, den Thermal Response Test (TRT), in einen aussagekräftigen hydrogeologischen Feldversuch durch die Einführung einer neuen Auswertemethode.

Der erste Teil dieser Arbeit beinhaltet drei separate Studien die sich mit dem TRT beschäftigen. Der TRT ist ein Feldversuch, um die Wärmetransportparameter des Untergrundes zu bestimmen. Dies ist bedeutend für die Planung von geothermischen Anlagen und besonders wichtig für die richtige Konfiguration der Erdwärmesonden (EWS). Der TRT bestimmt die thermische Leitfähigkeit des Untergrundes und den Bohrlochwiderstand der EWS. Über mehrere Tage wird das Wärmeträgerfluid künstlich am Einlass der EWS erwärmt und die thermische Antwort, die Temperaturentwicklung am Auslass, aufgezeichnet. Mit Hilfe der Kalibrierung der Kelvinschen Linienquellen werden die gesuchten Parameter bestimmt. Die erste Studie untersucht die verfälschenden Einflüsse einiger Vereinfachungen, die bei der Standard-TRT-Auswertung angenommen werden, durch die Interpretation von numerisch generierten Datensätzen. Die analysierten verfälschenden Einflussfaktoren, die nicht in der Kelvinschen Linienquelle berücksichtigt werden, aber von dem verwendeten numerischen Model, sind der Rohrabstand der EWS, die initiale uneinheitliche Temperaturverteilung im Untergrund und Veränderungen der thermischen Dispersivität des Untergrundes. Diese Studie bestimmt geringe Ungenauigkeiten für die verschiedenen Rohrabstände der EWS und moderate Ungenauigkeiten für die uneinheitliche Temperaturverteilung, die eine Abweichung von 10% leicht überschreitet. Jedoch wurde eine signifikante Ungenauigkeit für die unterschiedlichen thermischen Dispersivitäten bei einer

konstanten Darcygeschwindigkeit von $0,1 \text{ m Tag}^{-1}$ bestimmt, die zu einer Überschätzung der tatsächlichen thermischen Leitfähigkeit von 20% bis 190% führt.

Die zweite Studie greift diesen deutlich Einfluss des Grundwasserflusses auf die Standard-TRT-Auswertung auf und es wird ein neuartiger Auswerteansatz entwickelt, um diese Problematik zu lösen. Um diese Zielsetzung zu erfüllen, wird mit der *Moving line source* Gleichung eine geeignete analytische Lösung für den neuen Auswerteansatz gewählt. Die *Moving line source* Lösung wird durch einen numerisch bestimmten Korrekturterm erweitert, um mögliche verfälschende Einflüsse durch die fehlende Berücksichtigung der EWS-Geometrie zu vermeiden. Mittels dieses Korrekturterms ist es möglich eine integrale Darcygeschwindigkeit durch die TRT-Auswertung zu bestimmen. Dieser neue Ansatz wurde erfolgreich an drei literaturbasierten TRT-Datensätzen getestet.

Ziel der dritten Studie ist es den TRT als einen geothermischen Feldversuch in dem Anwendungsbereich der hydrogeologischen Feldversuche, wie zum Beispiel der Pumpversuch, zu etablieren. Diese Studie profitiert von der Tatsache, dass die thermischen Aquiferseigenschaften weniger variabel sind als die hydraulischen, insbesondere die hydraulische Leitfähigkeit. Daher ist es möglich die Spannbreite der hydraulischen Leitfähigkeit mit dem neuen TRT-Auswerteverfahren zu bestimmen, unter der Annahme von realistischen Intervallen für thermische Leitfähigkeit, volumetrische Wärmekapazität, thermische Dispersivität und thermischen Bohrlochwiderstand. Die vorgeschlagene hydraulische Charakterisierungsmethode wurde erfolgreich an Hand eines großmaßstäblichen geothermischen Laborversuchs und eines kommerziell ausgeführten TRTs getestet. Gleichzeitig stellt diese Untersuchung die Validierung der neuen TRT-Auswertemethode dar, die in der zweiten Studie entwickelt wurde.

Die vierte Studie untersucht einen thermischen Tracertest (TTT). Während dieses TTTs werden 16 m^3 an 22°C warmen Wasser in einen porösen Aquifer eingeleitet und die Wärmeausbreitung mittels eines stromabwärtsorientierten Profils aus fünf separaten Beobachtungsbrunnen überwacht. Das untersuchte Versuchsgelände Lauswiesen befindet sich in der Nähe von Tübingen, Deutschland. Basierend auf den Erkenntnissen von vorangegangenen Studien, wird ein numerisches Modell erstellt, um künstliche Ergebnisse zu erzeugen, die ein ideales Wärmetransportverhalten repräsentieren. Von den gemessenen und simulierten thermischen Durchbruchkurven wird die Ankunftszeit des Maximums und

dessen Temperatur bestimmt und für einen detaillierten Vergleich verwendet. Die hauptsächlich verantwortlichen Wärmetransportprozesse werden auf Grund dieses Vergleichs identifiziert. Diese sind die geschichtete Struktur des Aquifers, vertikal und horizontal orientierte bevorzugte Fließpfade und eine erzeugte instationäre Änderungen des hydraulischen Potentials wären der Eingabe des Tracers. Die Ergebnisse der TTT-Auswertung werden durch den ausführlichen Vergleich mit einer Direct-Push-Injection-Logging Messung bestätigt.

Content

| | |
|--|-----|
| Abstract | i |
| Kurzfassung..... | iii |
| Content | vi |
| 1 Introduction..... | 1 |
| 1.1 Background..... | 1 |
| 1.2 Heat transport in the shallow subsurface | 3 |
| 1.3 Thermal field test methods | 6 |
| 1.3.1 Thermal response test..... | 6 |
| 1.3.2 Thermal tracer test..... | 9 |
| 1.3.3 Test evaluation | 9 |
| 1.4 Thesis outline..... | 12 |
| 2 Numerical Sensitivity Study of Thermal Response Tests..... | 13 |
| 2.1 Introduction | 14 |
| 2.1.1 Nomenclature | 17 |
| 2.2 Methodology..... | 17 |
| 2.2.1 Line Source Theory | 17 |
| 2.2.2 Numerical Simulation | 19 |
| 2.3 Results and Discussion | 23 |
| 2.3.1 Pipe Position..... | 24 |
| 2.3.2 Non-uniform Initial Temperature Distribution | 26 |
| 2.3.3 Thermal Dispersion | 28 |
| 2.4 Conclusions | 30 |
| 3 Analytical approach to groundwater-influenced thermal response tests of grouted borehole heat exchangers | 33 |
| 3.1 Introduction | 34 |

| | | |
|-------|--|----|
| 3.1.1 | Nomenclature | 37 |
| 3.2 | TRT Models..... | 37 |
| 3.2.1 | Conductive Line Source | 37 |
| 3.2.2 | Moving Line Source..... | 38 |
| 3.2.3 | Two-dimensional Finite Element Model for TRT Simulation..... | 42 |
| 3.3 | Initial Evaluation | 44 |
| 3.3.1 | Thermal Borehole Resistance..... | 44 |
| 3.3.2 | TRT Evaluation With Moving Line Source..... | 46 |
| 3.4 | Correction | 50 |
| 3.4.1 | Correction Term | 50 |
| 3.4.2 | Correction Procedure..... | 53 |
| 3.5 | Application | 53 |
| 3.5.1 | Diersch Case..... | 54 |
| 3.5.2 | Dornstädter Case | 56 |
| 3.5.3 | Pannike Case | 57 |
| 3.6 | Conclusion | 58 |
| 4 | Hydraulic characterization of aquifers by thermal response testing: validation by large scale tank and field experiments | 61 |
| 4.1 | Introduction | 62 |
| 4.2 | Methodology..... | 64 |
| 4.2.1 | Technological and theoretical background..... | 64 |
| 4.2.2 | Parameter estimation procedure | 70 |
| 4.2.3 | Experimental setup..... | 76 |
| 4.3 | Results and discussion | 84 |
| 4.3.1 | Interpretation of the tank experiment | 84 |
| 4.3.2 | Interpretation of the field experiment..... | 87 |
| 4.4 | Summary and conclusions | 90 |

| | | |
|-------|--|-----|
| 5 | Thermal tracer testing in a heterogeneous sedimentary aquifer: Field experiment and numerical simulation | 93 |
| 5.1 | Introduction | 94 |
| 5.2 | Thermal tracer test set up at Lauswiesen site | 98 |
| 5.2.1 | Study site | 98 |
| 5.2.2 | Thermal tracer test..... | 99 |
| 5.2.3 | Direct-push injection logging..... | 101 |
| 5.2.4 | Numerical model | 102 |
| 5.2.5 | Evaluation methodology | 105 |
| 5.3 | Results and discussion | 106 |
| 5.3.1 | Calibration of the numerical model..... | 109 |
| 5.3.2 | Temperature evolution at injection well..... | 109 |
| 5.3.3 | Density effects vs. hydraulic heterogeneity | 110 |
| 5.3.4 | Downgradient propagation of the thermal plume | 111 |
| 5.3.5 | Comparison to DPIL | 113 |
| 5.4 | Conclusions | 114 |
| 6 | Summary and conclusions | 117 |
| 7 | Perspectives..... | 121 |
| 8 | References..... | 123 |
| | Acknowledgments | 141 |
| | Declaration of authorship..... | 143 |
| | Curriculum vitae..... | 145 |

1 Introduction

1.1 Background

Energy demand and climate change present some of the major challenges of the next century. On the one hand, the long term trend of the energy demand will increase and a safe energy supply is indispensable to ensure economic growth. On the other hand, the effects of climate change have to be mitigated. To fulfill these challenges, it is necessary to use the existing primary energy more efficiently and to find new energy resources which avoid or reduce greenhouse gas emissions.

Geothermal energy exhibits a great potential to solve the aforementioned challenges. *Bromley et al.* [2010] listed the following advantages of using geothermal energy: It is available virtually worldwide; it provides base load power and heat, respectively cold; it requires technologies that are available in both developed as well as developing countries and it possesses a small land-use footprint. Depending on the type of use and system employed to harvest the geothermal energy, a better understanding of the interaction between the individual components of the geothermal system and the heat transport in the underground is mandatory.

The definition of geothermal energy includes all kinds of energy stored as heat below the surface of the earth. Hence, there are different types of reservoirs within the earth, which might be used to attain geothermal energy. These reservoirs have different characteristics, for instance reservoir temperature or depth, which need to be considered to ensure an efficient use of the reservoir. According to *Banks* [2008], the geothermal reservoirs can be classified as a low, intermediate and high enthalpy systems. Intermediate and high enthalpy systems have high production temperatures ($> 80^{\circ}\text{C}$). These systems are usually planned to provide electric and thermal energy if the temperatures are sufficient [*Banks*, 2008]. The high temperatures in combination with the reservoir depth (usually 1000 m below the surface) require the consideration of specific technical aspects for the energy exploration and various geoscientific parameters to describe the reservoir itself [*Stober and Bucher*, 2012]. These technical aspects and geoscientific parameters are different from those of low enthalpy systems, which are only applied to generate thermal energy at low temperature levels from shallow depth. In generally, these low enthalpy systems exhibit extraction temperatures of approximately 25°C and the

depth varies from 1 up to 150 m [*Stober and Bucher, 2012*]. The studies enclosed within the present thesis focus on low enthalpy systems.

For certain applications, such as space heating, these low extraction temperatures require the application of an additional energy device, commonly a heat pump. The heat pump helps increase the temperature of the geothermal source to the temperature level required for the heating system [*Tholen and Walker-Hertkorn, 2008*]. To elevate the temperature level, the heat pump itself consumes auxiliary energy in the form of electricity [e.g. *Bayer et al., 2012*]. The amount of auxiliary energy consumption rises with an increasing temperature difference between the geothermal source and the heating system. To lower the temperature of a building, cooling applications, such as heat pump systems can be applied reverse to transfer heat from the building into the subsurface. The natural and undisturbed temperature regime of the shallow subsurface is typically very stable and varies only in the upper part due to diurnal temperature fluctuations [*Taylor and Stefan, 2009*]. This zone represents the geothermal reservoir used by a ground source heat pump system (GSHP). The thermal reservoir interacts in all directions with the surrounding environment, at the bottom a geothermal heat flux occurs, at the top there is a thermal interaction with the atmosphere and at the sides of the thermal reservoir there might be a heat flux due the advective and conductive heat transport. The direction of these heat fluxes across the reservoir boundaries depends on the temperature difference between the reservoir and the surrounding environments. Heat inside the thermal reservoir propagates by advection and thermal dispersion (see chapter 1.2 for more details on heat transport). To ensure a sustainable and efficient usage of this geothermal source, both the heat budget and the heat transport properties have to be considered. Based on this knowledge an adequate utilization technique can be developed. The shallow geothermal energy can be exploited by two types of systems, the groundwater heat pump (GWHP) and the ground source heat pump (GSHP). In GWHP systems or so called open systems heat and mass (groundwater) are exchanged with the subsurface. In general, the groundwater is extracted from a spring, dug well, drilled borehole or flooded mine [*Banks, 2008*]. Commonly, an open system consists of an extraction well, which heaves the groundwater and supplies the heat pump with this water, and a second well, the injection well, which passes the thermally used groundwater back into the aquifer [*Koenigsdorff, 2011*]. In contrast to this, closed systems only exchange heat with the subsurface. The main representatives of closed systems are vertical borehole heat exchanger (BHE), horizontal closed loops and energy piles [*Banks,*

2008]. The basic functionality of a closed loop system can be explained by using the example of a BHE, which is the most commonly used representative of this category [Bayer *et al.*, 2012]. A BHE is a drilled borehole equipped with a pipe system, for instance a single u-pipe, a double u-pipe or a coaxial pipe. The remaining surplus of the borehole, which is not occupied by the pipe system, is normally backfilled with a grouting material to guarantee the thermal connection between the pipes and the subsurface. The second task of the grouting material is to protect the subsurface from negative consequences, such as hydraulic short circuits between two aquifers, caused by the borehole. Inside the pipes a heat carrier fluid circulates, which exchanges thermal energy with the surrounding subsurface and transports the obtained thermal energy to the heat pump at the surface.

Such shallow geothermal systems are among the fastest growing renewable energy technologies in the world [Rybach, 2010]. Furthermore, most parts of this technology, like the heat pump, are already well established and today a great number of installations already exist. This is corroborated by the 2.8 million GSHP installed in the year 2010 worldwide [Lund *et al.*, 2011]. Bayer *et al.* [2012], who analyzed the current state of shallow geothermal installations in Europe, stated that there are over one million units installed in Europe and that this number will further increase. Blum *et al.* [2010] quantified the amount of shallow geothermal installations in Germany to approx. 100,000 units. All these three studies predict a recurrent growth of the number of GSHP systems. The amount of thermal energy supplied by the GSHP is small compared to the total amount of energy used for space heating. In the residential sector, Bayer *et al.* [2012] specified a percentage of less than 1% of GSHPs on the total heating energy amount. But this emphasizes that there is still a great growth potential and that this technology is far from reaching any level of market saturation.

1.2 Heat transport in the shallow subsurface

Heat propagation in the saturated porous media is controlled by three basic processes [de Marsily, 1986]. These are (1) heat transport through the solid phase, (2) heat transport by fluid movement and (3) heat exchange between the fluid and the solid phase. Both processes (1) and (2) result in a separate transport equation for heat in the fluid and solid phase. The interaction between these two transport equations is controlled by the heat exchange process (3). Due to the fast heat exchange rates between the fluid and the solid in a porous media, it is a common assumption to suppose an instantaneous thermal equilibrium in the porous media. For instance, de Marsily [1986] presented a study, which demonstrated that the temperature

difference between the solid and the fluid phase in a media composed of grains $< 1\text{mm}$ will be equilibrated in less than one minute. Because of the valid assumption of an instantaneous thermal equilibrium, there is usually no significant temperature difference between the solid and the fluid temperature of the porous media. Hence, the heat transport in the porous subsurface can be simplified to be governed only by heat transport through the solid and the fluid phase with a uniform temperature distribution in both phases. Based on the principles of heat conservation, the heat transport governing equation in the porous media can be expressed as [de Marsily, 1986]

$$\frac{\partial T}{\partial t} = \text{div}(D \cdot \text{grad}(T)) - \text{div}(v_{th}T) \quad (1-1)$$

Where T specifies the temperature of the porous media (K), D denotes the thermal dispersion coefficient ($\text{m}^2 \text{s}^{-1}$) and v_{th} represents the thermally retarded velocity ($\text{m} \text{s}^{-1}$). The heat transport by fluid movement is termed advection. In the present thesis the term convection is only used if the fluid movement is caused by temperature induced density differences. It should be noted that in porous media, the groundwater velocity required for advective/convective heat transport, is typically described by Darcy's law. Furthermore, it is necessary to consider that the advective heat transport velocity is retarded compared to the actual groundwater flow velocity. These effects of thermal retardation can be calculated by

$$v_{th} = v \frac{c_{pw}}{c_{pm}} \quad (1-2)$$

Where c_{pm} and c_{pw} are the volumetric heat capacity of the porous media and the groundwater ($\text{J m}^{-3} \text{K}^{-1}$). This thermally retarded velocity assumes a fictitious medium, which is completely streamed by groundwater, and disregards the actual velocity distribution caused by the heterogeneous structure of the pore channel network [de Marsily, 1986]. The effect of the existing variability of the groundwater velocity field, which is mainly caused by the granular structure of the porous media, is considered in the thermal dispersion coefficient D . This coefficient includes the isotropic and groundwater flow independent thermal diffusivity, which forms the quotient of the thermal conductivity and the volumetric heat capacity of the porous media. Further, this dispersion coefficient possesses a groundwater flow depending part. This part linearly links the v_{th} with a longitudinal, α_l , and two transversal dispersivities, α_t . Therefore, the thermal dispersion is a tensor encompassing a coefficient parallel to the groundwater flow direction and two coefficients transversal to the groundwater flow direction

[*de Marsily, 1986*]. In this thesis it is assumed that both transversally orientated thermal dispersion coefficients are equal. The resulting longitudinal and transversal thermal dispersion coefficients (D_l and D_t) are

$$D_l = \frac{\lambda_m}{c_{pm}} + \alpha_l v_{th} \quad (1-3)$$

$$D_t = \frac{\lambda_m}{c_{pm}} + \alpha_t v_{th} \quad (1-4)$$

Where λ_m represents the thermal conductivity of the porous media ($\text{W m}^{-1} \text{K}^{-1}$). The heat transport governing equation (Eq. 1-1) can be solved analytically or numerically. It should be noted, that thermal dispersion might be smaller than solute dispersion due to the heat exchange between the solid and fluid phase [*Molina-Giraldo et al., 2011a*]. In general, the analytical solution bases on a set of simplifications, but provides an exact solution of the entire space [*Mohrlok, 2008*]. These simplifications and assumptions are related to the parameters of the domain, the geometry of the system and the initial and boundary conditions of the problem. Based on these assumptions, suitable analytical solutions for various heat transport situations can be derived. For instance, several suitable solutions exist to simulate a BHE.

Various analytical solutions exist for different simplifications of the BHE geometry. The most important ones are the solutions with a representation of the BHE as a line-shaped [e.g. *Molina-Giraldo et al., 2011b*] or cylinder-shaped [e.g. *Sass and Lehr, 2011*] heat source and/or a heat source of infinite [e.g. *Diao et al., 2004*] or finite [e.g. *Zeng et al., 2002*] length. Furthermore, the applied analytical solutions consider constant initial and boundary conditions. This simplification can be overcome by a Laplace transformation [*Mohrlok, 2008*]. More frequently, utilizing the fact that energy is an extensive variable, the principles of spatial and temporal superposition are applied to simulate BHE arrays or BHEs with variable heat loads [e.g. *Diao et al., 2004*]. All these analytical solutions also assume that the hydraulic and thermal parameters are independent of time and temperature and that each of the parameters are homogeneously distributed. The analytical solutions also differ in the transport processes, which are assumed. There are solutions which only consider conductive heat transport [e.g. *Zeng et al., 2002*] and other which consider conductive and advective heat transport [e.g. *Carslaw and Jaeger, 1959; Molina-Giraldo et al., 2011b*].

Contrary to the analytical approaches, numerical solutions are able to represent more complex systems. Hence, they are suitable to solve transport problems with a complex geometry, highly variable boundary conditions, heterogeneous distributions of the initial conditions and/or the parameter distributions [Mohrlok, 2008]. In contrast to analytical solutions, numerical approaches calculate values only at a set of discrete numerical nodes. In general, three different numerical methods can be used to simulate heat transport in porous media: the finite difference method, the finite volume method and the finite element method. Based on these three different methods, there are several computer codes available to simulate subsurface heat transfer due to shallow geothermal systems. Hecht-Méndez *et al.* [2010] assembled a list of 18 different suitable numerical codes of varying complexity. The computer code complexity mainly depends on the ability to consider hydraulic and thermal processes alone or chemical processes in addition and on how the two, or respectively, three processes are coupled. More straightforward computer codes, such as AST/TWOW and VS2DH, possess a one way coupling between the hydraulic and thermal processes while more advanced numerical codes exhibit a full coupling between the involved processes (e.g. FEFLOW and FRACtrue).

1.3 Thermal field test methods

Temperature is one major intensive quantity of the subsurface. Therefore, it is obvious to use temperature measurements to examine the subsurface [Anderson, 2005; Saar, 2011]. This thesis presents evaluations of two different thermal field tests, the thermal response test (TRT) and the active thermal tracer test (TTT). Comparable to the classification of shallow geothermal systems, these field tests can also be distinguished by the different thermodynamic interaction of the heat source and the subsurface. Similarly to closed loop systems, the TRT applies a BHE as a heat source, which is a thermodynamic closed system. In correspondence to an open geothermal system, the source of an active TTT is a groundwater well, which is used to exchange heat and water with the aquifer.

1.3.1 Thermal response test

The TRT is the most standard field investigation technique for close shallow geothermal systems using a BHE. The basic principle of the TRT is to thermally stress the subsurface by injecting or extracting heat in or from the subsurface through a BHE. The thermal response is then evaluated to derive the major heat transport characteristics of the examined system. These characteristics are typically the effective thermal conductivity λ_{eff} and the thermal

borehole resistance R_b . In general, a TRT device consists of a circulation pump, which controls the flow rate of the heat carrier fluid, temperature sensors connected to a data logger to record the development of the heat carrier fluid temperature, and a heating or cooling device.

One of the major research topics related to the standard TRT is the accuracy of the obtained values λ_{eff} and R_b . The standard TRT evaluation encompasses a parameter estimation applying the Kelvin line source equation [e.g. *Gehlin*, 1998]. This approach exhibits several assumptions and not all effects which influence the TRT experiment are considered by this analytical solution. This nonobservance might have a tampering influence on the resulting parameters. *Signorelli et al.* [2007] analyzed by interpreting results of a numerical model, the tampering influences of borehole length, subsurface heterogeneity, groundwater movement and variable data quality on the resulting λ_{eff} values. The study “*Numerical sensitivity study of thermal response tests*” [*Wagner et al.*, 2012b] presented in chapter 2, adopts the methodology of *Signorelli*’s study to determine the tampering effects of different assumptions. Further, these analyses are extended by a sensitivity analysis of the result. As the standard TRT evaluation includes a simultaneous determination of λ_{eff} and R_b , the present study performs a sensitivity analysis of both resulting parameters and not only of λ_{eff} . Motivated by the study of *Signorelli et al.* [2007], which demonstrated that there is a tampering effect of a non-uniform initial ground temperature distribution (e.g. geothermal gradient) based on one artificial dataset, a systematic survey of this effect is performed. One of the most intensively studied tampering effect is additional heat transport by advection [e.g. *Signorelli et al.*, 2007; *Raymond et al.*, 2011b], but the effects of thermal dispersion, which are directly related to heat transport in environments with flowing groundwater (chapter 1.2), so far have not been analyzed. Further, *Raymond et al.* [2011b] already formulated the necessity to account for thermal dispersion in TRT interpretations. This need is taken up and a systematical evaluation of different thermal dispersion coefficients caused by varying thermal dispersivities is evaluated.

As mentioned above, the influence of groundwater movement on the result of a standard TRT evaluation is analyzed in several studies, which are based on numerical simulations [e.g. *Signorelli et al.*, 2007] or field experiments [e.g. *Witte*, 2001]. For instance, the study presented in chapter 2 [*Wagner et al.*, 2012b] determines an overestimation potential for λ_{eff} of 0.5 to 3.9 W m⁻¹ K⁻¹ and R_b of 0.012 to 0.022 m K W⁻¹ based on numerically generated TRT

datasets. Furthermore, *Carslaw and Jaeger* [1959] presented an adequate analytical solution more than 50 years ago which determines the heat propagation around an heat source, which is shaped like an infinite line, in an environment influenced by advection and conduction. In spite of the obvious demand and an existing analytical solution, there is no existing groundwater sensitive TRT evaluation relying on such an analytical equation. This analytical solution is the moving line source model. To overcome this need *Chiasson and O'Connell* [2011] and the study in chapter 3 [*Wagner et al.*, 2013] simultaneously present a TRT evaluation approach based on the moving line source equation. In contrast to the study of *Chiasson and O'Connell* [2011], the survey “*Analytical approach to groundwater influenced thermal response tests of grouted borehole heat exchangers*” [*Wagner et al.*, 2013] presented in chapter 3, analyzed the accuracy of the applied analytical solution to determine the actual thermal conductivity and Darcy velocity of the subsurface. This inspection relies on an intensive comparison between the input parameters of numerical generated TRT datasets and the resulting parameters of a moving line source based parameter estimation. Based on this systematic comparison, a correction term is developed to overcome the potentially distorting effects of not considering the geometry of the BHE.

Recently, *Anderson* [2005] and *Saar* [2011] presented the high potential of heat as a groundwater tracer. Additionally, there are already several studies on thermal field tests, which successfully evaluate thermal signals to perform a hydraulic characterization of the subsurface. For instance, there are active thermal tracer tests [e.g. *Ma et al.*, 2012; *Wagner et al.*, 2014b] or the heat perturbation flow meter [e.g. *Ochsner et al.*, 2005; *Gao et al.*, 2006]. Due to the fact that the theoretical study presented in chapter 3 [also see *Wagner et al.*, 2013] provides an evaluation framework to determine groundwater velocities based on TRTs, it is very reasonable to use a TRT for hydraulic characterizations. The study “*Hydraulic characterization of aquifers by thermal response testing: validation by large scale tank and field experiments*”, which is presented in chapter 4, picks this up and inspects the applicability of a TRT as a hydraulic characterization method. Due to the fact that the thermal properties of a porous aquifer vary in small ranges compared to the hydraulic properties, especially the hydraulic conductivity, the correction term based TRT evaluation in chapter 3 is used to obtain an integral hydraulic conductivity value of the subsurface. To validate this approach, the study presented in chapter 4 [*Wagner et al.*, 2014a] conducts a large scale tank experiment to be able to generate a groundwater influenced TRT in a well-known environment.

Furthermore, a field scale and commercially performed TRT is used to test the approach under realistic conditions. The obtained TRT dataset from this tank experiment and the field based TRT dataset are evaluated and the resulting hydraulic properties are compared to previous hydraulic characterization to validate the proposed approach.

1.3.2 Thermal tracer test

As aforesaid, there are several applications, which use heat as a tracer [e.g. *Anderson, 2005*]. One of these applications is the short term active thermal tracer test (TTT). In general, this TTT is applied for the characterization of an aquifer [e.g. *Ma et al., 2012*]. In spite of the fact that heat propagation in the subsurface can be quantified and the direct analogy between heat and solute tracer test, the TTT, is still not a standard method for aquifer testing. To establish the short term active TTT as a standard methodology, one essential requirement is an improved insight into the relevant heat transport phenomena influencing the TTT-result. Furthermore, it is important to share the implications from as many TTTs as possible to accelerate the establishment of the TTT as a standard hydrogeological investigation technique. Therefore the study “*Thermal tracer testing in a sedimentary aquifer: field experiment (Lauswiesen, Germany) and Numerical simulation*” presented in chapter 5 presents a TTT experiment which determines relevant heat transport processes and is upfront with the observed experimental difficulties. To achieve these objectives, the study compares the results of the TTT to another hydrogeological field investigation (direct push injection logging measurements) and a corresponding numerical model. The TTT incorporates one injection well, which is used to inject 16 m³ of 22°C warm water within 8 h into the aquifer and five downgradient observation wells to record the transport of the thermal plume. Based on the recommendations of *Bellin and Rubin [2004]*, the main focus of the interpretation is set on the peak arrival time of the thermal tracer. The comparison of measured and simulated TTT results are used primarily to improve the understanding of the thermal interaction between aquifer and aquitard, the distinction of hydraulic heterogeneities and density effects and influences of the layered aquifer structure on the heat propagation. The results of the TTT are in agreement with the findings of *Lessoff et al. [2010]*.

1.3.3 Test evaluation

Both thermal field tests share the same principle: heat is injected into the subsurface and the measured thermal response is interpreted to get new insights of the subsurface thermal

properties. Therefore the interpretation process of the measured datasets can be carried out by the same methodology. This methodology is based on the principles of optimization.

In the present investigation, the general aim of the optimization procedures focuses on the determination of a set of model properties, such as thermal or hydraulic conductivity, which result in the best agreement between the TRT or TTT experiment and a corresponding model. Therefore the optimization is used to perform a parameter estimation or an inverse modeling, respectively. To be able to estimate the optimal parameter set, a model is needed, which represents the real system, for instance a field test and considers the searched set of properties, for example thermal conductivity and/or hydraulic conductivity. Based on this model and the measured results of the field experiment, an objective function can be formulated which quantifies the difference between both. *Loague and Green* [1991] presented a comprehensive review of suitable formulations of such an objective function. All studies included in this thesis apply the root mean squared error (RMSE) to scale the difference between the measured and simulated values to express the objective function.

Additionally, a suitable search algorithm is needed to find the optimal parameter set. The most simple discrete search algorithm, respectively, technique is the “brute force” grid search method [*Venkataraman*, 2009]. This method first constructs a parameter grid of the searched parameters with a predefined resolution of each parameter. The value of the objective function is obtained for each grid point and all related values are compared. Consequently, the grid point with the optimal value of the objective function, which might be the highest, lowest or nearest to a certain target value, features the searched or optimal parameter set. In general, this approach requires numerous evaluations of the objective function to find an adequate solution, which might cause a long duration of the optimization procedure. But this approach always examines the entire parameter grid and therefore this solution represents a global optimum with respect to the parameter grid. In contrast to the global optimum, which represents the best solution of the entire parameter grid, there is the local optimum. This exhibits the best solution of a certain parameter grid sector, but not of the entire array. More efficient search algorithms, which in general require less objective function evaluations, implicate a risk to find only a local optimum. The second search algorithm applied in this thesis is the Nelder-Mead simplex algorithm [*Nelder and Mead*, 1965], which is more efficient, but entails the risk of finding only a local optimum. This algorithm is able to optimize any function with n searched parameters. The algorithm evaluates the objective

function at the $n + 1$ vertices of a simplex. For example, if the searched parameter set consists of the hydraulic and thermal conductivity, the algorithm determines the value of the objective function for three different parameter combinations. The three parameter pairs are the vertices of the first simplex. The search algorithm skips the vertices with the worst value of the objective function. To construct the missing vertices of a new simplex, a parameter combination is determined by applying a reflection, expansion, contraction and shrinkage step. The Nelder-Mead simplex algorithm is a quite robust search algorithm, but it is not completely shielded to converge in a local minima or contracting some parameters as constant too early in the optimization procedure.

Both of these search algorithms are applied to find the best parameter combinations in the enclosed studies. The studies presented in chapter 2 and 5 uses the “brute force” grid search method approach. The study enclosed in chapter 3 applies the Nelder-Mead simplex algorithm to find the optimal solution and the study of chapter 4 employs a combination of both search algorithms.

1.4 Thesis outline

This work is a cumulative dissertation and the four enclosed studies of this work are integrated in the chapters 2 – 5. The major objective of the first study (chapter 2) is to reveal a deeper insight into the influences of the shank spacing, initial non-uniform temperature distributions (e.g. geothermal gradient), and thermal dispersion on a Kelvin line source based TRT evaluation. The main objective of the second study (chapter 3) is the development of a new groundwater sensitive TRT evaluation approach, which can be used to additionally determine the integral Darcy velocity of an aquifer. The primary objective of the third study (chapter 4) is to demonstrate that data from TRT measurements can be applied for a hydraulic characterization of the subsurface. The general objective of the fourth study (chapter 5) is to determine how much information of the hydraulic properties can be derived from the interpretation of a TTT experiment.

2 Numerical Sensitivity Study of Thermal Response Tests

Reproduced from: Wagner, V., Bayer, P., Kübert, M., Blum, P. (2012a), Numerical sensitivity study of thermal response tests, Renewable Energy, 41(0), 245-253, doi: 10.1016/j.renene.2011.11.001. The final publication is available at sciencedirect.com.

Abstract: Thermal conductivity and thermal borehole resistance are basic parameters for the technical and sustainable design of closed ground source heat pump (GSHP) systems. One of the most common methods to determine these parameters is the thermal response test (TRT). The response data measured are typically evaluated by the Kelvin line source equation which does not consider all relevant processes of heat transfer in the subsurface. The approach only considers conductive heat transfer from the borehole heat exchanger (BHE) and all transport effects are combined in the parameters of effective thermal conductivity and thermal borehole resistance. In order to examine primary effects in more detail, a sensitivity study based on numerically generated TRT data sets is performed considering the effects of (1) the in-situ position of the U-shaped pipes of borehole heat exchangers (shank spacing), (2) a non-uniform initial thermal distribution (such as a geothermal gradient), and (3) thermal dispersivity. It will be demonstrated that the shank spacing and the non-uniform initial thermal distribution have minor effects (less than 10%) on the effective thermal conductivity and the determined borehole resistance. Constant groundwater velocity with varying thermal dispersivity values, however, has a significant influence on the thermal borehole resistance. These effects are even more pronounced for interpreted effective thermal conductivity which is overestimated by a factor of 1.2 to 2.9 compared to the real thermal conductivity of the saturated porous media.

2.1 Introduction

The utilization of shallow geothermal energy is becoming increasingly popular, which is mainly due to the rising costs of fossil fuels and its potential to avoid additional or even reduce CO₂ emissions [Blum *et al.*, 2010; Saner *et al.*, 2010]. The most popular way to exploit shallow geothermal energy resources is the use of ground source heat pump (GSHP) systems. They extract energy from the ground to depths of about 400 m by horizontal or vertical borehole heat exchangers (BHEs). In the latter, a heat carrier fluid is circulated in closed pipes that transfer heat or cold to the heat pumps. The pipes are installed in boreholes and are often backfilled with a bentonite-cement suspension for safety and stability reasons. To ensure the efficiency of such systems, appropriate dimensioning of the GSHP system is essential. Only if the extracted amount of energy is equal or close to the amount of energy which can be replenished naturally, will the GSHP system work efficiently and sustainably over its lifetime. The extractable amount of energy mainly depends on the thermal properties and the hydrogeological conditions of the ground as well as on the properties of the grouting material.

Thermal properties commonly are estimated in situ by a thermal response test (TRT) which was developed by *Morgensen* [Morgensen, 1983]. During the TRT, a constant amount of energy is injected into [Gehlin, 1998] or extracted [Witte *et al.*, 2002] from the ground by using a BHE and the temperature development of the circulating heat carrier fluid is recorded. Standard interpretation of TRTs follows the line source theory [Witte *et al.*, 2002]. The parameters obtained are the effective thermal conductivity, λ_{eff} , which integrates all thermal effects of the subsurface along the entire BHE length, and the thermal borehole resistance, R_b , which describes the heat transfer inside the entire BHE. To characterize the expected performance of a BHE, all relevant heat transfer processes in the subsurface are parameterized by two integrative terms, λ_{eff} and R_b . However, it is often impossible to identify the reasons of specific parameter values, since the interference of the dominant heat transfer processes cannot be resolved. In order to clarify the role of different effects on λ_{eff} and R_b , several field [Witte, 2001; Roth *et al.*, 2004; Sanner *et al.*, 2005; Esen and Inalli, 2009; Kübert *et al.*, 2009; Gustafsson and Westerlund, 2010; Raymond *et al.*, 2011b] and modeling studies [Gehlin and Hellström, 2003; Wagner and Clauser, 2005; Signorelli *et al.*, 2007; Marcotte and Pasquier, 2008; Zanchini and Terlizese, 2008; Acuña and Palm, 2009; Raymond *et al.*, 2011b] were performed. From field studies, it is known that groundwater flow results in an increase of λ_{eff} [Witte, 2001; Kübert *et al.*, 2009]. Esen and Inalli [Esen and Inalli, 2009] suggested that

increasing the depth of the analyzed BHEs yields a decrease of R_b . Variable daily air temperature causes fluctuations in the recorded temperature time curve of the circulating heat carrier fluid, which introduce uncertainty in TRT interpretation [Roth *et al.*, 2004]. An enhanced thermal conductivity of the grouting material improves R_b [Sanner *et al.*, 2005]. Increasing heat injection rates of groundwater-filled boreholes results in a decrease of R_b [Gustafsson and Westerlund, 2010]. Raymond *et al.* [2011b] demonstrated that geological heterogeneity (e.g. layering) can result in an overestimation of λ_{eff} . The results of TRT simulations confirm these observations like the enhancing effect on λ_{eff} of groundwater flow [Signorelli *et al.*, 2007] and reveal the influence of additional parameters, especially of the type of aquifer [Gehlin and Hellström, 2003], heat capacity of the subsurface [Wagner and Clauser, 2005], horizontal configuration of the BHE pipes [Acuña and Palm, 2009], and changes in the heat carrier fluid density during a TRT [Zanchini and Terlizzese, 2008].

The effects of different methods to calculate the mean heat carrier fluid temperature [Marcotte and Pasquier, 2008] and the impact of vertical temperature variations [Raymond *et al.*, 2011b] are analyzed based on numerical models. For example, high values of groundwater flow velocity yield elevated λ_{eff} values. Another crucial factor is the shank space defined by Lamarche *et al.* [Lamarche *et al.*, 2010] as the distance between the centers of the BHE pipes. A small shank spacing or a lower thermal conductivity of the grouting material results in high R_b values. The exact in-situ position of the individual U-shaped pipes results in a major uncertainty which can hardly be quantified, even if a pipe spacer is used during installation.

The shank spacing will also be one of three factors in the focus of the present study. A number of studies are dedicated to factors determining the value of R_b . Some studies examined the thermal borehole resistance of a single U-pipe BHE [Acuña and Palm, 2009; Sharqawy *et al.*, 2009a; Lamarche *et al.*, 2010] and others focused on double U-pipe BHE [Zeng *et al.*, 2003; De Carli *et al.*, 2010]. However, these studies did not consider the evaluation of R_b using TRTs. Here, the effects of various pipe positions on the R_b values obtained from TRT interpretation will be analyzed and compared to actual (“true”) R_{b-num} values determined by numerical simulation. In addition, the influence of the shank spacing on the resulting λ_{eff} will be evaluated. For this, valid pairs of estimated R_b and λ_{eff} values will be studied as a function of the shank spacing.

Signorelli et al. [2007] demonstrated for one numerically simulated TRT that the non-uniform initial ground temperature distribution due to the natural vertical geothermal gradient, which is not considered by the line source theory, results in a detectable difference between the obtained λ_{eff} and the true thermal conductivity of the porous medium, λ_m . *Raymond et al.* [2011b] confirm these findings by analyzing a TRT conducted in a waste rock. This waste rock contains iron-sulfide minerals which react exothermally with water and oxygen and cause an abnormally high geothermal gradient ($0.3 \text{ }^\circ\text{C m}^{-1}$). The TRT is evaluated with a numerical model and based on the standard line source approach. The thermal conductivity value of the numerical analysis is approximately 14% lower than the value of the line source based evaluation. The work reported here was based on their findings and will focus on a systematic analysis of the influence of various non-uniform initial temperature distributions on the TRT result. Additionally, the correlation between R_b and λ_{eff} will be studied.

Several studies [*Witte*, 2001; *Gehlin and Hellström*, 2003; *Signorelli et al.*, 2007] evaluated the influence of convective heat transfer, i.e. groundwater flow, on TRT interpretation (in particular on λ_{eff}). However, these studies did not consider the effects of thermal dispersion. Although *Raymond et al.* [2011b] mentioned the need to also account for thermal dispersion in TRT interpretation, no sensitivity study was performed. In contrast to this, *Molina-Giraldo et al.* [2011a] found that dispersion-dominated aquifers result in smaller temperature changes close to the BHE and shorter thermal plumes. The present study will therefore also concentrate on the effects of thermal dispersion on the TRT and a detailed analysis of convection-influenced TRTs will be performed.

The main objective of this study is to obtain deeper insight into the influence of the three factors of shank spacing, non-uniform initial temperature distribution (e.g. geothermal gradient), and thermal dispersion on the interpretation of TRTs. Furthermore, the difference between estimated and true parameter values characterizing the BHE and subsurface under various conditions will be determined. For this purpose, a high-resolution finite element BHE model with coupled heat and mass transport will be developed to generate artificial TRT data sets with well-known initial and boundary conditions. The generated data will be analyzed by two common line source based evaluation approaches, linear regression and the two-variable parameter fitting method.

2.1.1 Nomenclature

The nomenclature used in chapter 2 is compiled in Table 1

Table 1 Nomenclature of chapter 2.

| | |
|----------------------|---|
| T | temperature ($^{\circ}\text{C}$) |
| q | heat transfer rate per unit length (W m^{-1}) |
| R_b | thermal borehole resistance (m K W^{-1}) |
| r | radius (m) |
| t | time (s) |
| Ei | exponential integral |
| u | integration variable |
| m | slope of the linear regression ($^{\circ}\text{C}$) |
| n | number of time steps evaluated |
| L | length of the borehole heat exchanger (m) |
| cp | volumetric heat capacity of the porous media ($\text{MJ m}^{-3} \text{K}^{-1}$) |
| cp_f | volumetric heat capacity of the heat carrier fluid ($\text{MJ m}^{-3} \text{K}^{-1}$) |
| Q_f | volume flow rate of the heat carrier fluid ($\text{m}^3 \text{s}^{-1}$) |
| <i>Greek symbols</i> | |
| λ | thermal conductivity ($\text{W m}^{-1} \text{K}^{-1}$) |
| κ | thermal diffusivity ($\text{m}^2 \text{s}^{-1}$) |
| γ | Euler's constant |
| <i>Subscripts</i> | |
| f | fluid |
| bw | borehole wall |
| sub | subsurface |
| eff | effective property value |
| num | numerically determined |
| lin | determined by linear regression |
| par | determined by parameter estimation |
| m | property of the porous media |
| 0 | initial or undisturbed value |
| mea | measured value |
| in | inflow |
| out | outflow |

2.2 Methodology

2.2.1 Line Source Theory

Kelvin's line source theory [Carslaw and Jaeger, 1959] is often used to evaluate a TRT [Gehlin, 1998; Witte et al., 2002; Signorelli et al., 2007]. The BHE is approximated as an infinite line source in a homogeneous, isotropic, and infinite medium, which injects or extracts a constant amount of energy (q). The temporal and spatial temperature changes around the line source are derived by [Witte, 2001; Gehlin, 2002]:

$$T_{sub}(r,t) - T_0 = \frac{q}{4\pi\lambda_{eff}} \int_{\frac{r^2}{4\kappa t}}^{\infty} \frac{e^{-u}}{u} du = \frac{q}{4\pi\lambda_{eff}} Ei \left[\frac{r^2}{4\kappa t} \right] \approx \frac{q}{4\pi\lambda_{eff}} \left[\ln \left(\frac{4\kappa t}{r^2} \right) - \gamma \right] \quad (2-1)$$

where q (W m^{-1}) is the heat injection rate per unit length of a borehole, λ_{eff} ($\text{W m}^{-1} \text{K}^{-1}$) the effective thermal conductivity of the subsurface, and κ ($\text{m}^2 \text{s}^{-1}$) the thermal diffusivity of the subsurface. The mean fluid temperature ($T_f = (T_{in} + T_{out}) / 2$) [Signorelli *et al.*, 2007]) of the circulating heat carrier fluid can be accessed by including a thermal borehole resistance term, R_b , in Eq. (2-1) [Signorelli *et al.*, 2007]:

$$T_f - T_{bw} = qR_b \quad (2-2)$$

The thermal borehole resistance depends mainly on the geometry (shank spacing, pipe and well diameter, number of pipes, and depth of the BHE) as well as on the physical parameters of the BHE, such as thermal properties of the BHE material, flow rate of heat carrier fluid in the BHE, and fluid properties [Pahud and Matthey, 2001]. This yield:

$$\begin{aligned} T_f(t) = T_{bw}(t) + qR_b &= \frac{q}{4\pi\lambda_{eff}} Ei \left[\frac{r_{bw}^2}{4\kappa t} \right] + T_0 + R_b q \\ &\approx \frac{q}{4\pi\lambda_{eff}} \ln(t) + q \left[R_b + \frac{1}{4\pi\lambda_{eff}} \left(\ln \left(\frac{4\kappa t}{r_{bw}^2} \right) - \gamma \right) \right] + T_0 \end{aligned} \quad (2-3)$$

The logarithmic approximation of Eq. (2-3) is a linear function of the logarithm of time. One possibility to graphically evaluate the TRT is by linear regression of the measured fluid temperature in logarithmic time. The slope (m) of the straight line is used to quantify λ_{eff} as follows:

$$\lambda_{eff} = \frac{q}{4\pi m} = \frac{q}{4\pi} \frac{\ln(t_2) - \ln(t_1)}{T_f(t_2) - T_f(t_1)} \quad (2-4)$$

In the same manner, R_b is determined by the y-axis intercept. The other possibility consists in a more rigorous two-variable parameter fitting method [Roth *et al.*, 2004]. This approach minimizes the misfit (e.g. root mean squared error, RMSE) between model and observation by a combined adjustment of R_b and λ_{eff} [Marcotte and Pasquier, 2008]:

$$RMSE = \left[\frac{1}{n} \sum_{i=1}^n (T_{mea} - T_f)^2 \right]^{0.5} \quad (2-5)$$

Due to measurement impreciseness and data noise, no perfect fit can be obtained and instead of one optimal parameter combination, it is desirable to also evaluate valid parameter pairs of R_b and λ_{eff} . Validity has to be decided on for each specific case and is determined by setting a threshold of tolerable RMSE. Here, the valid parameter pairs are searched for by exhaustive grid search. Reasonable intervals of R_b and λ_{eff} are discretized on a sufficient level of detail and interpolated response surfaces of fit are obtained through complete testing of all possible parameter pairs. In the current study the acceptable error of the parameter fitting method is set to an RMSE of 0.14°C based on the typical uncertainty of the temperature difference of 0.14°C determined by Witte et al. [Witte et al., 2002], which is supposed to represent the measurement error of a TRT.

2.2.2 Numerical Simulation

In contrast to the application of the line source equation, numerical models allow for the simulation of coupled subsurface physical and hydraulic processes during a TRT. The numerical model can be used to simulate the relevant processes during a TRT under realistic conditions. Although using real field data would be even more desirable, synthetic simulations are attractive, since all processes and their specifications are completely known. By comparison to standard line source theory-based interpretation, the significance of the individual effects to the standard parameters, R_b and λ_{eff} , can be quantified accurately.

In previous studies, 1D finite difference BHE models [Shonder and Beck, 1999], 2D finite volume BHE models [Yavuzturk et al., 1999], 2D finite element BHE models [Zanchini and Terlizze, 2008], 3D finite difference BHE models [Wagner and Clauser, 2005], and 3D finite element BHE models [Signorelli et al., 2007] were used. Due to the three-dimensionality of heat transport caused by a BHE in the subsurface, a 3D simulation is the most favourable option [Signorelli et al., 2007]. The complex geometry of a BHE can be represented by finite element meshes [Esen et al., 2009]. Therefore, finite element-based simulations are frequently used to simulate BHE [Marcotte and Pasquier, 2008; Lamarche et al., 2010; Diersch et al., 2011a; b]. A common and versatile commercial finite element software platform for computationally efficient simulations of 3D heat transport is FEFLOW [Diersch, 2006].

Since the release of the FEFLOW version 5.4, a BHE model has been implemented directly in the software, in which the BHE is simulated as an embedded vertical 1D finite element in the finite element matrix [Diersch, 2006]. However, this implementation does not provide the exact spatial temperature distribution inside the BHE. This prevents a detailed analysis of R_b based on numerical results. Within the framework of the present study, an alternative single BHE model based on the study by Signorelli *et al.* [2007] was developed in FEFLOW and verified for conduction- as well as convection-dominated aquifer systems [Wagner, 2010]. The BHE is assumed to be installed in a confined sandy aquifer. The flow field around a single BHE is hardly influenced by the BHE and therefore simulated in steady state, whereas the heat transport is simulated transiently. The entire 3D model has a size of $100 \text{ m} \times 90 \text{ m} \times 165 \text{ m}$ (length \times width \times depth; Fig. 1), which is large enough to minimize boundary effects for the period of a TRT (e.g. 40 h to 90 h). The dimensions of the fully discretized BHE are listed in Table 1.

Table 2 Detailed dimensions of the simulated borehole heat exchanger.

| | Value |
|--|-------|
| Radius of the borehole, r_b , (m) | 0.075 |
| Inner radius of the pipe, r_{pins} , (m) | 0.013 |
| Outer radius of the pipe, r_{pout} , (m) | 0.016 |
| Depth of the BHE, D_{BHE} , (m) | 100 |

The distance between borehole wall and the pipe wall is often unknown. To determine the uncertainty, several numerical simulations with varying pipe positions are analyzed. The model is discretized by 191,940 prism elements equally distributed in 35 horizontal layers. The finite element resolution is telescopic: It increases towards the BHE and reaches a maximum at the pipe wall (Fig. 1), where the steepest temperature gradients are expected. The distance between nodes varies between approximately 20 m at the model boundary and approximately 0.001 m at the pipe wall. The thickness of the horizontal layers ranges between 0.03 m and 39 m. The layer offset is smallest at the bottom of the BHE, where the highest vertical temperature gradients are expected.

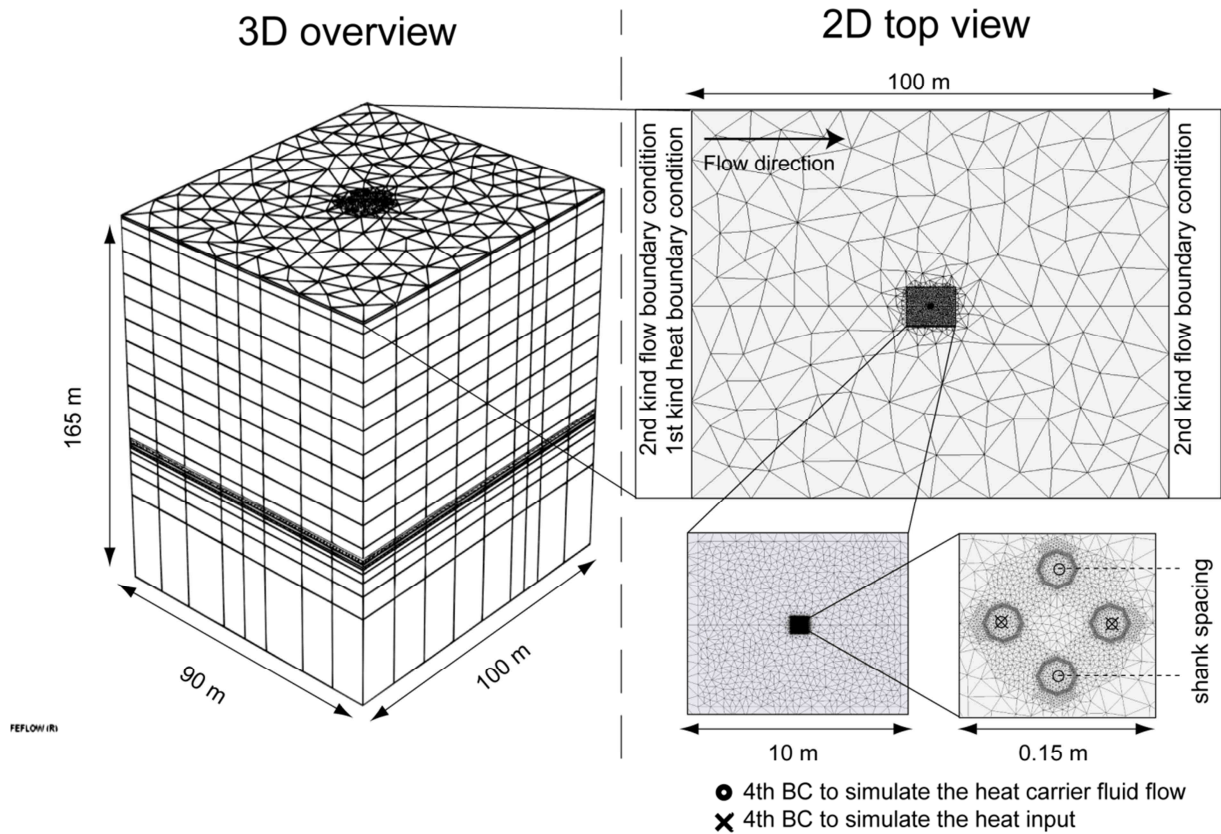


Fig. 1. Left: 3D overview of the model domain and discretization. Right: 2D top view of the model domain and the used boundary conditions (BC).

Thermal and hydraulic properties of the different compartments of the finite element mesh are given in Table 2. The selected values are based on reported real values, except for the thermal conductivity of the pipe material and the part of the mesh representing the heat carrier fluid. The heat transfer between the turbulently flowing heat carrier fluid and the pipe wall can be approximated by a one-dimensional series connection of thermal resistances, which gives the fitted thermal conductivity of the pipe material. Due to turbulent flow within the BHE, lateral heat transfer to/from the heat carrier fluid is very fast. To represent this in the model, thermal conductivity of the elements representing the heat carrier fluid is set very high [Diersch *et al.*, 2011a]. Clausen [2008] demonstrated that a thermal conductivity of $20 \text{ W m}^{-1} \text{ K}^{-1}$ is sufficient to represent this turbulent flow. Furthermore, a modification of the volumetric heat capacity for the part of the mesh representing the heat carrier fluid is recommended by Diersch *et al.* [2010]. The volumetric heat capacity of this part should therefore be very small (e.g. $1 \text{ J m}^{-3} \text{ K}^{-1}$).

Table 3 Hydraulic and thermal properties of different model compartments.

| Property | Hydraulic conductivity, K , (m s^{-1}) | Thermal conductivity of the porous media, λ_m , ($\text{W m}^{-1}\text{K}^{-1}$) | Volumetric heat capacity of the porous media, cp , ($\text{MJ m}^{-3}\text{K}^{-1}$) |
|---|---|--|--|
| Subsurface | 1.5×10^{-3} a) [Hähnlein et al., 2010] | 2.1 a) [Palmer et al., 1992] | 2.8 a) [Palmer et al., 1992] |
| Grouting material | 6×10^{-8} a) [Herrmann, 2008] | 0.8 a) [Herrmann, 2008] | 2.3 b) [Niekamp et al., 1984; Gauthier et al., 1997] |
| Pipe material | 1×10^{-19} c) [Pannike et al., 2006] | 0.39 b) [Signorelli et al., 2007] | 1.6 a) [Signorelli et al., 2007] |
| Heat carrier fluid (mesh) | 1×10^{-19} c) [Pannike et al., 2006] | 20.0 b) [Clausen, 2008] | 1×10^{-6} c) [Diersch et al., 2010] |
| Heat carrier fluid (discrete feature element) | - | 0.6 a) [Signorelli et al., 2007] | 4.2 a) [Signorelli et al., 2007] |

a) Reported realistic values; b) estimated based on real values; c) estimated to be able to run the model and avoid hydraulic interactions between the discrete feature elements and the part of the FE mesh representing the grouting material and the subsurface.

To simulate flow of the heat carrier fluid, elements of lower dimension, i.e. discrete feature elements [Diersch, 2005], are often connected with the 3D finite element mesh [Witte, 2001; Gehlin and Hellström, 2003; Diersch, 2006]. The shank spacing of the simulated BHE is equal to the distance between the connected discrete feature elements representing the center of each pipe (Fig. 1). Convective heat transport through the heat carrier fluid is simulated only within the discrete feature elements. Heat transport of the connected mesh representing the inner parts of the pipe is approximated by conduction only [Diersch, 2006]. The flow of the heat carrier fluid is defined by a fourth-type boundary condition (BC) [Diersch, 2006]. In FEFLOW the fourth-type BC describes a singular point source, which describes the injection or withdrawal rate of water/mass/energy into/from a single node or into/from a number of nodes. To simulate the energy transfer to the circulating BHE fluid, a fourth-type BC is used. Constant values are assigned to both fourth-type BC, therefore the BHE fluid is circulating with a constant flow rate and a constant energy injection rate to BHE fluid. This arrangement is very similar to a TRT device used in the field. Here, the flow rate of the heat carrier fluid and the energy transfer to the heat carrier fluid are held constant by the TRT device. Thus, the heat transfer rate, q , of the simulated BHE can be calculated based on the difference between inlet temperature, T_{in} , and outlet temperature, T_{out} , the volume flow rate of the heat carrier fluid, Q_f , and the volumetric heat capacity of the heat carrier fluid, c_{pf} :

$$q = \frac{c_{pf} Q_f (T_{in} - T_{out})}{L} \quad (2-6)$$

Based on Eq. (2-6) we calculated for each test case the average heat transfer rate, q , of the examined evaluation period of the BHE.

Groundwater flow, if applicable, is simulated by a second-type BC (Neumann) that assigns a constant flux to model boundary nodes [Diersch, 2006]. The temperature of the groundwater, which enters the model domain, is controlled by a first-type BC (Dirichlet), which assigns a certain temperature value to a selected node [Diersch, 2006].

The numerical model is applied to simulate a BHE, which injects energy of a known rate into the subsurface. The resulting synthetic time series of the temperature development of the heat carrier fluid represent the measured (artificial) data set of a TRT. In separate subsequent analyses, the influence of the geometry of the BHE as well as of naturally occurring non-uniform initial temperature distributions, e.g. vertical geothermal gradients and thermal dispersivities, on standard TRT-based interpretation are investigated. For this purpose, evaluation intervals of 50 h and a starting point of 40 h are selected, which is considered a period sufficient to obtain reliable results [Signorelli *et al.*, 2007]. Furthermore, to improve the comparability of the parameters obtained, equal starting points and the same duration of the evaluation interval are set for all experiments.

2.3 Results and Discussion

By way of example, Fig. 2 illustrates two numerically generated TRT data sets. Additionally, the linear regression based on Eq. (2-3) is shown.

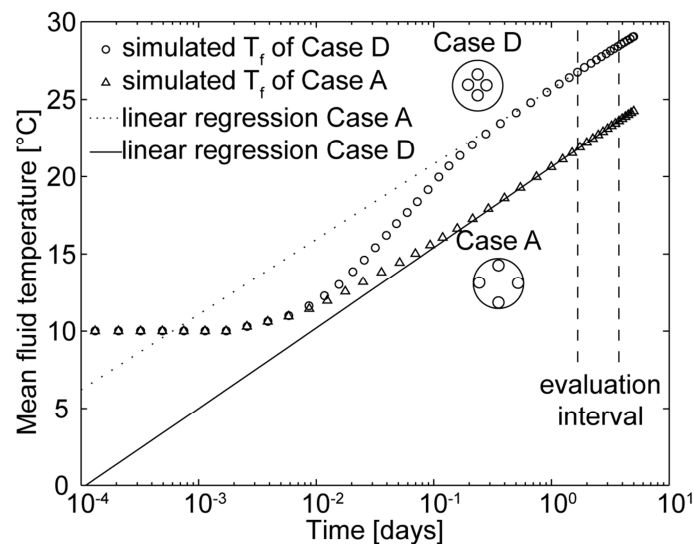


Fig. 2. Comparison of two numerically generated temperature time series of the mean fluid temperature T_f at variable shank spacings. Additionally, the result of the linear regression is presented.

2.3.1 Pipe Position

To exclusively analyze the effects of different shank spacings, no groundwater flow is considered and the initial temperature of the entire model is assumed to be uniform. These conditions comply with those commonly assumed for application of the line source equation. Different shank spacings are simulated by variants of the numerical model grid that is adjusted to the cross section geometry of the BHE. The setup of the models is illustrated in Fig. 3 showing different sections through the BHE, with decreasing distance of the symmetrically arranged tubes from Case A to D. The simulated shank spacings are 0.115 m, 0.092 m, 0.071 m, and 0.051 m in Cases A to D, respectively.

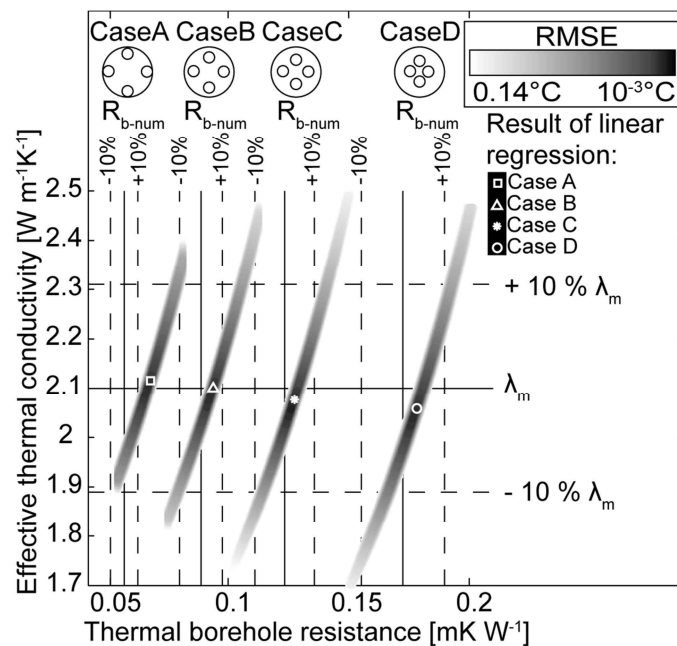


Fig. 3. Results of the two-variable parameter fitting method and the linear regression method for four different BHE shank spacings compared to the thermal conductivity of the porous media (λ_m) and the R_{b-num} value. The evaluated time interval lasts from 40 h to 90 h and only parameter pairs with an RMSE value smaller than 0.14°C are presented.

The results of the analysis are also presented in Fig. 3. For both parameter estimation techniques, the linear regression and the parameter fitting method, the effective thermal conductivities (λ_{eff}) identified sufficiently approximate the given thermal conductivity of the porous media (λ_m). According to the way the parameter values are derived, they are further distinguished by $\lambda_{eff-lin}$ and $\lambda_{eff-par}$. Table 3 shows that the best fitted values of λ_{eff} are identical for both methods. Fig. 3 also reveals that several parameter pairs of $\lambda_{eff-par}$ and R_{b-par} exist within the valid RMSE range ($<0.14^\circ\text{C}$). Valid pairs are positively correlated, indicating an ill-posed parameter estimation problem. If the acceptable error interval of estimated parameter

values is set to $\pm 10\%$ [Eugster, 2002], the detected pairs are mostly within these limits. With the given RMSE threshold, however, valid solutions spread beyond the 10% interval. Since the RMSE threshold is an arbitrary tolerance level that accounts for measurement uncertainty and noise, setting a stricter threshold may be problematic in practice, although this would improve identifiability of λ_{eff} and R_b in the ideal case.

The effective thermal conductivities obtained decrease with decreasing shank spacing and only in Case B is λ_{eff} similar to the “true” λ_m specified in the numerical model. Nevertheless, the differences between the $\lambda_{eff-lin}$ and λ_m values obtained are small and lie within an interval of -2% and +1%. This demonstrates that the derived λ_{eff} is an apparent and integral value integrating the properties of the grouting material and the aquifer. In general, the smaller the shank spacing is and the larger the distance to the ambient ground, the greater is the influence of the grouting material and, hence, the smaller is the derived effective thermal conductivity. The overestimation by 1% determined for Case A is due the deviation of the simulated system from the ideal shape assumed by the line source. In this particular case, interpretation by a cylinder source equation appears to be more suitable.

In contrast to its minor influence on the interpretation of thermal conductivity, the effect of changing shank spacing on the best fitted value of R_b is significant (Fig. 3). This agrees with the observations by Acuna *et al.* [2009], who studied the thermal borehole resistance of single U-pipe BHEs by a steady-state approach. We determined the same promoting effect of increasing shank spacing on R_b obtained by TRTs for a double U-pipe system. Again, the best results of the linear regression (R_{b-lin}) and the parameter fitting method (R_{b-par}) are in agreement. Borehole resistance values, R_{b-lin} and R_{b-par} , are comparable to those derived directly by Eq. (2-2) from the numerical model (R_{b-num}). For using this equation, the actual difference between borehole wall temperature (T_{bw}) and carrier fluid temperature (T_f) is determined by the simulated temperatures. T_f is extracted at the discrete feature element and T_{bw} is determined at eight equally scattered points on the borehole wall. To account for 3D effects, the weighted mean R_{b-num} value of four different layers (depth of 0 m, 15 m, 55 m, and 95 m) is calculated. The R_{b-num} value is considered to be most suitable for representing the actual heat transfer inside the BHE (Fig. 3).

The estimated values of R_{b-lin} and R_{b-par} agree with R_{b-num} within an interval of $\pm 10\%$, except for Case A. The reason of the higher discrepancy in this case is the direct contact between the

pipes and the ambient ground, which substantially disturbs the temperature distribution at the borehole wall. Thus, the assumption of a uniform T_{bw} is not fulfilled and the standard R_b calculation method is no longer suitable. Due to the unrealistic shape of Case A, the evaluation procedure is not adopted for this test case. However, Case A is included in this study as it offers insight into the theoretically minimum possible value of R_b . Although the fitting error is small for the Cases C-D, the values of R_{b-lin} and R_{b-par} systematically overestimate R_{b-num} . This is interpreted as an indication of 3D effects explicitly simulated by the numerical model, but not covered by the line source equation. Case B represents intermediate conditions, where these artifacts appear to be negligible and the actual parameters λ_m and R_{b-num} can be estimated perfectly. Therefore, the remainder of this study will focus on the shank spacing simulated by Case B.

Table 4 Results of linear regression and parameter fitting in comparison to originally simulated values (λ_m and R_{b-num}) for four different shank spacings. The evaluated time interval is between 40 h and 90 h.

| Pipe position | Case A | Case B | Case C | Case D |
|--|--------|--------|--------|--------|
| Shank spacing (m) | 0.115 | 0.092 | 0.071 | 0.051 |
| Heat transfer rate per unit length, calculated by Eq. (2-6), q (W m^{-1}) | 59 | 61 | 58 | 52 |
| Thermal borehole resistance of the numerical simulation, R_{b-num} (m K W^{-1}) | 0.057 | 0.089 | 0.124 | 0.173 |
| Thermal borehole resistance determined by linear regression, R_{b-lin} (m K W^{-1}) | 0.068 | 0.094 | 0.128 | 0.178 |
| Thermal borehole resistance determined by parameter estimation, R_{b-par} (m K W^{-1}) | 0.068 | 0.094 | 0.128 | 0.178 |
| Thermal conductivity of porous media, λ_m ($\text{W m}^{-1} \text{K}^{-1}$) | 2.10 | 2.10 | 2.10 | 2.10 |
| Effective thermal conductivity determined by linear regression, $\lambda_{eff-lin}$ ($\text{W m}^{-1} \text{K}^{-1}$) | 2.12 | 2.10 | 2.08 | 2.06 |
| Effective thermal conductivity determined by parameter estimation, $\lambda_{eff-par}$ ($\text{W m}^{-1} \text{K}^{-1}$) | 2.12 | 2.10 | 2.08 | 2.06 |

2.3.2 Non-uniform Initial Temperature Distribution

To analyze the effects of a non-uniform initial temperature distribution of the subsurface on the TRT result, the model with the fixed pipe configuration of Case B is modified. While constant thermal and hydraulic material properties are kept as before (see Table 2) and groundwater flow is neglected, initial temperature increases with depth according to a specific geothermal gradient. To simulate realistic geothermal gradients, the initial temperature field is calculated separately by steady-state simulations with different geothermal heat fluxes at the bottom boundary of the model and a constant temperature at the surface of the model (Table 4).

According to *Pollack et al.* [1993], a geothermal heat flux range between 0.05 and 0.11 W m^{-2} is considered to be realistic. Based on the given extreme values, temperature gradients of 23.7°C km^{-1} and 52.2°C km^{-1} are determined for the numerical model, which are below the unnaturally high gradient of 300°C km^{-1} analyzed in the special case by *Raymond et al.*

[2011b]. The initial ambient temperature values in the model are calculated based on the two temperature gradients selected and assuming a fixed temperature value of 10°C at a depth of 50 m. In this way, the simulations of the two geothermal gradients remain comparable.

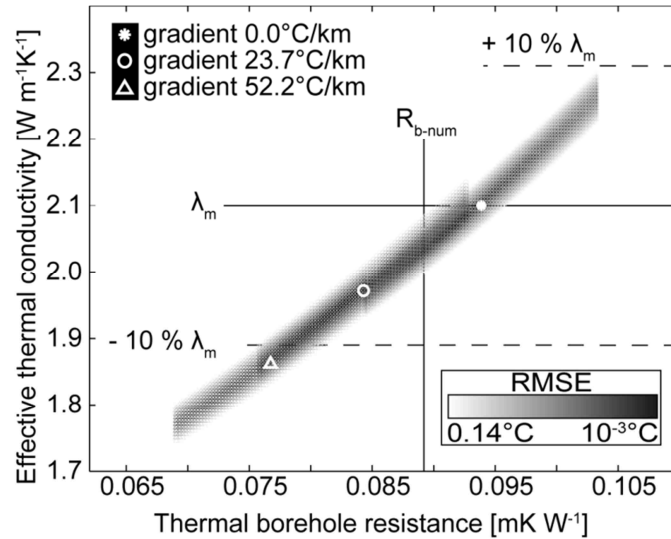


Fig. 4. Results of the two-variable parameter fitting method and the linear regression method for three different initial temperature distributions compared to the thermal conductivity of the porous media and the R_{b-num} values. The latter are given in Table 4. The evaluated time interval lasts from 40 h to 90 h and only parameter pairs with an RMSE value smaller than 0.14°C are presented here.

Both line source evaluation approaches yield comparable results (relative difference less than 1%). However, the best fitted λ_{eff} values are smaller than the input values of the numerical simulation selected (Fig. 4). For high geothermal gradients (52.2°C km⁻¹), the acceptable error exceeds $\pm 10\%$ (Fig. 4) [Eugster, 2002]. Fig. 4 illustrates again that a wide range of valid parameter pairs of $\lambda_{eff-par}$ and R_{b-par} exists and acceptable parameter values are correlated positively. This validity range is shifted along the direction of correlation by increasing the value of the geothermal gradient. This outcome demonstrates that a depth-dependent initial temperature field prevents reliable line source based TRT evaluation. The geothermal gradient influences the horizontal temperature gradient towards the BHE. The amplified depth-dependent heat propagation which cannot be considered by the line source theory leads to an apparently higher thermal conductivity than the real one.

As shown above, the borehole resistance R_b reflects the heat transport inside the BHE and, thus, depends on geometry and physical properties of the BHE itself. Hence, it can be expected that R_b is quasi-independent of the subsurface properties and that the TRT parameter values obtained are constant and comparable to those computed for the negligible geothermal

gradient (0.089 m K W^{-1} , Table 3). This is true for the value of R_{b-num} which is determined directly from the numerical model (Table 4). In contrast to this, R_{b-lin} and R_{b-par} values obtained from the TRT seem to be influenced significantly by the geothermal gradient (Table 4).

For the geothermal gradients evaluated, the resulting R_{b-lin} and R_{b-par} values vary in the range between 0.077 m K W^{-1} and 0.094 m K W^{-1} . The line source based TRT evaluation with a constant initial temperature yields the slightly overestimated value of $R_b = 0.094 \text{ m K W}^{-1}$ (see Fig. 3). At an enhanced geothermal gradient, the estimated value of R_b decreases. The relative error of the line source evaluation for the high geothermal gradients selected even exceeds the acceptable error range of -10% (Fig. 4) [Eugster, 2002]. This relationship between estimated borehole resistance and geothermal gradient apparently is artificial and does not represent the real heat transfer inside the BHE. This positive correlation illustrated in Fig. 4 might be caused by the temperature variations inside and outside the BHE along the total length, leading to depth-dependent R_b values.

Table 5 Results of the parameter fitting method, linear regression, and the FEFLOW input values (λ_m and R_{b-num}) for three different initial temperature distributions which can be described by a constant geothermal gradient. All simulations are based on a BHE with the geometry of Case B. The evaluated time interval is between 40 h and 90 h.

| | | | |
|--|-------|-------|-------|
| Heat flux (W m^{-2}): | 0.00 | 0.05 | 0.11 |
| Resulting geothermal gradient ($^{\circ}\text{C km}^{-1}$): | 0.0 | 23.7 | 52.2 |
| Heat transfer rate per unit length, calculated by Eq. (2-6), q (W m^{-1}) | 61 | 58 | 55 |
| Thermal borehole resistance of the numerical simulation, R_{b-num} (m K W^{-1}) | 0.089 | 0.089 | 0.089 |
| Thermal borehole resistance determined by linear regression, R_{b-lin} (m K W^{-1}) | 0.094 | 0.084 | 0.077 |
| Thermal borehole resistance determined by parameter estimation, R_{b-par} (m K W^{-1}) | 0.094 | 0.083 | 0.077 |
| Thermal conductivity of porous media, λ_m ($\text{W m}^{-1} \text{K}^{-1}$) | 2.10 | 2.10 | 2.10 |
| Effective thermal conductivity determined by linear regression, $\lambda_{eff-lin}$ ($\text{W m}^{-1} \text{K}^{-1}$) | 2.10 | 1.97 | 1.86 |
| Effective thermal conductivity determined by parameter estimation, $\lambda_{eff-par}$ ($\text{W m}^{-1} \text{K}^{-1}$) | 2.10 | 1.96 | 1.86 |

2.3.3 Thermal Dispersion

A third aspect analyzed is the effect of longitudinal and transverse thermal dispersion on TRT interpretation. Again, artificial TRT data sets are generated using the numerical model that simulates a BHE with the pipe configuration of Case B. A uniform horizontal Darcy velocity of 0.1 m day^{-1} is assumed for the aquifer. This threshold is recommended by Signorelli et al. [Signorelli et al., 2007] to be the upper limit for TRT evaluations based on the line source theory. The thermal dispersivities are varied and a constant relationship $\alpha_t = 0.1 \times \alpha_l$ is assumed [Molina-Giraldo et al., 2011a]. Molina-Giraldo et al. [2011a] demonstrate the variability of the reported α_l and α_t values which are mainly influenced by the relationship

applied for the description of thermal dispersion. Hence, a wide range of α_l values between 0 and 2 m is analyzed here in order to represent possible values for a field scale of 10 m [Molina-Giraldo et al., 2011a]. The results are depicted in Fig. 5.

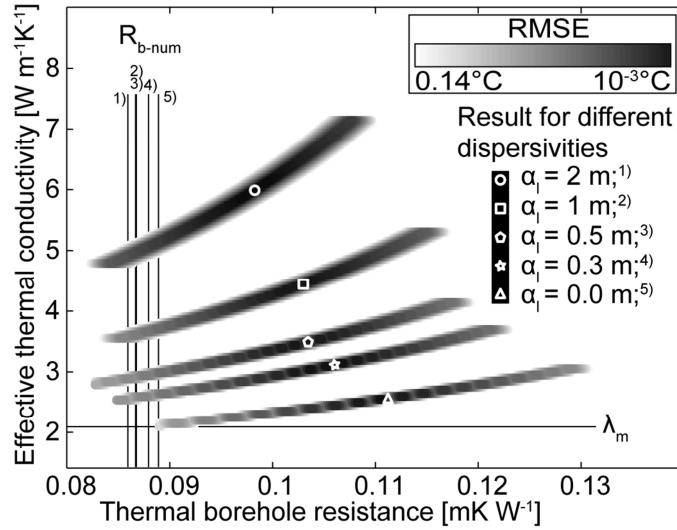


Fig. 5. Result of the two-variable parameter fitting method and the linear regression method for five different thermal dispersivities (constant Darcy velocity of 0.1 m day^{-1}) compared to the thermal conductivity of the aquifer and the R_{b-num} values. The latter are given in Table 5. The evaluated time interval lasts from 40 h to 90 h and only parameter pairs with an RMSE value smaller than 0.14°C are presented. Superscript numbers specify the thermal dispersivities belonging to a corresponding R_{b-num} value.

Both parameter estimation techniques yield similar $\lambda_{eff-lin}$ and $\lambda_{eff-par}$ values with a difference of less than 1% (Table 5). Both evaluation approaches are therefore considered to be equally suitable for the TRT-based λ_{eff} determination in these cases. Again, the parameter estimation with an RMSE tolerance of 0.14°C yields a correlated group of $\lambda_{eff-par}$, R_{b-par} pairs. The λ_{eff} values obtained are significantly higher than the original value of λ_m in the numerical model. They are higher than λ_m by a factor between 20% ($\alpha_l = 0$) and 190% ($\alpha_l = 2$), which clearly exceeds the acceptable 10% error assumed for a TRT [Eugster, 2002]. The effect of increasing thermal dispersivity on the valid λ_{eff} value range is explained by the relationship between α_l and α_t and the effective thermal dispersion coefficient which is one key parameter of the heat transport equation in porous media [Domenico and Schwartz, 1998]. Heat transport, including dispersion, results in an increase of λ_{eff} (Table 5). Thus, TRT evaluation of convection-dominated conditions should not only consider the effect of convection, but also the impact of dispersion.

As in all previous results, the R_{b-lin} and R_{b-par} values obtained are identical. A slightly negative correlation between thermal dispersivity and determined borehole resistance is found. The calculated R_{b-num} values decrease by up to 3% compared to the conduction-dominated value of 0.089 m K W^{-1} (Table 3). The decrease by 3% might be caused by dispersive effects into the BHE, which decrease the thermal resistance between the borehole wall and the heat carrier fluid. This is also reflected by the line source based best estimates of R_b . However, these values are significantly higher than those in the model. They also span a broad validity range depending on the given dispersivity. By neglecting the effects of thermal dispersion, the best line source based fit yields an overestimation of 14% compared to R_{b-num} . This discrepancy increases with the degree of dispersion up to 25% for $\alpha_l = 2 \text{ m}$. Under these conditions, the standard line source equation obviously is not applicable. Consequently, estimated parameter values are not reliable.

Table 6 Results of the two-variable parameter fitting method, the linear regression method, and the FEFLOW input values (λ_m and R_{b-num}) for six different thermal dispersivity values. The evaluated time interval is 40 h - 90 h.

| Longitudinal dispersivity, α_l (m) | 2 | 1 | 0.5 | 0.3 | 0 |
|--|-------|-------|-------|-------|-------|
| Heat transfer rate per unit length, calculated by Eq. (2-6), q (W m^{-1}) | 61 | 61 | 61 | 61 | 61 |
| Thermal borehole resistance of the numerical simulation, R_{b-num} (m K W^{-1}) | 0.086 | 0.087 | 0.087 | 0.088 | 0.089 |
| Thermal borehole resistance determined by linear regression, R_{b-lin} (m K W^{-1}) | 0.098 | 0.103 | 0.103 | 0.106 | 0.111 |
| Thermal borehole resistance determined by parameter estimation, R_{b-par} (m K W^{-1}) | 0.098 | 0.103 | 0.103 | 0.106 | 0.111 |
| Thermal conductivity of porous media, λ_m ($\text{W m}^{-1} \text{K}^{-1}$) | 2.10 | 2.10 | 2.10 | 2.10 | 2.10 |
| Effective thermal conductivity determined by linear regression, $\lambda_{eff-lin}$ ($\text{W m}^{-1} \text{K}^{-1}$) | 5.99 | 4.44 | 3.48 | 3.11 | 2.56 |
| Effective thermal conductivity determined by parameter estimation, $\lambda_{eff-par}$ ($\text{W m}^{-1} \text{K}^{-1}$) | 6.00 | 4.45 | 3.49 | 3.13 | 2.58 |

2.4 Conclusions

A finite element model of a double U-pipe BHE was developed to generate artificial TRT data sets. Based on these data sets, the influence of selected natural subsurface conditions, such as depth-dependent temperature variation and thermal dispersion, was investigated. Furthermore, the effect of the shank spacing within the BHE on TRT interpretation was assessed by simultaneous λ_{eff} and R_b estimation. From the results of this study, the following conclusions can be drawn:

- The TRT parameters (R_{b-lin} , R_{b-par} and $\lambda_{eff-lin}$, $\lambda_{eff-par}$) obtained for different shank geometries represent the real parameters of the subsurface (λ_m) and the BHE (R_{b-num}) with sufficient accuracy. The shank spacing analyzed varied between 0.051 and 0.115 m, the resultant error of the estimated λ_{eff} values was less than 2%. However, the borehole resistance is strongly dependent on the shank spacing. With increasing shank spacing, the borehole resistance decreases as the influence of the grout material is reduced. At the same time, the error of line source based R_b estimation increases.

The BHE more and more disagrees with the ideal line-shaped heat source. In practice, a TRT evaluation based on the cylinder source equation, which was analyzed by *Sass and Lehr* [2011], might improve the result for large shank spacing, such as in Case A.

- A typical geothermal gradient (0°C per 100 m to 5.2°C per 100 m) results in an underestimation of λ_{eff} and R_b by the standard line source based approach. The estimation error may exceed 10% for a gradient of 5.2°C per 100 m. This has to be accounted for when TRTs are conducted in areas with a relatively high geothermal gradient. Furthermore, the effects observed may also be induced by artificial temperature variations in the subsurface, for instance, by surrounding geothermal systems, local heat sources, such as sewage systems or other underground facilities, especially in urban areas.
- Apart from convection, also thermal dispersion was found to influence the TRT and its interpretation. Numerically generated TRTs influenced by a constant Darcy velocity (0.1 m day⁻¹) and various dispersivities (α_l between 0 and 2 m) result in a deviation from the "true" values of the model from 0.5 W m⁻¹ K⁻¹ to 3.9 W m⁻¹ K⁻¹ for λ_{eff} and from 0.012 m K W⁻¹ to 0.022 m K W⁻¹ for R_b , respectively. Hence, further studies of convection-dominated TRTs should also consider the effects of thermal dispersion. In practice, we recommend to consider not only groundwater flow, but also the effects of thermal dispersion for convection-influenced TRTs in highly heterogeneous aquifers.

This numerical study clearly showed the limits of the standard TRT evaluation when the test performed is influenced by extreme shank spacing, high geothermal gradients or significant dispersivity values. To overcome this restriction, improved concepts are needed to consider and quantify the analyzed effects, especially thermal dispersivity. TRT interpretation also has to account for feasible parameter ranges instead of best fits within a small function fitting tolerance only. The results of the numerical study here showed that typical case-specific valid ranges of positively correlated borehole resistance and effective thermal conductivity values exist.

3 Analytical approach to groundwater-influenced thermal response tests of grouted borehole heat exchangers

Reproduced from: Wagner, V., Blum, P., Kübert, M., Bayer, P. (2013), Analytical approach to groundwater-influenced thermal response tests of grouted borehole heat exchangers, Geothermics, 46(0), 22-31, doi: 10.1016/j.geothermics.2012.10.005. The final publication is available at sciencedirect.com.

Abstract: For ground-source heat pump (GSHP) systems, the thermal response test (TRT) is commonly used to determine the heat transport parameters of the subsurface. The main limitation of this approach is the assumption of pure conductive heat transport, which might result in significant deviations. Based on the moving line source theory, a parameter estimation approach is introduced, which is sensitive to conduction and advection. This approach is calibrated and successfully tested against three different test cases. The presented analytical approach therefore expands the field of application of the TRT to advection-influenced conditions beyond a Darcy velocity of 0.1 m day^{-1} .

3.1 Introduction

The heat stored in the shallow subsurface is of growing interest to geothermal energy use. In the upper hundreds of meters of the earth's crust, the temperature usually does not reach much more than 20°C [e.g., *Taniguchi and Uemura*, 2005; *Zhu et al.*, 2011]. Thus, the energy is only useful for space heating and air conditioning systems and is ideally extracted from wells or boreholes (in general to a depth of around 150 m [e.g., *Hecht-Méndez et al.*, 2010]) combined with heat pumps. Alternatively, the ground may be used as storage medium for waste heat or for cooling purposes [*Sanner et al.*, 2003]. The most common variants of geothermal systems are ground-source heat pumps (GSHPs), where vertical boreholes act as borehole heat exchangers (BHEs) [*Rybach and Eugster*, 2010]. A heat carrier fluid is circulated in closed tubes installed in the boreholes. In the heating mode, the injection temperature is slightly lower than the temperature of the ground. Circulation in the subsurface warms up the fluid and by operating the heat pump, the collected energy is extracted above, thus cooling the ambient ground. Temperature anomalies develop, and the radial temperature gradient forces the heat flow towards the BHE.

Since the geological, geophysical, and hydrogeological conditions that control the heat transfer processes and extraction efficiency vary, field investigation campaigns are suggested for larger-scale systems to ensure appropriate planning of shallow geothermal installation. The thermal response test (TRT), which is conducted in BHEs before heat mining begins is an established technique [*Morgensen*, 1983; *Gehlin*, 2002; *Sanner et al.*, 2005; *Signorelli et al.*, 2007; *Beier et al.*, 2011; *Raymond et al.*, 2011a; *Raymond et al.*, 2011c]. By monitoring the effect of short-term heating (or cooling), the thermal properties of the ground and the heat transfer efficiency between ground and BHE are interpreted.

In standard experiments, a heated or cooled fluid is injected and the temperature development, i.e. the response of the ground, is monitored at the BHE outlet. The slower the temperatures of the heat carrier fluid increase, the more heat is lost in the ground and, thus, the higher is the interpreted in-situ effective thermal conductivity. The temperature time series are commonly evaluated based on the Kelvin line source theory that assumes an infinite, homogeneous and isotropic medium with a constant heat source [*Carslaw and Jaeger*, 1959]. This evaluation provides the effective thermal conductivity (λ_{eff}) as well as the thermal borehole resistance (R_b), which is a measure of the heat transfer performance in the borehole. Both parameters are used for a case-specific planning and efficient operation of the GSHP-system.

Standard TRT interpretation exhibits several shortcomings. It assumes a homogenous subsurface, no axial heat transport, uniform initial temperature distribution, and it approximates the BHE shape as an infinite line. *Bandos et al.* [2009] presented an analytical solution to overcome the limitations caused by the assumption of an infinite line shape. Another significant shortcoming is that only conductive heat transport is considered [e.g., *Signorelli et al.*, 2007]. However, shallow geothermal systems are frequently installed in water-saturated underground. In aquifers, advective heat transfer due to groundwater flow can be significant [e.g., *Witte*, 2001]. Accordingly, the effective thermal conductivity (λ_{eff}) obtained based on the Kelvin line source theory is an apparent parameter, which increases with Darcy velocity. Several studies have demonstrated the significant influence of groundwater flow [*Witte and Gelder*, 2006] and ambient air temperature variations [*Bandos et al.*, 2011] on TRT results. *Witte* [2001] established a advection-dominated aquifer by performing a TRT, while groundwater was being extracted from a well 5 m away from the BHE. A comparison to the results of an undisturbed TRT showed an increase in the λ_{eff} value by a factor of 1.38. This relationship was also investigated by *Bozdog et al.* [2008], who performed four different TRTs in one BHE and correlated the obtained λ_{eff} and R_b values with the observed different hydraulic gradients. Their field measurements clearly indicated the influence of groundwater table fluctuations, which govern groundwater flow velocities, on the TRT results. The influence of groundwater flow is also examined by several theoretical studies. For instance, *Chiasson et al.* [2000] numerically simulated TRTs to analyze the role of groundwater flow velocity and different evaluation periods with respect to the value of λ_{eff} that would be obtained by the line-source approach. They demonstrated that the resulting thermal conductivity value is an effective one and does not represent the thermal conductivity of the subsurface. *Signorelli et al.* [2007] comprehensively analyzed those effects and confirmed the findings by *Witte et al.* [2001] that λ_{eff} increases continuously with evaluation time. In essence, the line source-based TRT evaluation of advection-dominated systems results in ambiguous λ_{eff} values. *Signorelli et al.* [2007] conclude that BHE dimensioning based on λ_{eff} in advection-dominated systems is rather problematic, because of the increasing instability of the resulting values.

A number of remedies have been suggested to reliably evaluate TRTs influenced by groundwater flow. One possibility to detect the influence of groundwater flow is a stepwise TRT evaluation based on the Kelvin line source theory [e.g., *Sanner et al.*, 2005]. *Witte*

[2001] interpreted an increasing λ_{eff} value with increasing evaluation time step size as an indicator for groundwater flow. Another possibility is an enhanced TRT [Wagner and Rohner, 2008], where depth-depending temperature series during and/or after the heating period are evaluated [Fujii *et al.*, 2009]. Wagner and Rohner [2008] showed how specific layers with groundwater flow (enhanced λ_{eff} values) can be estimated. However, these concepts provide no information about the actual Darcy velocity. To overcome this, parameter estimation approaches based on numerical simulations [Raymond *et al.*, 2011b] or alternative analytical equations [Katsura *et al.*, 2006] were suggested. Raymond *et al.* [2011b] numerically quantified that the TRT examined at a field site was influenced by a groundwater flow velocity smaller than 10^{-5} m s⁻¹. Based on several simulation results with a groundwater flux between 10^{-6} and 10^{-8} m s⁻¹ and λ_m values between 2.35 and 2.65 W m⁻¹ K⁻¹, the measured temperature values could be reproduced [Raymond *et al.*, 2011b]. In a different context, Katsura *et al.* [2006] analyzed the heat response of a thermal probe in a sand-filled cylinder influenced by different water flow velocities. By calibration of the moving line source equation [Carslaw and Jaeger, 1959] to the measured thermal response it was possible to derive the groundwater velocity with a relative error less than 20% [Katsura *et al.*, 2006].

Previous studies have demonstrated the ambiguous character of the parameters determined by line source-based TRT evaluation, especially if groundwater flow influences the system. The objective of this study is therefore to develop an analytical approach to groundwater-influenced TRTs, which provides parameters more suitable for a detailed simulation of conductive and advective heat transport in the subsurface. For this purpose, an approach in line with the one by Katsura *et al.* [2006] is developed. Furthermore, we introduce a correction term to consider the effects caused by the lower hydraulic conductivity of a grouted BHE on the apparent (i.e., estimated) Darcy velocity in the vicinity of the BHE. This correction term is calibrated by artificially generated high-resolution TRT temperature time series and embedded in a parameter estimation framework. Finally, the applicability of this concept for the simultaneous determination of ground thermal conductivity, λ_m , and Darcy velocity, v , is discussed based on a set of scenarios adopted from related studies.

3.1.1 Nomenclature

The nomenclature used in chapter 3 is compiled in Table 7.

Table 7 Nomenclature of chapter 3.

| | |
|-----------------------------|---|
| C | correction factor (-) |
| c_p | volumetric heat capacity ($\text{MJ m}^{-3} \text{K}^{-1}$) |
| D | thermal dispersion coefficient ($\text{m}^2 \text{s}^{-1}$) |
| d_s | shank spacing (m) |
| Ei | exponential integral |
| k | hydraulic conductivity (m s^{-1}) |
| Pe | Péclet number (-) |
| q | heat transfer rate per unit length (W m^{-1}) |
| r | radius (m) |
| r_{pin} | inner pipe radius (m) |
| r_{pout} | outer pipe radius (m) |
| R_b | thermal borehole resistance (m K W^{-1}) |
| T | temperature ($^{\circ}\text{C}$) |
| t | time (s) |
| t_c | time criterion (s) |
| u | integration variable |
| v | Darcy velocity (m day^{-1}) |
| v_{th} | heat transport velocity (m day^{-1}) |
| x, y | Cartesian coordinates (m) |
| Greek symbols | |
| α | dispersivity (m) |
| λ | thermal conductivity ($\text{W m}^{-1} \text{K}^{-1}$) |
| κ | thermal diffusivity ($\text{m}^2 \text{s}^{-1}$) |
| γ | Euler constant (-) |
| Subscripts and superscripts | |
| f | heat carrier fluid |
| bw | borehole wall |
| sub | property of the subsurface |
| g | property of the grouting material |
| eff | obtained effective property value (without correction) |
| m | property of the porous medium |
| w | property of the groundwater |
| 0 | initial or undisturbed value |
| l | longitudinal |
| t | transversal |
| * | value corrected by C |

3.2 TRT Models

3.2.1 Conductive Line Source

The most widely used procedure to evaluate a TRT is based on the Kelvin line source theory. This approach approximates the BHE as an infinite line source in a homogeneous, isotropic and infinite medium, which injects or extracts a constant amount of energy (q) by conductive heat transport only. The temporal and spatial temperature changes around the line source can

be calculated as follows [e.g. *Carslaw and Jaeger*, 1959; *Gehlin*, 2002; *Signorelli et al.*, 2007]:

$$T_{sub}(r, t) - T_0 = \frac{q}{4\pi\lambda_{eff}} \int_{\frac{r^2}{4\kappa t}}^{\infty} \frac{e^{-u}}{u} du = \frac{q}{4\pi\lambda_{eff}} E_i \left[\frac{r^2}{4\kappa t} \right] \approx \frac{q}{4\pi\lambda_{eff}} \left[\ln \left(\frac{4\kappa t}{r^2} \right) - \gamma \right] \quad (3-1)$$

The maximum error of the logarithmic approximation of the exponential integral is less than 10%, if the time criterion $t \geq t_c \geq 5 r_{bw}^2 \kappa^{-1}$ is fulfilled [*Hellström*, 1991]. This error range assumes that substantial disturbances on the recorded temperatures are absent and the test is properly executed. To be able to calculate the mean fluid temperature, the thermal resistance R_b between the borehole wall and the circulating heat carrier fluid has to be considered. This leads to the following extension of Eq. (3-1):

$$T_f - T_{bw} = q \cdot R_b \quad (3-2)$$

$$\begin{aligned} T_f(t) = T_{bw}(t) + qR_b &= \frac{q}{4\pi\lambda_{eff}} E_i \left[\frac{r_{bw}^2}{4\kappa t} \right] + T_0 + R_b q \\ &\approx \frac{q}{4\pi\lambda_{eff}} \ln(t) + q \left[R_b + \frac{1}{4\pi\lambda_{eff}} \left(\ln \left(\frac{4\kappa t}{r_{bw}^2} \right) - \gamma \right) \right] + T_0 \end{aligned} \quad (3-3)$$

To determine the effective thermal properties (λ_{eff} and R_b), two similar approaches are possible. The recorded TRT data are either fitted by a two-variable parameter estimation technique [*Roth et al.*, 2004] or by a linear regression based on the logarithmic approximation of Eq. (3-3) [*Gehlin*, 2002; *Signorelli et al.*, 2007]. A TRT evaluation based on the Kelvin line source theory does not consider the effects of groundwater flow and simplifies all possible heat transfer processes of the subsurface as purely conductive transport with an effective thermal conductivity, λ_{eff} . Therefore, it is not possible to determine the relevant heat transport parameters for advection-dominated conditions using Eq. (3-3).

3.2.2 Moving Line Source

To determine adequate parameters for the simultaneous heat transport by advection and conduction, another analytical equation is necessary. *Carslaw and Jaeger* [1959] derived a suitable analytical equation, which simulates a constant line source of infinite length in a homogeneous and infinite medium and in its extended version additionally accounts for

advection and hydrodynamic dispersion [Metzger *et al.*, 2004; Molina-Giraldo *et al.*, 2011a].

The temperature difference caused by the line source is calculated by:

$$T_{sub}(x, y, t) - T_0 = \frac{q}{4\pi c_{pm} \sqrt{D_l D_t}} \exp\left[\frac{v_{th} x}{2D_l}\right] \int_0^{\frac{v_{th}^2 t}{4D_l}} \exp\left[-\left(\frac{x^2}{D_l} + \frac{y^2}{D_t}\right) \frac{v_{th}^2}{16D_l u} - u\right] \frac{du}{u} \quad (3-4)$$

Equivalent to the approach by Sutton *et al.* [2002], the fluid temperature of a BHE can be accessed by adding a thermal borehole resistance term. Eq. (3-4) is extended as follows if the Cartesian coordinates fulfill the condition $x^2 + y^2 = r_{bw}^2$:

$$T_f(x, y, t) = \frac{q}{4\pi c_{pm} \sqrt{D_l D_t}} \exp\left[\frac{v_{th} x}{2D_l}\right] \int_0^{\frac{v_{th}^2 t}{4D_l}} \exp\left[-\left(\frac{x^2}{D_l} + \frac{y^2}{D_t}\right) \frac{v_{th}^2}{16D_l u} - u\right] \frac{du}{u} + T_0 + R_b q \quad (3-5)$$

Eqs. (3-4) and (3-5) account for an effective heat transport velocity (v_{th}) and an effective thermal dispersion coefficient (D_l and D_t). These parameters are determined as follows:

$$v_{th} = v_{eff} \frac{c_{pw}}{c_{pm}} \quad (3-6)$$

$$D_l = \frac{\lambda_{m-eff}}{c_{pm}} + \alpha_l v_{th} \quad (3-7)$$

$$D_t = \frac{\lambda_{m-eff}}{c_{pm}} + \alpha_t v_{th} \quad (3-8)$$

In contrast to λ_{eff} , $\lambda_{m,eff}$ in fact is an obtained value, but only represents the properties of the porous medium and contains no advective portion.

Eq. (3-5) additionally accounts for advective heat transport, but it still carries some simplifying assumptions. Similar to Eq. (3-2) for standard TRT interpretation, the effects of thermal disturbance, such as from vertical heat flow along the natural vertical geothermal gradient, are neglected. However, Wagner *et al.* [2012b] demonstrated that this only introduces a minor error in standard TRT interpretation. Disturbances from buoyancy effect

are also ignored. *Hecht-Méndez et al.* [2010] demonstrated this as a valid assumption for the simulation of common GSHP systems. Furthermore, *Gehlin et al.* [2003] reported that the thermosiphon effect, which is caused by a vertical groundwater flow inside the borehole, can be neglected for properly grouted BHE. It is important to emphasize that our TRT interpretation only provides subsurface properties averaged over the total length of the BHE. Both Eq. (3-3) and Eq. (3-5) yield integral parameter sets to characterize the subsurface, and are not suited for resolving heterogeneous properties of the ground. Eq. (3-5) also assumes advective heat transport in a porous media, and the application to fractured rocks is restricted. For the latter, the evaluation by *Gehlin and Hellström* [2003] is therefore recommended.

We suggest a parameter estimation approach that calibrates Eq. (3-5) to temperature time series of a TRT, which uses the Nelder-Mead algorithm as explained for example by *Lagarias et al.* [1998]. This minimizes the root mean squared error (RMSE) between observed (in this study: the numerically generated dataset) and calculated data (Eq. (3-5)) by varying a defined set of functional parameters. The RMSE determines the accuracy of the fitting, and thus can be utilized to compare different calibration results. In general, when calibrating models to measurements in natural systems, the complex coupled processes involved often make it impossible that one unique set of valid model parameter values can be determined. For a given tolerance on the RMSE of the calibrated model it is thus suggested to estimate possible parameter ranges and, if they exist, to also extract correlations among different parameters [*Maier et al.*, 2009]. This insight is in particular valuable for ill-posed problems like the TRT evaluation based on Eq. (3-5), where solutions to the inverse problem are non-unique. For the estimation of $\lambda_{m,eff}$ and v_{eff} this is considered by setting a threshold on the RMSE equivalent to the expected measurement error of 0.1°C, which *Witte et al.* [2002] mentioned as the accuracy of a temperature sensor. In reality, the measurement error might be different, because of the applied type of sensor, the kind of combination of temperature sensors and/or the temperature dependency of the sensor itself. To inspect whether acceptable locally optimal or close-optimal solutions to the error function exist, multiple randomly initialized Nelder-Mead-based minimization runs (here: 15) are applied. In this way, we gather sufficient sets of $\lambda_{m,eff}$ and v_{eff} pairs.

Eq. (3-5) is not suitable for TRT interpretation with a real BHE, since it does not explain the complex heat transfer inside the BHE. This was not relevant in the study by *Katsura et al.* [2006], who suggested the moving line source equation to evaluate the temperature difference

in a sand- filled cylinder caused by a needle-shaped heating device in a laboratory experiment. In our approach, similar to that by *Katsura et al.* [2006], the effects of mechanical thermal dispersion are neglected in Eq. (3-5) in a first step. This is considered an acceptable simplification that reduces the number of unknown parameters. More details on potential errors introduced by this simplification are comprehensively discussed by *Molina-Giraldo et al.* [2011a] and *Wagner et al.* [2012b].

The second step computes a single representative borehole wall temperature, which is necessary for application of Eq. (3-5). The representative borehole wall temperature here is an integral value of the entire BHE. In contrast to a conduction-dominated system, the heat propagation in an advection-dominated system is not radially symmetric. Consequently, temperatures at the borehole wall are not constant. To account for the asymmetric heat distribution around a BHE influenced by groundwater flow, we calculate a mean borehole wall temperature measured at eight positions. These positions are predefined on the BHE cross section and depicted in Fig. 6.

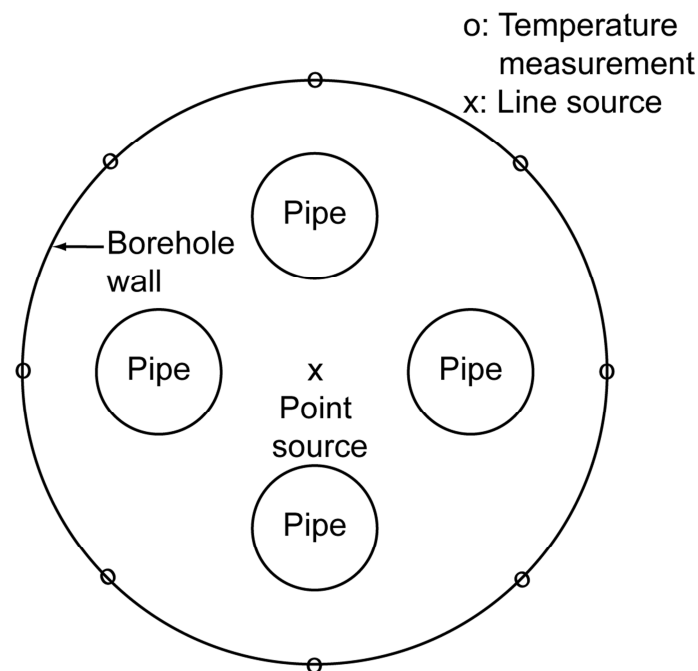


Fig. 6. Cross section of a BHE with central evaluation position of the line source equation and the temperature measurement locations at the borehole wall for calculation of mean temperature in the case of groundwater flow.

The amount of energy transported by conduction and advection can be compared by the Péclet number Pe [Domenico and Palciauskas, 1973]. Barcenilla *et al.* [2005] suggested the following formulation to calculate the Péclet number, Pe , of a BHE:

$$Pe = \frac{vr_{bw}}{\kappa} = \frac{vr_{bw}c_{pm}}{\lambda_m} \quad (3-9)$$

3.2.3 Two-dimensional Finite Element Model for TRT Simulation

The applicability of the moving line source equation (Eq. 3-5) to evaluate the thermal response of a BHE is tested by comparing analytical to realistic numerical simulation. For this, a two-dimensional (2D) high-resolution finite element model in FEFLOW 5.4 [Diersch, 2006] is developed. The latter is developed by comparison to a more comprehensive 3D finite element model presented by Wagner *et al.* [2012b]. It is able to predict the complex heat transfer between the several parts of the BHE (heat carrier fluid, pipe wall and grout material), the porous medium, and the moving groundwater. In contrast, Eq. (3-5) considers the entire system as a line-shaped heat source in a homogeneous medium. Errors caused by this simplification can be evaluated by comparison between the numerical simulation and the results of Eq. (3-5). The numerical model specifications of simulated BHE geometry are listed in Table 8 and shown in Fig. 7, and the assumed material properties are provided in Table 9.

Table 8 Geometric settings of simulated borehole heat exchanger (BHE) in the numerical model (Fig. 7).

| | Value |
|--|-------|
| Radius of the borehole, r_{bw} , (m) | 0.075 |
| Inner radius of the pipe, r_{pin} , (m) | 0.013 |
| Outer radius of the pipe, r_{pout} , (m) | 0.016 |
| Shank spacing, d_s , (m) | 0.093 |

Table 9 Hydraulic and thermal properties of different numerical model compartments.

| Property | Hydraulic conductivity, k , (m s^{-1}) | Thermal conductivity of porous medium, λ_m , ($\text{W m}^{-1} \text{K}^{-1}$) | Volumetric heat capacity of porous medium, c_{pm} , ($\text{MJ m}^{-3} \text{K}^{-1}$) |
|------------------------------|--|--|--|
| Subsurface | 1.5×10^{-3} ^{a)} [Hähnlein et al., 2010] | 2.1 ^{a)} [Palmer et al., 1992] | 2.8 ^{a)} [Palmer et al., 1992] |
| Grout material | 6×10^{-8} ^{a)} [Herrmann, 2008] | 0.8 ^{a)} [Herrmann, 2008] | 2.3 ^{b)} [Niekamp et al., 1984; Gauthier et al., 1997] |
| Pipe material | 1×10^{-19} ^{c)} [Pannike et al., 2006] | 0.39 ^{b)} [Signorelli et al., 2007] | 1.6 ^{a)} [Signorelli et al., 2007] |
| Heat carrier fluid (surplus) | 1×10^{-19} ^{c)} [Pannike et al., 2006] | ≥ 20.0 ^{b)} [Clausen, 2008] | 4.2 ^{a)} [Diersch et al., 2010] |

^{a)} reported realistic values; ^{b)} estimated based on real values; ^{c)} estimated to be able to run the model and avoid hydraulic interactions between the discrete feature elements and the part of the finite element mesh representing the grouting material and the subsurface.

Implementation of the BHE and the surrounding aquifer in the numerical grid is illustrated in Fig. 2. The discretization is refined for the parts with the highest expected gradients. This is the BHE itself and the downgradient eastern part of the subsurface, where the temperature plume evolves. Groundwater flow is simulated by a 2nd type boundary condition (BC) at the western and eastern boundary of the model, which assigns a constant flux [Diersch, 2006]. The temperature of the inflowing groundwater is controlled by a 1st BC, which assigns a constant temperature value to certain nodes. The temperature value is equal to the initial temperature of the entire system. The heat is injected in the surplus of the pipes by a 4th type BC, which defines cell-specific energy extraction/injection per time. The turbulent heat propagation inside the pipe is simulated by an enhanced thermal conductivity of the pipe surplus [Diersch et al., 2010].

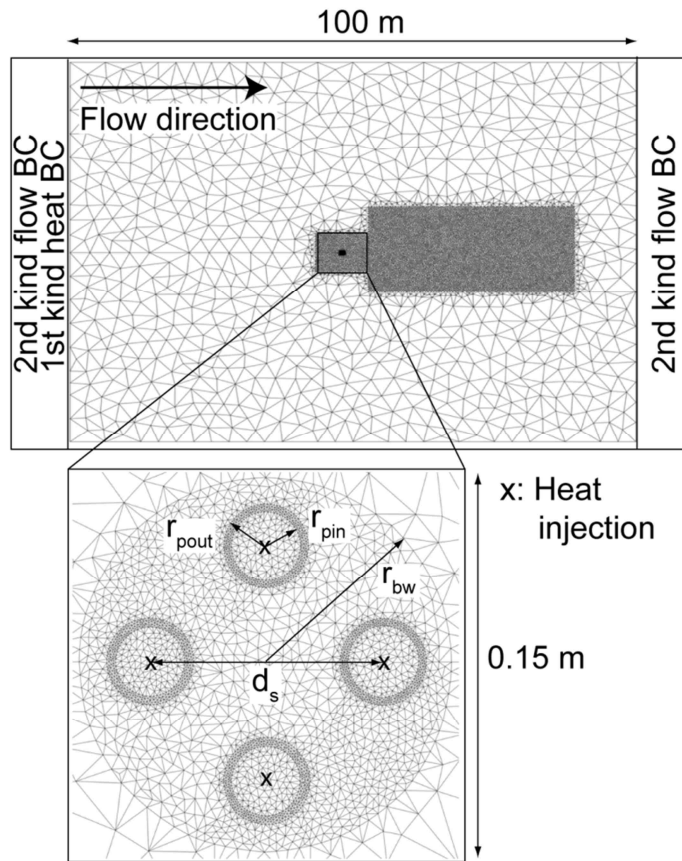


Fig. 7. Overview of model domain, spatial discretization, boundary conditions (BC), and parameters to characterize the simulated borehole heat exchanger (BHE). The shape of the BHE is defined by shank spacing d_s , borehole radius r_{bw} , outer pipe radius r_{pout} , and inner pipe radius r_{pin} .

3.3 Initial Evaluation

3.3.1 Thermal Borehole Resistance

In an initial evaluation, the numerical model is employed to examine the influence of hydraulic parameters on the calculated borehole resistance, R_b , of a completely grouted BHE. Conditions in ungrouted and groundwater filled BHE might be different, reflected by a more transient behavior inside the BHE [e.g. *Gustafsson and Gehlin, 2008; Gustafsson and Westerlund, 2010; Gustafsson and Westerlund, 2011*]. The latter is calculated based on Eq. (3-2) and the simulated temperature values of the borehole wall, T_{bw} , and of the fluid, T_f . The borehole wall temperature T_{bw} is the arithmetic mean of temperature values which are obtained from nodes located at the boundary between the subsurface and the grout material. The position of the nodes applied to obtain the latter temperature values are specified in Fig. 6. The mean heat carrier fluid temperature, which is evaluated by the TRT approach, is the average temperature determined at the center nodes of each pipe (Fig. 7).

Using the numerical model, it is possible to determine R_b for every simulation time step (Fig. 8). All thermal settings remain unchanged. The BHE is simulated with variable Darcy velocities, v , in the aquifer and two different hydraulic conductivities, k_g , of the grout material (Fig. 8). The first case analyzes R_b with respect to increasing v . In order to prevent the BHE from acting as hydraulic resistor, the hydraulic conductivity of the grouting material is set equal to the hydraulic conductivity of the subsurface ($k_g = k_{sub}$). Thus, groundwater flow penetrates the BHE, and conductive and advective heat transports inside the BHE occur. The additional advective component promotes heat transfer inside the BHE and therefore thermal borehole resistance, R_b , decreases with increasing Darcy velocity, v . If significant amounts of groundwater penetrate the grouted part of a BHE, adverse impacts on the grouting material might also occur.

The second case considers the more realistic hydraulic conductivity k_g contrast between grout and aquifer ($k_g \ll k_{sub}$). *Hermann* [2008] measured hydraulic conductivity values of several grout materials, and accordingly a typical value of $k_g = 6 \times 10^{-8} \text{ m s}^{-1}$ is selected here. Under such conditions, groundwater flows mainly around the BHE. The heat transfer inside the grout is considered purely conductive and only in the aquifer heat is transported by both conduction and advection. As a consequence, the calculated R_b values are nearly independent of the Darcy velocity (Fig. 8). The determined R_b time series of the second case shows small variations of the R_b values at the early time steps. The promoting effect of groundwater flow on the heat transport in the subsurface decreases the period of time to reach thermal steady-state conditions of the entire system (subsurface and BHE). To verify the obtained results, R_b values with an identical BHE setup are calculated based on the steady-state multipole method, which is implemented in the software Earth Energy Designer - EED [*Hellström and Sanner, 2000*]. For all cases with a negligible advective heat transport inside the BHE, both approaches result in comparable values (discrepancy below 0.5%) for the time interval of 20 h to 70 h. This time interval is also applied for subsequent TRT interpretations.

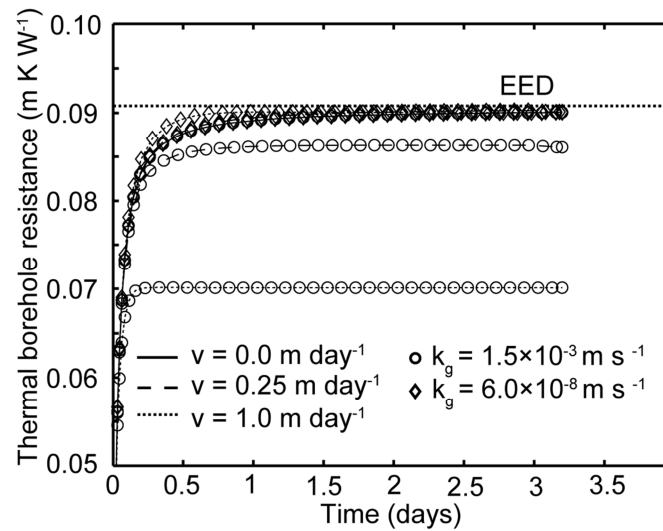


Fig. 8. Temporal sequence of thermal borehole resistance calculated from the numerical simulation result for different Darcy velocities, v , and hydraulic conductivity values, k_g , of the grouting material. The obtained results are compared to simulation by EED.

There are several similar methods available to determine R_b [e.g. *Lamarche et al.*, 2010; *Bauer et al.*, 2011], if the specifications of the BHE are known, like hydraulic and thermal properties of the grout material, U-tube spacing, borehole diameter. *Chiasson and O'Connell* [2011] demonstrated a good agreement of R_b values calculated by the multipole method and a moving line source parameter estimation approach. This means that in principle, no TRT is necessary to estimate this parameter, which is also assumed in the current study. Hence, the borehole resistance can be excluded from the evaluation of a TRT. Instead, it is predetermined as a case-specific constant, and the only unknowns, therefore, are v and λ_m . This facilitates the parameter estimation procedure, which is already difficult for standard TRT interpretation. The inversion problem revealed to be ill-posed in the studies by *Marcotte et al.* [2008] and *Wagner et al.* [2012b], which showed multiple λ_{eff} and R_b pairs yielding valid solutions. Accordingly, we also assess the determinability of TRT parameters in our proposed analytical approach for groundwater-influenced TRT.

3.3.2 TRT Evaluation With Moving Line Source

Several numerically generated TRT temperature time series are generated to analyze the suitability of the moving line source equation, Eq. (3-5), for determination of the Darcy velocity. Since a BHE is made up of different materials with specific property values, this violates the assumption of a homogeneous medium in Eq. (3-5). Thus, fitting TRT data might potentially cause errors for the results. Thermal properties are less variable than hydraulic properties, and therefore interpretation of purely conductive systems with the standard line

source equation is feasible. *Signorelli et al.* [2007] analyzed numerically generated TRTs and showed that the error caused by the thermal conductivity difference between the grouting material and the subsurface of $\Delta\lambda = 2.2 \text{ W m}^{-1} \text{ K}^{-1}$ is less than 5%. The difference of the model in our study is even smaller ($\Delta\lambda = 1.3 \text{ W m}^{-1} \text{ K}^{-1}$, Table 9). This property contrast becomes even smaller when a thermally enhanced grout material is used to backfill the BHE, which becomes increasingly popular. The effect of this parameter difference is presented in Fig. 9a. The spatial temperature distribution calculated by Eq. (3-5) only deviates inside the BHE in comparison with the results of the numerical model. The heat transfer inside the BHE is approximated by the thermal borehole resistance; therefore, the temperature value at the borehole wall is relevant for TRT evaluation and, thus, the temperatures resulting at the borehole wall of the analytical solution and the numerical model are identical. Hence, we assume that the influence of the thermal conductivity contrast can be neglected.

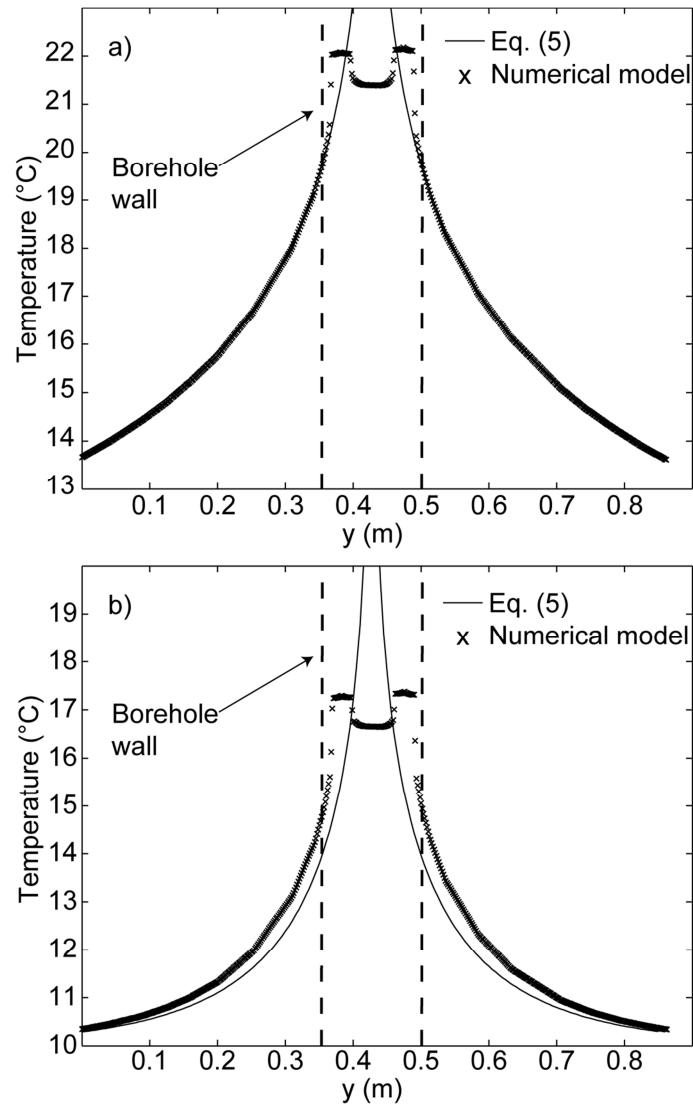


Fig. 9. Comparison of the spatial temperature distribution around a BHE perpendicular to the flow direction calculated using Eq. (3-5) and the numerical model presented in chapter 3.2.3. a) Temperature distribution for a pure conductive heat transfer around a BHE; b) Temperature distribution for a conductive and advective heat transfer around a BHE (Darcy velocity: $v = 0.5 \text{ m day}^{-1}$).

The borehole resistance, R_b , should not be influenced by groundwater flow in the BHE-surrounding porous medium, and its value may be determined separately. Therefore, in the next analysis our focus is set exclusively on Darcy velocity, v , and thermal conductivity. Thermal borehole resistance values are fixed as given in Table 9. The question is, how well does the effective Darcy velocity (v_{eff}), determined by Eq. (3-5), approximate the known value of v specified in the numerical model? The results are based on repeated simulations of different hydraulic conditions, and parameter estimations with Eq. (3-5) and are illustrated in Fig. 10. According to *Witte et al.* [2002], all determined effective Darcy velocities are suitable

with an RMSE smaller than the temperature measurement error of 0.1°C . The average validity range of v_{eff} is smaller than $\pm 2.5\%$ of the optimal fit, which denotes that the moving line source delivers a satisfactory result. The observed discrepancy between chosen v and best-fitted v_{eff} is unsatisfactory. The true value of Darcy velocity, v , is always underestimated, and the calculated conformance ratio even decreases non-linearly for higher groundwater velocities. For a high Darcy velocity of $v = 2 \text{ m day}^{-1}$, for example, the best-fitted Darcy velocity is about 50% below the input value. For low values ($< 0.2 \text{ m day}^{-1}$), conduction dominates the heat transport and consequently the sensitivity of the advective component decreases. Under these conditions, the validity range of v_{eff} clearly exceeds $\pm 2.5\%$, indicating that a small uncertainty in the thermal conductivity value causes significant relative errors of v_{eff} in this domain and, thus, a precise determination of the ratio v_{eff}/v is not possible.

This discrepancy between input and best-fitted Darcy velocity is mainly caused by the difference between the hydraulic conductivities of the grouting material and the aquifer. The latter (k_{sub}) applied in the current study is 2.5×10^4 times higher than that of the grouting material. Thus, the Darcy velocity is noticeably reduced in the close vicinity of the source, i.e. the BHE, which also explains why the best-fitted Darcy velocities are increasingly underestimated for increasing input velocities v . This effect is shown for the conduction and advection-influenced system in Fig. 9b. The determined temperature at the borehole wall calculated using Eq. (3-5) and the numerical model differ not only inside the BHE like in the case of conductive heat transfer, but also at the borehole wall. The deviation inside the BHE is reflected by the thermal borehole resistance R_b , but the discrepancy of T_{bw} values still remains. The latter hampers the application of Eq. (3-5), and instead only time-consuming numerical simulation appears to be suitable. However, as a systematic error is introduced by an evident process, a straightforward parametric approach is favored for practical applications. Hence, a correction term is included in the estimation procedure by Eq. (3-5), which is described in the subsequent chapter.

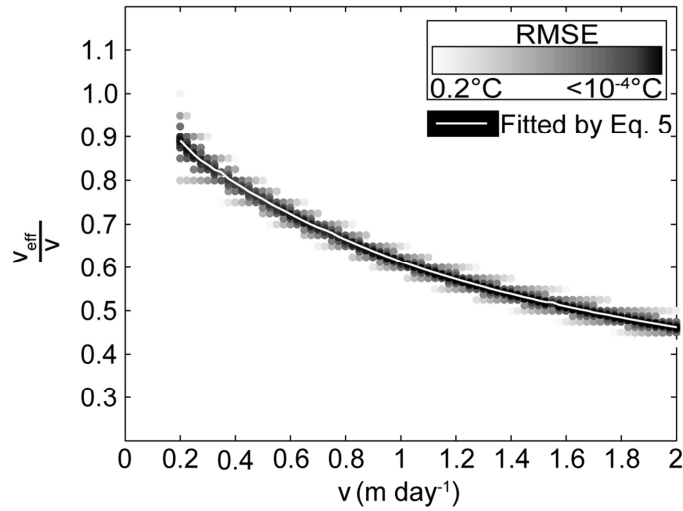


Fig. 10. Result of the evaluation of numerically generated TRT temperature time series (influenced by different Darcy velocities) based on the moving line source equation. Maximum tolerance of fitting error is set to an RMSE of 0.2°C.

3.4 Correction

3.4.1 Correction Term

A correction term, C , is introduced to balance the difference between v_{eff} and v :

$$v \approx v_{eff}^* = \frac{v_{eff}}{C} \quad (3-10)$$

For various hydraulic and thermal conditions, the ratio v_{eff}/v is calculated to obtain a robust specification of the correction term, which can be used to estimate a corrected Darcy velocity v_{eff}^* . Numerical simulations with a thermal conductivity range of the porous medium λ_m from 1.2 to 5.2 W m⁻¹ K⁻¹ and a Darcy velocity v interval from 0.01 to 3.5 m day⁻¹ are performed and analyzed. Furthermore, the ratio v_{eff}/v is calculated for three different R_b values and four different extraction or injection rates, respectively (Fig. 11).

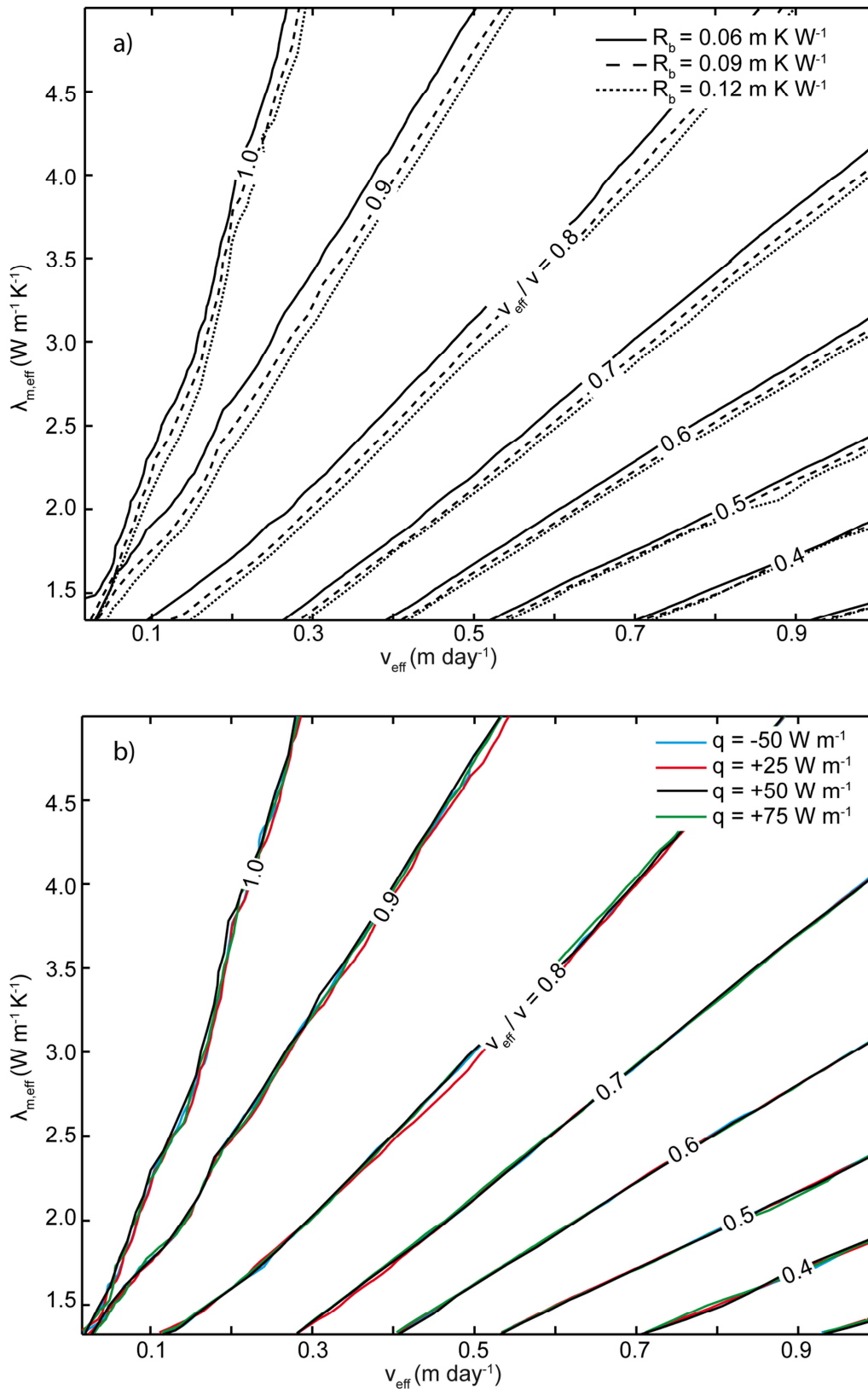


Fig. 11. Relation between the resulting parameters of the TRT evaluation based on Eq. (3-5) ($\lambda_{m,eff}$ and v_{eff}) and the determined ratio v_{eff}/v , which is based on numerical simulations. a) using three different R_b values and an heat transfer rate of 50 W m⁻¹; b) using four different q values and an thermal borehole resistance of 0.09 m K W⁻¹.

The determined ratio v_{eff}/v does not vary significantly for the three different R_b values, which is expected, because R_b is only related to the heat transfer inside the BHE. Thus, it is possible to exclude R_b from a TRT evaluation procedure and determine R_b separately. The focus of the TRT evaluation is therefore on the heat transfer from the borehole wall to the subsurface (or vice versa). The ratio v_{eff}/v shows a clear linear correlation between the obtained Darcy velocity, v_{eff} , and the determined thermal conductivity of the porous medium, $\lambda_{m,eff}$. The wavering curve shape of the v_{eff}/v ratio arrays 0.9 and 1.0 (Fig. 11) are mainly caused by the decreasing influence of advective heat transport, resulting in a substantial uncertainty of the determined v_{eff} value. The determined ratio v_{eff}/v is even less influenced by the applied heat transfer rate. This is expected, because the heat transfer rate is simulated by the moving line source (Eq. (3-5)).

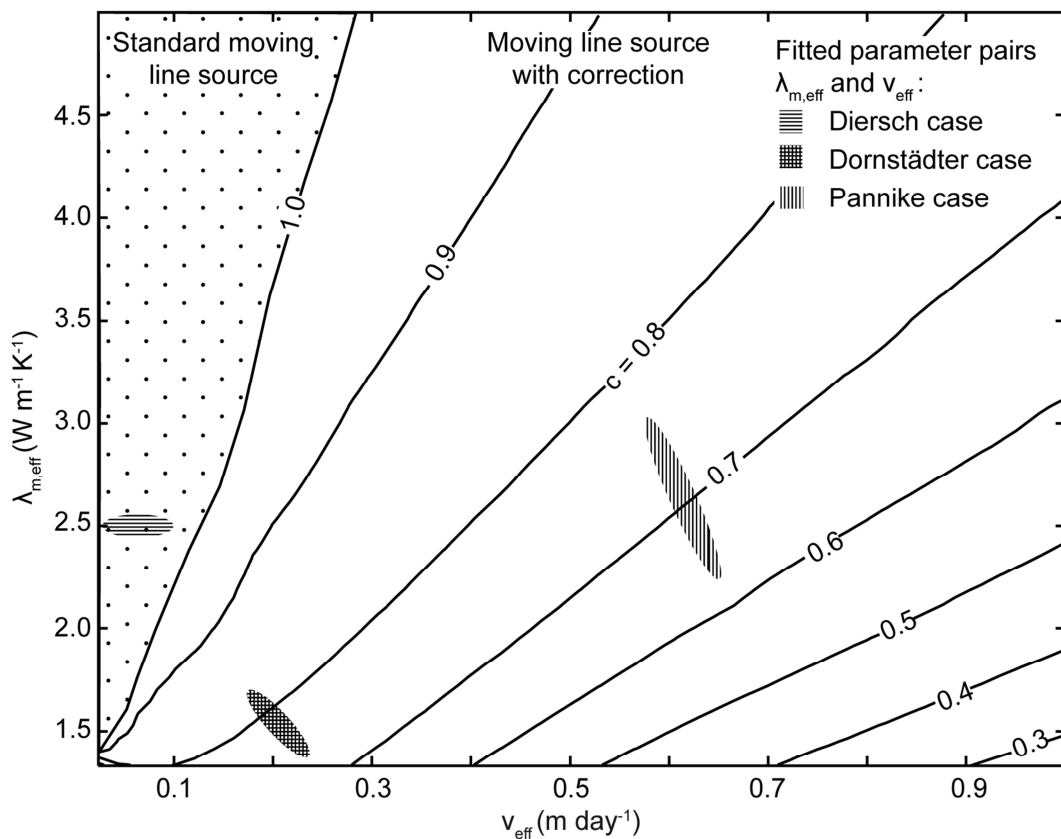


Fig. 12. Relation between the resulting parameters of the TRT evaluation based on Eq. (3-5) ($\lambda_{m,eff}$ and v_{eff}) and the determined correction term C . For the dotted parameter range of $\lambda_{m,eff}$ and v_{eff} , no correction is required, and for the white parameter range a correction of v_{eff} based on Eq. (3-10) is suggested. Parameter pairs ($\lambda_{m,eff}$ and v_{eff}) of the three studied test cases presented in chapter 3.5 are marked as: \times Diersch-case; o Dornstädter-case; $+$ Pannike-case.

To transfer the results to an applicable correction term C , only the averages of v_{eff}/v for the three analyzed R_b values and four different extraction or injection rates are determined, which

are shown Fig. 7. As explained previously, the determination of v_{eff}/v starts to become vague for low groundwater velocities. This inaccuracy also affects the determined C values. Thus, we defined a field of application ($C < 1$) in which the resulting Darcy velocity v_{eff} of the moving line source evaluation (Eq. (3-5)) should be corrected by C . Inside this area v_{eff} systematically underestimates v , and outside of this area (dotted range in Fig. 12) no correction of the obtained v_{eff} value is required.

3.4.2 Correction Procedure

We suggest a three-step procedure to quantify both thermal (R_b , λ_m) and hydraulic (v) parameters from the TRT.

- (1) Determine R_b by an external approach. In our study, we used the numerical results (Fig. 8).
- (2) Estimate $\lambda_{m,eff}$ ($= \lambda_m$) and v_{eff} by fitting the moving line source (Eq. (3-5)) to the measured temperature time series.
- (3) Obtain v_{eff}^* ($= v$) by correction of v_{eff} (Eq. (3-10)) with C taken from Fig. 12. For low v_{eff} , no correction is necessary ($C = 1$).

3.5 Application

To assess the proposed correction procedure for realistic GSHPs, three reported test cases are taken from the literature representing the field of application shown in Fig. 12 (Table 10). Based on the provided conditions, numerical TRT temperature time series are simulated and illustrated in **Fig. 13**. All other settings are listed in Tables 6 and 7. The generated temperature time series are evaluated by the proposed correction approach and the resulting parameter values are compared to the assigned input values to assess the procedure.

Table 10 Thermal conductivities λ_m and λ_g , calculated thermal borehole resistances R_b , and Darcy velocities v from the three case studies for the application of the proposed correction procedure.

| | Diersch case | Dornstädter case | Pannike case |
|--|--------------------|--------------------|--------------------|
| Thermal conductivity of the grout, λ_g , ($\text{W m}^{-1} \text{K}^{-1}$) | 2.3 ^{a)} | 0.5 ^{b)} | 0.8 ^{b)} |
| Thermal borehole resistance, R_b , (m K W^{-1}) | 0.05 ^{c)} | 0.14 ^{c)} | 0.09 ^{c)} |
| Thermal conductivity of the porous medium, λ_m , ($\text{W m}^{-1} \text{K}^{-1}$) | 2.5 ^{a)} | 1.5 ^{a)} | 2.7 ^{a)} |
| Darcy velocity, v (m day^{-1}) | 0.05 ^{a)} | 0.25 ^{a)} | 0.86 ^{a)} |
| Péclet number, Pe (-) | 0.05 ^{c)} | 0.4 ^{c)} | 0.8 ^{c)} |

a) values from literature *Diersch et al.* [2010], *Dornstädter et al.* [2008] or *Pannike et al.* [2006], respectively; b) values estimated; c) values calculated based on the reported values and using Eq. (3-9); d) values calculated based on Eq. (3-2) and the numerical result.

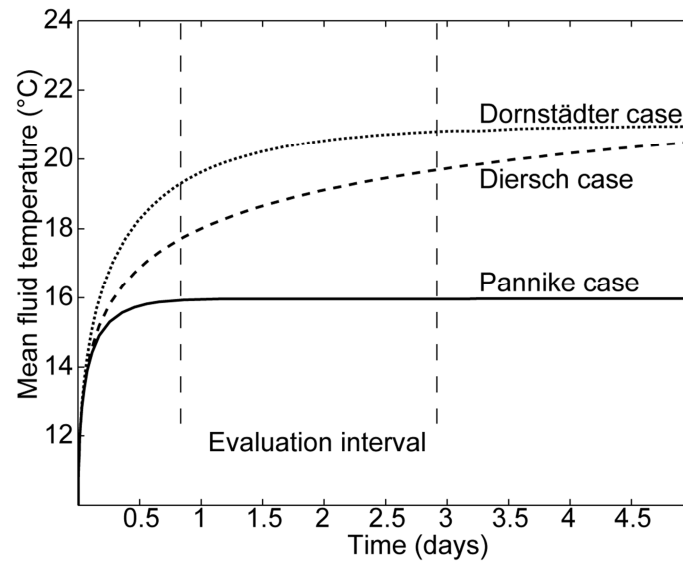


Fig. 13. Numerically generated temperature time series of the three evaluated test cases (Diersch case, Dornstädter case, Pannike case).

3.5.1 Diersch Case

Diersch et al. [2010] simulated a shallow geothermal energy storage system installed in South-West Germany. The entire energy storage system consists of 80 BHEs, which are placed in a circular field with a radius of 15 m [*Diersch et al.*, 2011b]. Each installed BHE is influenced by an underlying limestone aquifer with $\lambda_m = 2.4 \text{ W m}^{-1} \text{ K}^{-1}$ and a maximum reported Darcy velocity of $v = 0.05 \text{ m day}^{-1}$. Based on both parameters an artificial temperature time series is generated by the numerical model and evaluated with the presented approach. This case study represents these conditions with lowest Darcy velocity and is dominated by conductive heat transport, which is also indicated by the small Péclet number ($Pe = 0.05$).

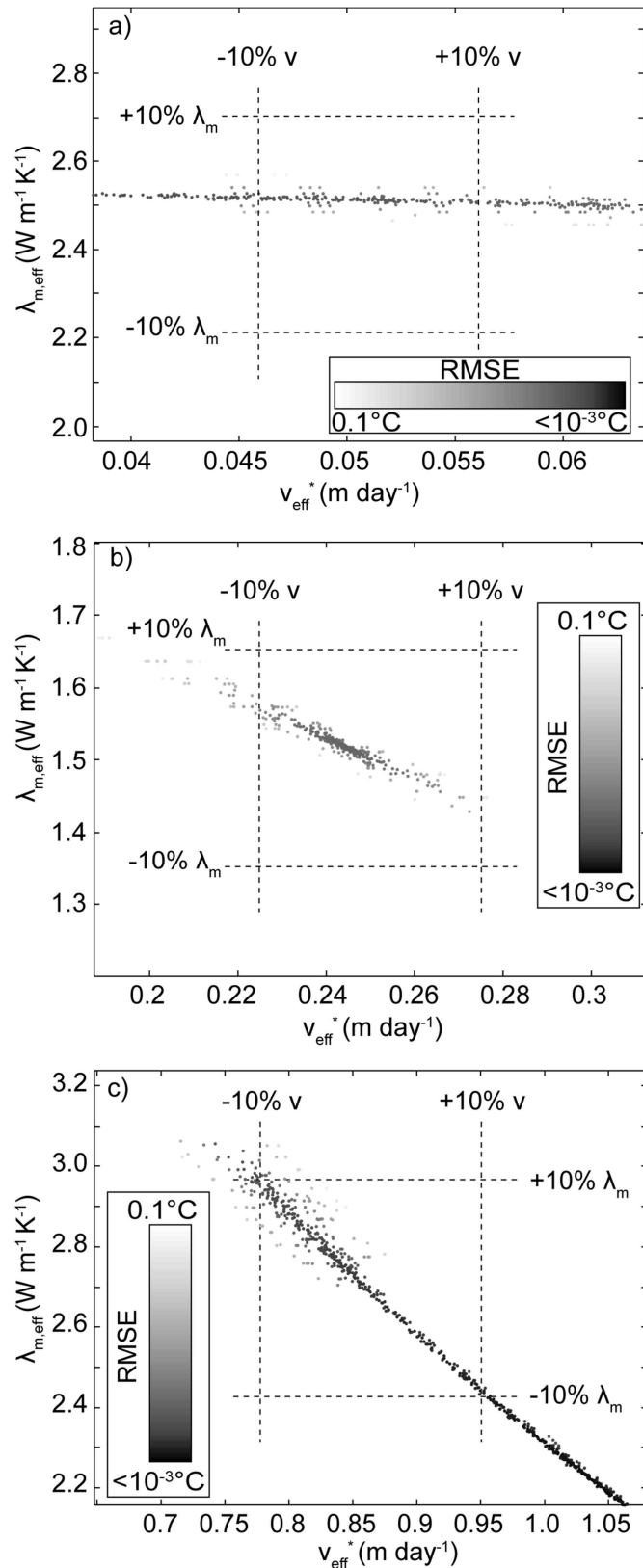


Fig. 14. Valid parameter pairs of $\lambda_{m,eff}$ and v_{eff}^* for an $\text{RMSE} \leq 0.1^\circ\text{C}$. Dashed lines delineate the predefined tolerance window of $\pm 10\%$ around the initial values listed in Table 10 for the different cases. a) Diersch case ; b) Dornstädter case; c) Pannike case.

The results of the Diersch case TRT evaluation are shown in Fig. 14a. The competitive character of conductive and advective heat transport is indicated by a minor negative correlation. Still, the thermal conductivity focuses in a small range between 2.4 and 2.55 W m⁻¹ K⁻¹. This only means a slight potential overestimation of the given value of $\lambda_m = 2.4 \text{ W m}^{-1} \text{ K}^{-1}$. Conduction dominates the heat transfer ($Pe = 0.04$), and the small contribution by advection therefore may be misinterpreted as a higher impact from conduction. Under such conditions, however, extracting the role of advection is a challenging task. Even if feasible solutions of $\lambda_{m,eff}$ and v_{eff} very close to the real values are found, the range of possible v_{eff}^* results exceeds the predefined validity interval of $\pm 10\%$. This confirms our expectations for the limited applicability of the presented approach for aquifers with low groundwater velocities. Obviously, even if λ_m can be estimated very well, more information can hardly be extracted from the TRT interpretation procedure. At most, it can be concluded that a very small Darcy velocity ($v < 0.1 \text{ ms}^{-1}$) is present.

3.5.2 Dornstädter Case

Dornstädter et al. [2008] evaluated an enhanced TRT by a Péclet number analysis. The studied BHE is 57 m deep and is influenced by an aquifer with $\lambda_m = 1.5 \text{ W m}^{-1} \text{ K}^{-1}$ and a maximum reported Darcy velocity of $v = 0.25 \text{ m day}^{-1}$. The aquifer ranges from 7 m to 14 m below ground level and is mainly built up of gravel. The hydraulic and thermal settings are used to generate an artificial TRT dataset, which is evaluated by the presented approach. From the selected case studies, the Dornstädter case represents the intermediate variant, with considerable but not extreme Darcy velocity. The calculated Pe indicates that the Dornstädter case is more influenced by advective heat transport than the Diersch case, but less than the following Pannike case. Nevertheless, in the Dornstädter case, conductive heat transport is more pronounced.

Again, the fitting procedure provides a nearly linear correlation of the possible solutions for $\lambda_{m,eff}$ and v_{eff}^* , which is presented in Fig. 14b. This reflects the similar effects of conduction and advection, although the higher contribution from advection yields a steeper trend, i. e., a more pronounced negative correlation. In contrast to the Diersch case, the estimated results for both parameters comply very well with the real values. Even if – for the given tolerance of the RMSE – numerous results are valid, the possible solution pairs only slightly exceed the $\pm 10\%$ boundary. Thus, we conclude that for conditions similar to this Dornstädter case ($Pe = 0.4$), the presented corrected moving line source procedure turns out to be very efficient.

3.5.3 Pannike Case

Pannike et al. [2006] analyzed numerically the thermal plume caused by a BHE in several aquifers with varying hydraulic and thermal properties, which are typical of northern Germany. We extract the case with the highest Darcy velocity $v = 0.86 \text{ m day}^{-1}$ and a thermal conductivity of the porous medium $\lambda_m = 2.7 \text{ W m}^{-1} \text{ K}^{-1}$. The conditions from the Pannike study are used to generate an artificial TRT dataset influenced by the highest Darcy velocity for testing the presented TRT evaluation approach. Based on the high Darcy velocity, the resulting Péclet number is $Pe = 0.8$, which indicates that heat is transported in comparable proportions by conduction and advection.

Similar to the previous cases, the results of the TRT evaluation show a negative linear correlation between λ_m and v_{eff}^* (Fig. 14c), which is further pronounced by the relatively high contribution from advective heat transport. Here, valid parameter values are nearly proportional. A relative change in v_{eff}^* is balanced by the same relative change in $\lambda_{m,eff}$. For the given RMSE threshold $\leq 0.1^\circ\text{C}$, the parameters span a broad range, which not only meets but also exceeds the $\pm 10\%$ error window. For example, for the given $v = 0.86 \text{ m day}^{-1}$, v_{eff}^* values are found to be between 0.6 and 1.1. The true thermal conductivity $\lambda_m = 2.7 \text{ W m}^{-1} \text{ K}^{-1}$ is equally over- and underestimated with values between $\lambda_{m,eff} = 2.0$ and $3.5 \text{ W m}^{-1} \text{ K}^{-1}$. In practice, this means that by the procedure at least a considerable influence of advection can be detected and also a plausible range can be determined. In the specific Pannike case, close-to-reality solutions can be found by taking the (visual) mean (or statistical median) from Fig. 14c, but in practice this might be biased by measurement errors or other sources of noise. Often, it is possible to further confine reasonable ranges of the expected thermal conductivity based on rock or sediment facies. For example, *Woodside and Messmer* [1961] and *Popov et al.*

[1999] presented several methods to estimate ranges of thermal conductivity for unconsolidated materials, which could be used as constraints to improve the estimation of the prevailing Darcy velocity.

Finally, we could demonstrate for all studied test cases that the resulting parameters of the presented evaluation procedure are representative properties of the subsurface. The Diersch case, which represents a low-advection case, shows that no further correction is necessary and the evaluation is not sensitive for the estimation of the Darcy velocity within the assigned

relative error range. The Dornstädter case, which represents a medium-advection case, shows that the proposed correction approach results in acceptable estimates for $\lambda_{m,eff}$ and v_{eff}^* . Although the R_b value of the simulated BHE exceeds the used R_b range for determination of the correction term C , the accuracy of the estimated parameters is very high. This is evidence that the field of application might exceed the considered R_b range for the determination of C (Fig. 12). The Pannike case, which represents the highly advective case, reveals the non-uniqueness of the inverse problem, which prevents an unequivocal estimation of $\lambda_{m,eff}$ and v_{eff}^* . However, the accuracy can be efficiently improved, if the representative thermal conductivity of the porous medium can be constrained. Nevertheless, four main challenges still remain: First, the effect of subsurface heterogeneity has to be analyzed in more detail and in particular, if the examined BHE is only partially groundwater-influenced. Secondly, the influence of different evaluation times should be further analyzed. Thirdly, the heat capacity ratio between the groundwater and the solid might also influence the result of the evaluation. Finally, the validation of the presented evaluation procedure in the field is necessary.

3.6 Conclusion

In this study, an innovative analytical approach to the evaluation of groundwater-influenced TRTs is introduced and applied using three different case studies from the literature. The approach includes a correction procedure to mitigate the error that is caused by the hydraulic parameter contrast between the grouting material and the subsurface. The derived procedure is verified by high-resolution numerical simulations.

With the results of the numerical simulations we demonstrate that for a wide range of groundwater-influenced TRTs, the Darcy velocity cannot be determined simply by the moving line source theory. Hence, we derived a correction procedure to overcome the limitations of a line-shaped heat source in a homogeneous flow field describing a BHE. The analyses of three TRT test cases are performed to assess the simultaneous determination of $\lambda_{m,eff}$ and v_{eff}^* . Due to the competitive character of conductive and advective heat transport around a BHE, the assessment of all three test cases results in an array of possible solutions and not only in a single valid parameter pair. However, all solution sets contain possible “true” parameter combinations and $\lambda_{m,eff}$ and v_{eff}^* always exhibit a negative correlation.

For conduction-dominated cases ($Pe < 0.1$), the result obtained by the moving line source theory cannot be further improved by the correction approach. The evaluation procedure

results in a wide range of valid v_{eff}^* values, which exceeds the given error tolerance interval of $\pm 10\%$. In contrast, the resulting thermal conductivity value $\lambda_{m,eff}$ matches rather precisely the value assigned in the numerical simulation. For the moderate test case, with a Pe number in the range of 0.1 to 0.8, an excellent distinction between advective and conductive contribution could be achieved. Almost all possible parameter pairs ($\lambda_{m,eff}$ and v_{eff}^*) are within the $\pm 10\%$ error interval. The results of the test case with the highest Darcy velocity ($v = 0.9 \text{ m day}^{-1}$) show that even for a small error tolerance ($RMSE < 0.1$), a broad range of parameter pairs of λ_{eff} and v_{eff}^* provide suitable results. However, based on the significant negative correlation between $\lambda_{m,eff}$ and v_{eff}^* , the latter however can be more precisely determined, if the representative thermal conductivity of the porous medium is estimated. Thus, for high Pe numbers ($Pe \geq 0.8$), the TRT could also be used as a hydraulic test method.

4 Hydraulic characterization of aquifers by thermal response testing: validation by large scale tank and field experiments

Reproduced from: Wagner, V., Bayer, P., Bisch, G., Kübert, M., Blum, P., (201x): Hydraulic characterization of aquifers by thermal response testing: validation by large scale tank and field experiments. Water Resources Research, (in revisions)

Abstract: Thermal response tests (TRT) are a common field method in shallow geothermics to estimate thermal properties of the ground. During the test, a constantly heated fluid is circulated in closed tubes within a vertical borehole heat exchanger (BHE). The observed temperature development of the fluid is characteristic for the thermal properties of the ground and the BHE. We show that, when the BHE is installed in an aquifer with significant horizontal groundwater flow, this test can also be used for hydrogeological characterization of the penetrated subsurface. An evaluation method based on the moving line source equation and considering the natural occurring variability of the thermal transport parameters is presented. It is validated by application to a well-controlled, large-scale tank experiment with 9 m length, 6 m width and 4.5 m depth, and by data interpretation from a field scale test. The tank experiment imitates an advection influenced TRT in a well-known layered aquifer. The field experiment was recorded with a 100 m deep BHE, installed in a gravel aquifer in southwest Germany. The evaluations of both experiments result in similar hydraulic conductivity ranges as determined by standard hydraulic investigation methods such as pumping tests and sieve analyses. Thus, advection influenced TRTs could also potentially be used to determine integral hydraulic conductivity of the subsurface.

4.1 Introduction

The use of temperature signals in hydrogeological field investigation has been suggested for decades [e.g., *Stallman*, 1963; *Bravo et al.*, 2002], and has recently gained significant attention, especially in the context of surface-groundwater interaction [*Cardenas*, 2010; *Lautz*, 2010]. *Anderson* [2005] and *Saar* [2011] emphasized the often unexplored potential of using natural temperature variations as a cheap, expressive and complementary means to support hydraulic characterization of groundwater flow conditions, water balancing, and modeling on local and basin scale. So far, less interest has been on application of artificial thermal signals, which are actively induced in field measurement campaigns. Reasons for this are that standard applications and interpretation procedures do not exist, that established alternative hydrogeological investigation methods coexist, and that generation of substantial and far reaching thermal signals is challenging, time consuming, and potentially costly.

In most studies with artificial heat perturbation, understanding coupled hydraulic-thermal processes is of particular interest. Evolution of thermal anomalies from injection of hot or cold water is mainly studied in the context of geothermal energy use of shallow aquifers [*Parr et al.*, 1983; *Palmer et al.*, 1992]. Thermal monitoring downgradient or in the vicinity of an artificial heat source has been gaining attention for active thermal tracer testing. *Hurtig et al.* [1994] initiated the use of distributed thermal sensors (DTS) at the Grimsel test site in Switzerland. Hot and cold water was injected in the crystalline hard rock to successfully identify fractures by thermal fluid logging. *Ma et al.* [2012] demonstrated that additional information can be exploited from combining Bromide tracer with hot water at the Hanford site, Washington. Both tracers could be used for the calibration of a groundwater and heat transport model, but density effects and intra borehole flow were identified as critical factors for the interpretation of vertical temperature variations [*Klepikova et al.*, 2011].

In contrast to this “open test design”, where mass and heat is exchanged with the subsurface, there are experiments that employ temperature signals from hydraulically closed devices without water exchange between device and soil or aquifer. *Byrne et al.* [1967] were among the first to use conductive heating devices to characterize soil water flux. In their application, a solid cylinder shelters the heater and the temperature sensors, but it significantly distorts the flow field. More recently developed devices measure thermal perturbations from a central wire, and these can be classified by the specific sensor arrangement. There are one-dimensional (1D) [e.g., *Ochsner et al.*, 2005; *Gao et al.*, 2006], two-dimensional (2D) [e.g.,

Greswell et al., 2009] and three-dimensional (3D) configurations [e.g., *Angermann et al.*, 2012]. In these studies, analytical solutions were employed to determine water flux, except of *Hopmans et al.* [2002], who applied the numerical HYDRUS-2D model for the analysis. *Ochsner et al.* [2005] emphasized that a systematical misfit between recorded and modeled data exists, which can be overcome by introducing a correction term that mitigates the advection component. *Gao et al.* [2006] explained this misfit by wall flow effects caused by the sensor.

“Closed” thermal perturbation, common in hydrogeology and soil science, is confined to miniature field investigation techniques such as heat perturbation flow meter or heat pulse sensor [Greswell et al., 2009; Angermann et al., 2012]. A related method for investigating ground thermal parameters, the thermal response test (TRT), is established in larger scale geothermal applications. Typically, vertical boreholes of about 50-200 m are drilled, equipped with one or two U-tubes, and a heat carrier fluid is circulated to facilitate energy transfer between subsurface and an aboveground heat pump or resistance heater. The borehole-tubes installation is also termed borehole heat exchanger (BHE). During the TRT, the temporal development of the artificially heated fluid over a period of one or more days is analyzed. The recorded temperatures are used to calibrate analytical or numerical models to obtain the BHE-specific borehole resistance, and the thermal conductivity of the ambient ground [e.g., *Gehlin*, 2002]. Commonly, advective heat transport in penetrated aquifers is ignored. If aquifers are present then it is accounted for by introducing an effective thermal conductivity that is typically larger than the actual one describing conduction only [e.g. *Witte*, 2001].

The influence of groundwater flow on TRTs has been examined in experimental and theoretical studies. To quantify the influence experimentally, two different strategies were presented. The first one compares a groundwater-influenced TRT to one conducted in comparable geology [e.g., *Chiasson and O'Connell*, 2011]. Alternatively, a forced gradient (e.g., by groundwater extraction) TRT is contrasted with results from undisturbed conditions [Witte, 2001]. The influence of groundwater flow on the TRT result is also analyzed by numerically generated datasets [e.g., *Signorelli et al.*, 2007; *Raymond et al.*, 2011b; *Wagner et al.*, 2012b; *Sharqawy et al.*, 2013]. Fitting the analytical line source model [e.g., *Mogensen*, 1983; *Signorelli et al.*, 2007], or the cylinder source model [Gehlin, 2002] is most common for TRT evaluation. Apart from these analytical models, there are numerical 1D [e.g., *Gehlin*, 2002], 2D [Witte et al., 2002] and 3D models [e.g., *Signorelli et al.*, 2007; *Raymond et al.*,

2011b] applied for more detailed TRT analysis. However, many of these standard analytical models (i.e. line and cylinder source models) neglect advective heat transport in the ground. To overcome this limitation, *Chiasson and O'Connell* [2011] and *Wagner et al.* [2013] suggested a conduction and advection sensitive model calibration approach for the TRT analysis. In *Wagner et al.* [2013], we revealed that there is a systematical misfit between actual and estimated Darcy velocities. Comparable to the approach by *Ochsner et al.* [2005] and *Gao et al.* [2006] for heat injection devices, a correction term is introduced.

The main objective of the current study is to determine the integral hydraulic conductivity of an aquifer by thermal response testing. The study builds up on the theoretical analysis presented in *Wagner et al.* [2013]. We introduce the TRT evaluation as a method to characterize – exclusively – the groundwater flow regime, and validate the evaluation procedure in laboratory and field applications. This changes the motivation of standard TRT application, which is mainly focused on thermal parameters, such as thermal conductivity and thermal borehole resistance, describing heat conduction from heated BHE. We recognize, in line with the results by the study of *Ma et al.* [2012] on “open” thermal tracer testing, that thermal conduction and dispersion are much less sensitive than hydraulic parameters (i.e. hydraulic conductivity) for advection-influenced systems. In the following, moderate value ranges of thermal parameters to describe heat transport in aquifers are discussed. First, the technical principles of TRT are briefly explained. Second, the moving line source based TRT interpretation to determine the vertically integrated Darcy velocity of an aquifer is introduced. By applying Darcy’s law, an integral aquifer hydraulic conductivity value is estimated. Then comprehensive large-scale tank and field experiments are described, one at a laboratory in Stuttgart and one at a field site in the town of Schwanau, Germany. These are used for validation. Finally, we discuss the applicability of the developed method, and conclude upon its robustness and potentials for improvements.

4.2 Methodology

4.2.1 Technological and theoretical background

Closed geothermal systems are frequent applications for low-enthalpy thermal energy provision. In Europe alone, there are currently far more than one million reported installations [*Bayer et al.*, 2012]. The technological principle is straightforward: in the tubes of one or multiple adjacent boreholes a heat carrier fluid is circulated to establish a temperature gradient

between borehole and ground. This stimulates conductive heat transport from or towards the borehole heat exchanger (BHE). In the closed tubes, the heat carrier fluid transports heat or cold to an aboveground receptor, such as a heat pump that supplies the heating demand of buildings. For cooling, only a circulating pump or a reversible heat pump is used. The TRT is an established field experiment to support design of closed geothermal systems [Gehlin, 2002; Signorelli *et al.*, 2007; Sharqawy *et al.*, 2009b]. It is employed, usually in the planning or pilot phase, to gain insights into the heat transport characteristics of the ground and of the transition between ground and heat carrier fluid. The better the geothermal system can extract heat (or cold) from the ground, the smaller the required length of the borehole and the lower the installation costs [Blum *et al.*, 2011].

During the TRT, the heat carrier fluid is warmed up at the inlet of the borehole tube(s) and circulated for one or more days. By recording the temperature at the outlet, the heat loss to the ground is monitored. Assuming only conductive heat loss and integrating over the entire borehole length, the Kelvin line source theory is typically applied [e.g., Carslaw and Jaeger, 1959]. The analytical line source equation describes conductive heat transport from the borehole to the ground that is simulated as an infinitely small linear structure. In practice, a logarithmic approximation of the Kelvin line source theory is often used for the calibration by straight line fitting on semi-log scale to the temperature time series recorded during the TRT. This procedure is comparable to pumping test interpretation in hydrogeology.

The TRT is conducted to typically estimate the values of two thermal parameters such as the mean effective thermal conductivity of the ground and the thermal borehole resistance. According to Fourier's law, the thermal conductivity governs the conductive heat flux from or towards the borehole for a given temperature gradient. In many applications, the tubes are embedded in bentonite grout [Wagner *et al.*, 2013]. Detailed simulation of the transport processes between borehole wall and carrier fluid in the tubes requires advanced numerical models, which simulate the discrete parts of a BHE. Instead of this, in the analytical line source based simulation, the thermal borehole resistance R_b is introduced serving as the bulk parameter to quantify the thermal effects inside the BHE (Fig. 15).

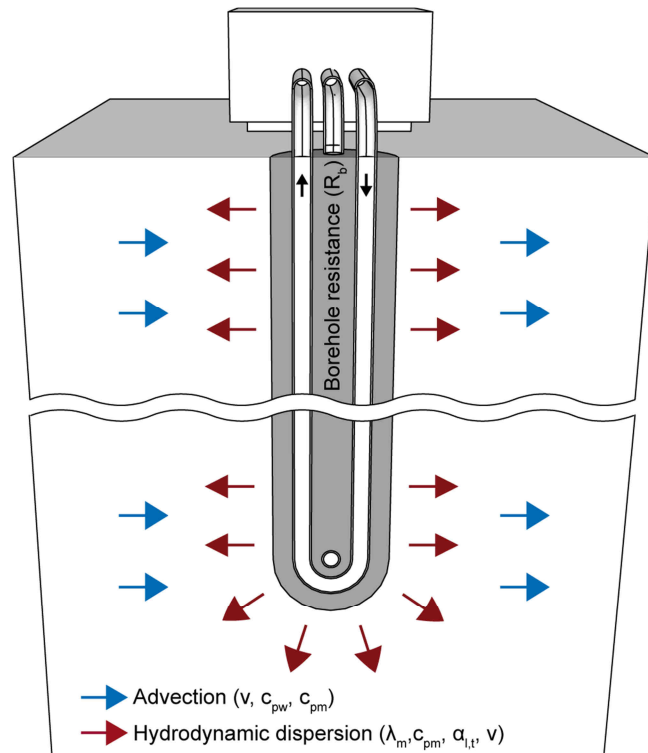


Fig. 15. Borehole heat exchanger (BHE) during a thermal response test (TRT) with heat transfer processes and parameters accounted for by the moving line source (Eq. (4-6)) (thermal borehole resistance R_b ; Darcy velocity v ; thermal conductivity of the porous media λ_m ; volumetric heat capacity of the porous media c_{pm} ; volumetric heat capacity of the groundwater c_{pw} ; longitudinal and transversal dispersivity α_l and α_t).

If BHEs operate in aquifers, advection commonly improves heat transfer and system efficiency. Since hydrogeological insight is often lacking, this process is not further examined and opportunities are lost for more economic (shorter) boreholes [e.g., *Blum et al.*, 2011]. Thus, recently, attention has grown towards the role of groundwater flow, and the additional advective heat transport component that balances thermal anomalies evolving around such BHEs. There are analytical [e.g., *Chiasson and O'Connell*, 2011; *Molina-Giraldo et al.*, 2011b] and numerical [e.g., *Signorelli et al.*, 2007; *Hecht-Méndez et al.*, 2010; *Raymond et al.*, 2011b] studies, which analyze the effects of simultaneous heat advection and hydrodynamic heat dispersion (Fig. 15). To be able to distinguish advective and conductive components in a groundwater influenced TRT, *Chiasson and O'Connell* [2011] and *Wagner et al.* [2013] suggest using the infinite moving line source model. The infinite moving line source equation approximates the BHE as an infinite line shape heat source (or sink) with a constant heat flux. The time-dependent temperature variation in the ground caused by the heat source is given by [*Carslaw and Jaeger*, 1959]

$$T_{sub}(x, y, t) - T_0 = \frac{q}{4\pi c_{pm} \sqrt{D_l D_t}} \exp\left[\frac{v_{th} x}{2D_l}\right] \int_0^{\frac{v_{th}^2 t}{4D_t}} \exp\left[-\left(\frac{x^2}{D_l} + \frac{y^2}{D_t}\right) \frac{v_{th}^2}{16D_l u} - u\right] \frac{du}{u} \quad (4-1)$$

In this study, T represents the temperature [$^{\circ}\text{C}$], x and y are the Cartesian coordinates [m] with the BHE at the origin, t is the time [s], q is the heat injection per unit length [W m^{-1}], c_{pm} is the volumetric heat capacity of the porous media [$\text{J m}^{-3} \text{K}^{-1}$] and u is the integration variable. Temperature T_0 describes the undisturbed conditions at the initial state.

Eq. (4-1) describes conductive and advective heat propagation in homogeneous porous media. The effective heat transport velocity is defined as

$$v_{th} = v \frac{c_{pw}}{c_{pm}} \quad (4-2)$$

where v is the Darcy velocity [m s^{-1}] and c_{pw} the volumetric heat capacity of the groundwater [$\text{J m}^{-3} \text{K}^{-1}$]. Subscript th denotes that the transport velocity (v_{th}) is thermally retarded. The effective thermal dispersion coefficients D [$\text{m}^2 \text{s}^{-1}$] are in longitudinal direction

$$D_l = \frac{\lambda_m}{c_{pm}} + \alpha_l v_{th} \quad (4-3a)$$

and in transversal direction

$$D_t = \frac{\lambda_m}{c_{pm}} + \alpha_t v_{th} \quad (4-3b)$$

The thermal conductivity of the porous media is λ_m [$\text{W m}^{-1} \text{K}^{-1}$]; α_l and α_t [m] represent the longitudinal and transversal dispersivities. For TRT interpretation, the temperature change of the ambient ground is calculated based on Eq. (4-1). The temperature difference inside the BHE is accounted for by the thermal borehole resistance R_b [m K W^{-1}], which is calculated as

$$R_b = \frac{T_f - T_{bw}}{q} \quad (4-4)$$

Temperature T_{bw} refers to the borehole wall and T_f to the heat carrier fluid. R_b relates the borehole wall temperature to the heat carrier fluid temperature [Sutton *et al.*, 2002]

$$T_f(x, y, t) = \frac{q}{4\pi c_{pm} \sqrt{D_l D_t}} \exp\left[\frac{v_{th} x}{2D_l}\right] \int_0^{\frac{v_{th}^2 t}{4D_l}} \exp\left[-\left(\frac{x^2}{D_l} + \frac{y^2}{D_t}\right) \frac{v_{th}^2}{16D_l u} - u\right] \frac{du}{u} + T_0 + R_b q \quad (4-5)$$

If the physical properties of the ground can be approximated as temperature independent, superposition can be applied to Eq. (4-5). Temporal superposition is used to consider multiple loads during the TRT, and consequentially, to facilitate a stepwise TRT evaluation. Spatial superposition is employed to account for locally variable effects of groundwater flow. During heating, advective heat transport causes an asymmetric borehole wall temperature with lower values at the upstream. This is resolved by multiple (here, six) superimposed line sources equally positioned at the borehole wall at (x_j, y_j) , which share the total heat injection rate of the TRT. Temporally and spatially superimposed Eq. (4-5) reads

$$T_f(t) = \sum_{i=1}^m \sum_{j=1}^n \frac{1}{n} (q_i - q_{i-1}) \frac{1}{4\pi c_{pm} \sqrt{D_l D_t}} \exp\left[\frac{v_{th} x_j}{2D_l}\right] \int_0^{\frac{v_{th}^2 (t_m - t_i)}{4D_l}} \exp\left[-\left(\frac{x_j^2}{D_l} + \frac{y_j^2}{D_t}\right) \frac{v_{th}^2}{16D_l u} - u\right] \frac{du}{u} + T_0 + R_b \frac{q_i}{n} \quad (4-6)$$

where m denotes the number of time steps and n the number of heat sources. At time step i , a total heat injection rate of q_i is applied to the BHE, with $t_0 = 0$ and $q_0 = 0$.

By formulating the moving line source equation in dimensionless form, one is able to obtain a set of universal thermal response curves. The dimensionless coordinates are obtained by referring to the BHE length H ; in x -direction: $x' = x H^{-1}$ and in y -direction $y' = y H^{-1}$. The dimensionless heat injection rate per unit length q' is formulated in the same manner, $q' = q q_{ref}^{-1}$. In line with the work of Molina-Giraldo *et al.* [2011b], a dimensionless temperature rise Θ is defined based on the temperature change ΔT : $\Theta = \Delta T c_{pm} D_l 4 \pi q_{ref}^{-1}$. Furthermore, the Fourier number $Fo = D_l t H^{-2}$, the Peclet number $Pe = v_{th} H D_l^{-1}$ and the effective thermal

dispersion ratio $\beta = D_l D_t^{-1}$ are defined. Based on these dimensionless parameters, Eq. (4-6) can be expressed in dimensionless form:

$$\Theta(q', x', y', \beta, Pe, Fo) = \sum_{i=1}^m \sum_{j=1}^n \frac{1}{n} (q'_i - q'_{i-1}) \sqrt{\beta} \exp\left[\frac{Pe x'}{2}\right] \int_0^{\frac{Pe^2 Fo}{4}} \exp\left[-(x_j'^2 + \beta y_j'^2) \frac{Pe^2}{16u} - u\right] \frac{du}{u} \quad (4-7)$$

In contrast to the approach by *Chiasson and O'Connell* [2011], *Wagner et al.* [2013] also considers the hydraulic effects of the grouting material inside the borehole on the estimated parameters. *Wagner et al.* [2013] built up a two-dimensional (2D) finite element model of a BHE in FEFLOW 5.4 [*Diersch, 2009b*]. By using a fully discretized BHE, this numerical model considers the complex heat propagation inside the BHE between the heat carrier fluid, pipe wall and the grout material, as well as advective and conductive heat transport in the surrounding ground. By comparing this high-resolution numerical model and Eq. (4-6), it was demonstrated that there is a systematic misfit between the Darcy velocities derived from realistic numerical and approximate moving line source models. The anticipated discrepancy of the numerical and analytical thermal response curves is caused by remarkable hydraulic conductivity contrast between the grouting material of the BHE and the ambient aquifer, which reaches typically more than three orders of magnitude, and which is not resolved by Eq. (4-6). In comparison, thermal properties of the grouting material and the aquifer are commonly in a comparable range. *Wagner et al.* [2013] demonstrated that Darcy velocity, v , in an aquifer is underestimated by Eq. (4-6) due to disregard of the low-permeable grout and therefore, the calibrated value reflects an effective Darcy velocity. This is comparable to the findings by *Ochsner et al.* [2005] for calibration of heat pulse models. The derived effective Darcy velocity, v_{eff} , however, may be adjusted by a numerically derived correction factor C to a corrected effective Darcy velocity v_{eff}^* , which is comparable to the aquifer Darcy velocity.

$$v \approx v_{eff}^* = \frac{v_{eff}}{C} \quad (4-8)$$

Appropriate values of C depend on effective thermal conductivity and effective Darcy velocity, $\lambda_{m,eff}$ and v_{eff} , as shown in Fig. 16. *Wagner et al.* [2013] analyzed possible effects of R_b values ranging from 0.06 m K W⁻¹ to 0.12 m K W⁻¹ and heat extraction/injection rates, q ,

varying from -50 W m^{-1} to 75 W m^{-1} on the discrepancy between v_{eff} and v . It was demonstrated that the obtained C values are robust and insensitive to these parameters.

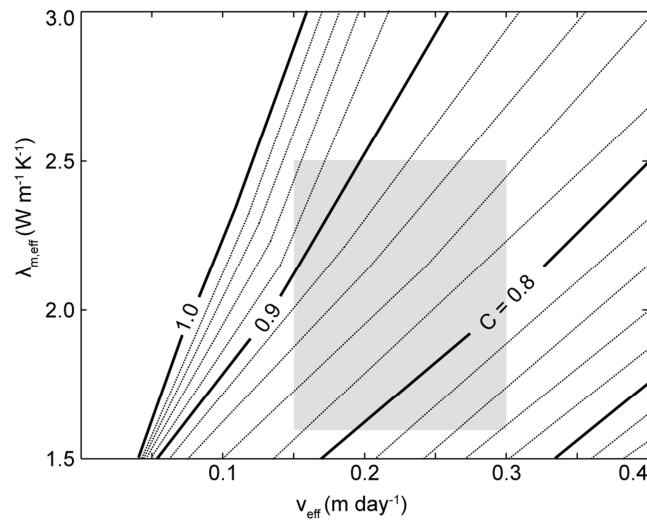


Fig. 16. Values for the correction factor C depending on effective thermal conductivity, $\lambda_{m,eff}$, and effective Darcy velocity, v_{eff} . The grey area depicts the value range for the examples chosen in the present study.

4.2.2 Parameter estimation procedure

A two-step parameter estimation procedure is applied to determine Darcy velocity of horizontal groundwater flow. If the hydraulic gradient is known, the hydraulic conductivity can be derived (Fig. 17). Hydraulic parameters such as the hydraulic conductivity, K , vary over orders of magnitude, and therefore natural occurring Darcy velocities are highly variable. In contrast, reasonable value ranges for thermal transport parameters in aquifers are much more constrained. Hence, here, we solely focus on the identification of effective Darcy velocity, v_{eff} , and K . The Nelder-Mead algorithm [Nelder and Mead, 1965; Lagarias et al., 1998; Bayer and Finkel, 2007] is used to determine v_{eff} , by fitting Eq. (4-6) to measured temperature time series. This is achieved by minimizing the root mean squared error (RMSE). Further thermal transport parameters are set fixed during the fitting step. In order to examine the variability of v_{eff} depending on the thermal transport parameter settings, the v_{eff} fitting step is repeated for alternative combinations. Given ranges of λ_m , c_{pm} , α_l and R_b are discretized and all combinations of these discretized parameter values are tested. This is exhaustive but, with an analytical model, the computational effort is moderate. Not all combinations enable satisfactory curve fitting, and a threshold for the RMSE is suggested to exclude non-plausible results. As a result, we obtain a complete set of possible v_{eff} , as well as the associated residuals

from the fitting, while assuming limited knowledge on thermal transport parameters. The derived v_{eff} values are corrected by Eq. (4-8) to estimate v , and we arrive at an estimate of K with the hydraulic gradient of the aquifer. This two-step parameter estimation procedure is a straightforward method, which may be replaced by any alternative. We favor the presented steps to capture all possible values of v_{eff} . Alternatively, this may also be studied with a Bayesian or evolutionary algorithm.

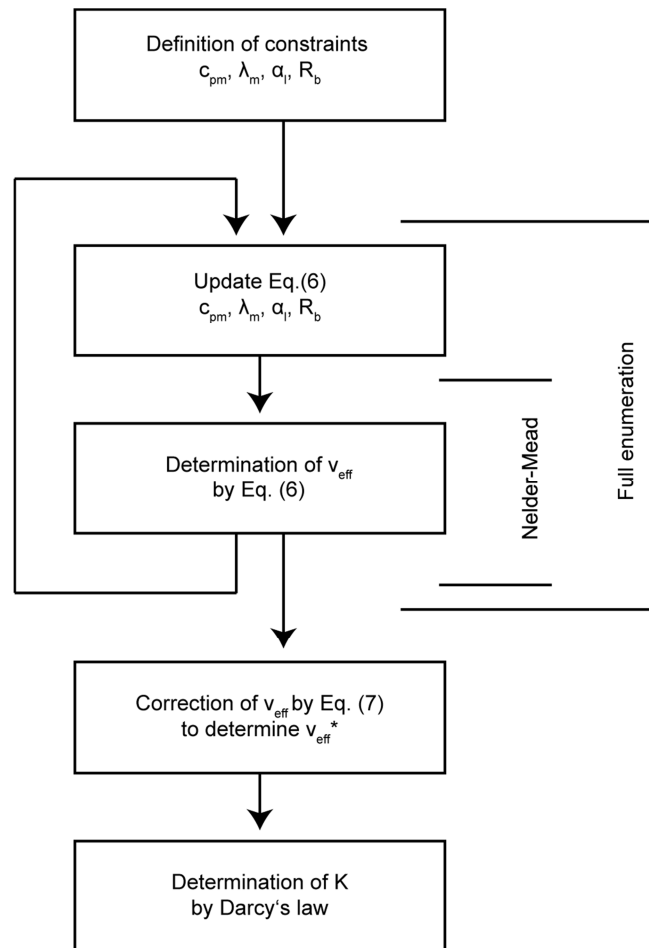


Fig. 17. Optimization schedule applied to combine a local Nelder-Mead optimization of v_{eff} , and full enumeration grid search on c_{pm} , λ_m , α_l and R_b . Determined v_{eff} values are corrected by Eq. (4-8) and if the hydraulic gradient is known, v_{eff}^* can be transferred to an integral hydraulic conductivity (K).

The more the value range of thermal parameters can be constrained, the more precisely the Darcy velocity can be determined. The thermal properties of aquifers are less variable than hydraulic properties [e.g. Parr *et al.*, 1983; Anderson, 2005], and by means of established empirical or statistical relationships they can be estimated at the field site [e.g., Woodside and Messmer, 1961; Menberg *et al.*, 2013b]. Support for this can be found when comparing case

studies on unconsolidated aquifers. For example, *Markle et al.* [2006] analyzed the evolution of a thermal plume in a glacial-outwash aquifer of the Tricks Creek wetland complex in southwest Ontario, Canada. Their main objective was to assess the impact of thermal disturbances on the subsurface and therefore, a detailed characterization of the hydraulic and thermal properties was performed. The volumetric heat capacity of the aquifer was $c_{pm} = 2.79 \pm 0.01 \text{ MJ m}^{-3} \text{ K}^{-1}$ and the thermal conductivity was $\lambda = 2.42 \pm 0.28 \text{ W m}^{-1} \text{ K}^{-1}$. In contrast to this small range of the thermal properties, the hydraulic conductivity measured at this site varies by three orders of magnitude ($1.8 \times 10^{-4} \text{ m s}^{-1} \leq K \leq 1.7 \times 10^{-2} \text{ m s}^{-1}$). At the prominent Borden test site, *Macfarlane et al.* [2002] and *Sudicky* [1986], among others, described the moderate heterogeneity of the studied aquifer ($1.0 \times 10^{-5} \text{ m s}^{-1} \leq K \leq 3.1 \times 10^{-4} \text{ m s}^{-1}$). In the field experiments by *Palmer et al.* [1992], the volumetric heat capacity was specified as $c_{pm} = 2.84 \text{ MJ m}^{-3} \text{ K}^{-1}$ and the variability of $\lambda_m = 2.1 \pm 0.3 \text{ W m}^{-1} \text{ K}^{-1}$ was comparably small. A third exemplary study site is located 32 km north of Mobile, Alabama. *Parr et al.* [1983] characterized the confined aquifer to assess its potential for thermal energy storage, and they obtained $c_{pm} = 2.78 \text{ MJ m}^{-3} \text{ K}^{-1}$ and $\lambda_m = 2.3 \pm 0.19 \text{ W m}^{-1} \text{ K}^{-1}$. A transmissivity of 1130 - 1140 m day^{-1} was determined by a standard pumping test. With an aquifer thickness of about 31 m and mean hydraulic conductivity around $K = 4.2 \times 10^{-3} \text{ m s}^{-1}$.

The volumetric heat capacity of porous media is commonly calculated by the arithmetic mean of the components [e.g. *Parr et al.*, 1983; *Palmer et al.*, 1992; *Markle et al.*, 2006]. For an idealized aquifer with one solid phase (i.e., mainly quartz) and one fluid phase (i.e., water) the volumetric heat capacity can be estimated by [e.g. *Rau et al.*, 2012]:

$$c_{pm} = nc_{pf} + (1-n)c_{ps} \quad (4-9)$$

where c_{pf} and c_{ps} are the volumetric heat capacities of the fluid and the solid phase (Note: if the fluid phase is water, c_{pf} is equal to c_{pw}). The porosity of unconsolidated materials is variable and for instance, in *Fetter* [2001], the porosity of sand and gravel mixture ranges typically from 20% to 35%, and may reach 50% in well sorted material. This yields a span of c_{pm} as illustrated in Fig. 18, which also captures those values reported above in the three case studies. Additionally, the values from the studied tank experiment (Table 11), which will subsequently serve as validation case for this study, are shown.

Appropriate estimation of thermal conductivity of saturated porous media, λ_m , is more challenging, because the value does not only depend on fraction of components or phases. There are several other factors, which are also relevant, such as bulk density, shape, size and arrangement of the grains [Markle *et al.*, 2006]. Accordingly, several methods to narrow down values of λ_m coexist. Maximum values are given by the arithmetic mean of component-specific quantities, and the harmonic mean denotes the minima [Woodside and Messmer, 1961]. The geometric mean describes a random distribution, which was successfully applied in a study by Menberg *et al.* [2013] validating the results of a TRT. A more specific, empirical approach is the one proposed by de Vries [1963]. It is particularly suited for unconsolidated soil, because it also considers the shape of the particles by the form factor g_i . For spherical particles $g_1 = g_2 = g_3 = 1/3$,

$$\lambda_m = \frac{n\lambda_f + (1-n)\lambda_s F_1}{n + (1-n)F_1} \quad (4-10)$$

$$F_1 = \frac{1}{3} \sum_{i=1}^3 \left[1 + \left(\frac{\lambda_s}{\lambda_f} - 1 \right) g_i \right]^{-1} \quad (4-11)$$

where the thermal conductivity of the fluid phase is λ_f , and of the solid phase λ_s . The factor F_1 defines the average temperature gradient in the fluid and solid phase.

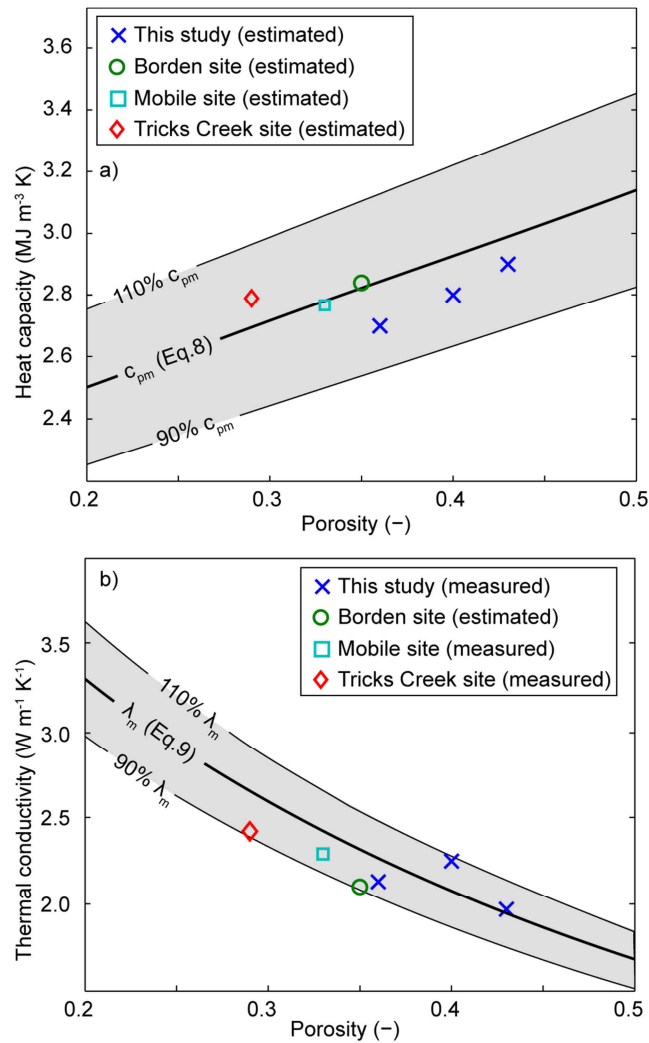


Fig. 18. a) Volumetric heat capacity values compared to estimates based on Eq. (4-9) for water/quartz system, with: $c_{pf} = 4.2 \text{ MJ m}^{-3} \text{ K}^{-1}$ and $c_{ps} = 2.1 \text{ MJ m}^{-3} \text{ K}^{-1}$. b) Thermal conductivity values compared to the range derived by Eq. (4-10). The thermal conductivity of the porous medium is calculated for a quartz solid phase with $6 \text{ W m}^{-1} \text{ K}^{-1}$, and water as fluid phase with $0.6 \text{ W m}^{-1} \text{ K}^{-1}$.

Fig. 18b) depicts obtained thermal conductivity value ranges for unconsolidated gravel/sand mixtures, assuming a two-phase system of spherical quartz grains and water. Again, this range captures the measured and reported (mean) values. Based on the findings from the exemplary measurements and the empirical relationships, values of λ_m vary within a small range, which is $2.2 \text{ W m}^{-1} \text{ K}^{-1} \pm 0.55 \text{ W m}^{-1} \text{ K}^{-1}$. This range represents a variability of $\pm 25\%$ around the mean thermal conductivity λ_m value. This variability is even less for the heat capacity, c_{pm} with a mean of $2.79 \text{ MJ m}^{-3} \text{ K}^{-1}$, and values that spread from $2.51 \text{ MJ m}^{-3} \text{ K}^{-1}$ to $3.07 \text{ MJ m}^{-3} \text{ K}^{-1}$, which is $\pm 10\%$ of the mean value. These limits are also adopted to constrain the parameter values in this study.

Differential advection leads to mechanical dispersion, which is quantified by thermal longitudinal and transversal dispersivity in Eqs. (3a) and (3b). It is commonly assumed that transversal dispersivity is one order of magnitude smaller than longitudinal dispersivity [e.g., *Bear and Cheng*, 2010; *Molina-Giraldo et al.*, 2011a]. This relationship is also applied for this study. In order to account for the scale-dependency of dispersion, appropriate dispersivity values are related to the field scale. *Molina-Giraldo et al.* [2011a] compiled longitudinal thermal dispersivity and corresponding field scales of previous studies. *Gelhar et al.* [1992] suggested taking the distance covered by transport during the experiment as a field scale. A rough estimate would be effective heat transport velocity times experimental duration. Until now, it is still not clear how thermal dispersivity compares to solute dispersivity [*Rau et al.*, 2012]. *Vandenbohede et al.* [2009] and *Bear* [1988] suspect that thermal is smaller than solute dispersivity, because heat propagates through the solid phase and the pore channels. In contrast, *de Marsily* [1986] found no differences in a combined solute and thermal tracer test. For our application, we suppose limited knowledge of appropriate dispersivity values and therefore, estimate the longitudinal dispersivity value based on the empirical relationship provided by *Neuman* [1990]:

$$\alpha_l = 0.017L_s^{1.5} \approx 0.017(v_{th}t_{TRT})^{1.5} \quad (4-12)$$

where the travel distance L_s is assumed to be equal to the product of the effective heat transport velocity, v_{th} , and the duration of the TRT, t_{TRT} . The travel distance can also represent the distance between the source and the observation point. For application purposes, we consider a range for the travel distance, with the borehole radius as the lower bound and the travel distance as upper bound.

While heat transport in the ambient ground is described in detail, heat transport inside the borehole is approximated by one parameter, the thermal borehole resistance, R_b . It relates the temperature difference between the heat carrier fluid and the borehole wall with the applied heat input rate per unit length. There are several approaches to estimate R_b based on the geometry and the material properties of the BHE [e.g., *Sharqawy et al.*, 2009a; *Lamarche et al.*, 2010]. *Bennet et al.* [1987] introduced the common multipole method. In this study, realistic R_b values are estimated using the multipole method implemented in the simulation software Earth Energy Designer (EED) [*Hellström and Sanner*, 2000]. Ranges are generated based on the known material properties of the BHE (pipe and backfilling material, heat carrier

fluid), the operation mode (volume flow rate of the heat carrier fluid and heat injection rate) and the geometry of the BHE (borehole radius, outer/inner pipe radius, number of pipes). The shank spacing, that is, the distance between the centers of the pipes in the borehole, is another unknown. Analogous to the work by *Acuña and Palm* [2009], the full range of feasible shank spacing variants is covered, from one extreme, where all pipes have direct contact in the centre of the borehole, to the other, where all pipes are symmetrically distributed at the borehole wall, to obtain the range of feasible R_b values.

4.2.3 Experimental setup

Two experiments were conducted to examine the suitability of the TRT for estimating Darcy velocity and deducing integral hydraulic conductivity. The first one is a well-controlled large-scale tank experiment. Here, all crucial hydraulic and thermal transport parameters are known or can be precisely determined. This experiment serves for validation of the moving line source based interpretation of monitored thermal response on the laboratory scale. However, laboratory experiments only approximate real in situ conditions. There are often limitations due to boundary or scaling effects, which might influence the results. Thus, the second experiment is a TRT performed at field scale, with moderate knowledge of the thermal and hydraulic parameters of the subsurface. We adopt this to validate our suggested approach at the field scale.

4.2.3.1 Tank experiment

A TRT tank experiment with a layered artificial aquifer was conducted at the research facility for subsurface remediation (VEGAS) at the University of Stuttgart (Fig. 19). Four grouted boreholes equipped with double U-tubes, which act as BHEs are installed in a water-saturated sand container of 9 m length, 6 m width and 4.5 m depth. The BHEs, with a radius of 0.1 m, penetrate the upper 4.3 m and, when ignoring the missing 20 cm on the bottom, can be approximated as fully penetrating. Due to the downscaling of this experiment, the length-width ratio of the used BHE (length / width = 4.3 m / 0.2 m = 21.5) is rather small. A second critical aspect of the laboratory experiment is the vicinity of the container bottom to the BHE, which might cause unsolicited boundary effects. From these BHEs, one is selected to conduct the TRT. It is located approximately 6 m away from the inflow boundary and approximately at the centerline of the container. The other BHEs are not used but implemented for other experiments [*Wagner et al.*, 2012a]. To ensure an optimal thermal connection between BHE and the subsurface, a thermally enhanced grouting material is selected (GWE ThermoSeal[®]).

Comparable to a standard TRT, tap water is taken as heat carrier fluid in the tubes. For this setting, the steady-state multipole method delivers R_b ranges between 0.04 and 0.10 m K W⁻¹, considering a shank spacing range from 0 m to 0.168 m.

Through controlled in and outflow devices, a constant hydraulic gradient can be established in the tank. For the TRT experiment, it is adjusted to 0.003. The artificial aquifer is composed of pure unconsolidated quartz of different well-sorted grain sizes. The five different layers, one of fine sand, two of middle sand and one of coarse sand, are sub-horizontal with an inclination of 3°. The structure is illustrated in Fig. 19, and detailed properties of the layers are listed in Table 11. The measured porosity of the fine sand layer is 0.40, the middle sand layers exhibit a porosity of 0.36 and the coarse sand layer possesses a porosity of 0.36. Hydraulic conductivity, K , ranges for the three different sand classes are determined by sieve curve analyses (Fig. 20) based on the empirical methods by *Hazen* [1893] and *Beyer* [1964]. For each layer, three different samples are analyzed. According to the validity ranges of these methods, the method by *Hazen* [1893] was solely applied for the coarse sand layer, and the method by *Beyer* [1964] was used for the middle sand layers. For the fine sand layer both methods are valid and therefore the widest resulting parameter range considering both methods is selected.

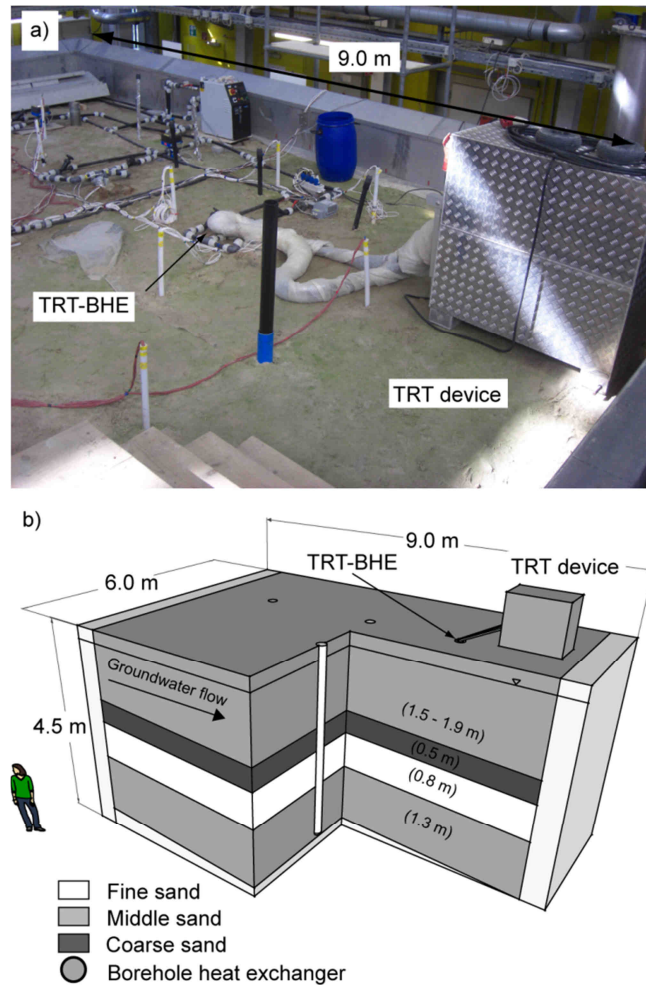


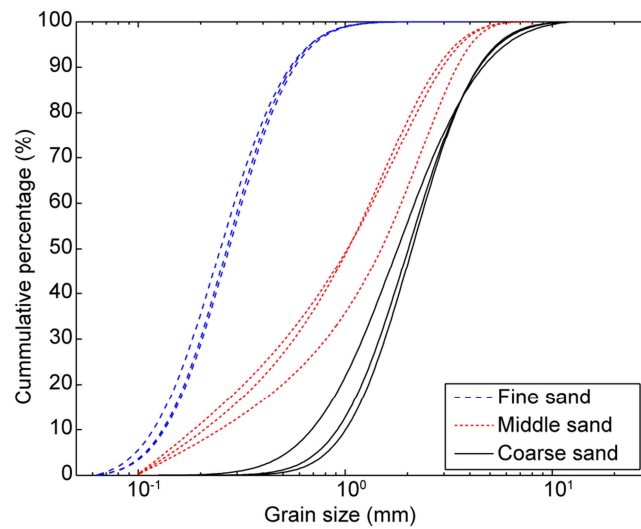
Fig. 19. a) Picture of the tank experiment; b) Schematic bird's eye view of the layered structure and geometries including the thicknesses of the layers.

Thermal conductivity of each layer is determined by laboratory measurements using the “TK04 thermal conductivity meter”, which is based on the line source method [Blackwell, 1954] with a measurement error of $\pm 5\%$. Due to the fact that each layer is built up of pure quartz sand, the volumetric heat capacity c_{pm} can be reliably calculated by a weighted arithmetic average of volumetric fraction of water and solid [e.g. Parr *et al.*, 1983; Palmer *et al.*, 1992; Markle *et al.*, 2006] (Table 11).

Table 11 Properties of the different sedimentary layers in the tank experiment.

| | Middle sand layer | | Coarse sand layer | | Fine sand layer | |
|--|------------------------------------|------------------------------------|------------------------------------|------------------------------------|------------------------------------|------------------------------------|
| | Min | Max | Min | Max | Min | Max |
| 10 % grains passed d_{10} (mm) | 0.19 | 0.25 | 0.70 | 1.00 | 0.12 | 0.13 |
| 60 % grains passed d_{60} (mm) | 1.31 | 1.87 | 2.35 | 2.15 | 0.29 | 0.31 |
| Uniformity index U () | 6.9 | 7.5 | 3.1 | 2.4 | 2.4 | 2.4 |
| Hydraulic conductivity K (m s^{-1}) | 2.9×10^{-4} ^{b)} | 5.0×10^{-4} ^{b)} | 5.7×10^{-3} ^{a)} | 1.2×10^{-2} ^{a)} | 1.2×10^{-4} ^{b)} | 2.0×10^{-4} ^{a)} |
| Volumetric heat capacity c_{pm} ($\text{MJ m}^{-3} \text{K}^{-1}$) | 2.73 | 2.73 | 2.84 | 2.84 | 2.93 | 2.93 |
| Thermal conductivity λ_m ($\text{W m}^{-1} \text{K}^{-1}$) | 2.02 | 2.24 | 2.14 | 2.36 | 1.87 | 2.07 |

^{a)} determined by method by *Haze* [1893]; ^{b)} determined by method by *Beyer* [1964].


Fig. 20. Grain size distribution from repeated sieve analyses of the three different sandy materials of the tank experiment.

A TRT was employed for a period of 8 days. During the test, sensors recorded the temperature of the heat carrier fluid at one-minute resolution. To minimize the atmospheric influences, the sensors were positioned directly at the in- and outflow of the BHE. The TRT was divided in two separate phases. During the initial heating phase of three days a constant heat load of 130 W m^{-1} was applied. Then, the behavior during a five-day recovery phase with no heat load was monitored. The recorded temperature development during the entire TRT is presented in Fig. 21.

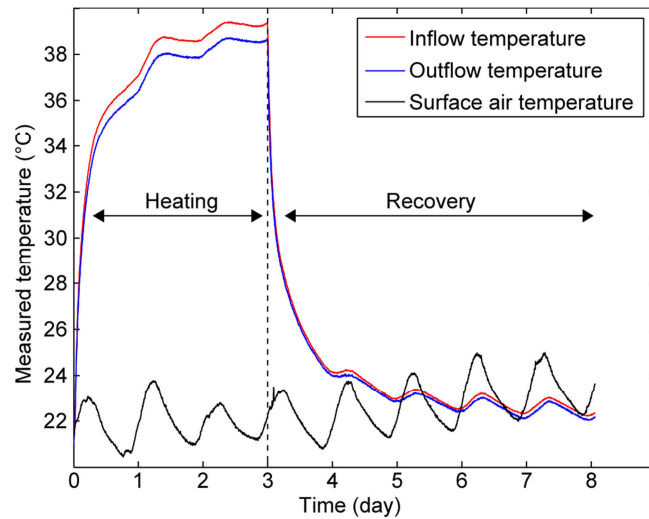


Fig. 21. Measured temperature development of the heat carrier fluid temperature at the inflow and outflow of the BHE during the TRT experiment at the tank experiment. Additionally, the air temperature in 0.1 m above the surface is shown.

Evaluation based on Eq. (4-6) assumes a homogenous aquifer. To be able to examine the applicability of the presented approach, integral parameters of the artificial aquifer are quantified. Water flow and heat propagation is nearly parallel to the sub-horizontal layering, and therefore, an equivalent homogenous media can be calculated by the arithmetic means of the layer properties (Table 12). Based on the minimum and maximum observed values, property ranges of the equivalent homogenous media are calculated. For the thermal conductivity, $\pm 0.55 \text{ W m}^{-1} \text{ K}^{-1}$ ranges are listed in Table 12, which are typical for natural porous aquifers. Although the measurement error of the determined thermal conductivity values is evidently below this range ($\pm 0.11 \text{ W m}^{-1} \text{ K}^{-1}$), we applied the wider parameter range ($\pm 0.55 \text{ W m}^{-1} \text{ K}^{-1}$) to inspect the robustness of the parameter estimation procedure. Ranges of the thermal dispersivity values α_l are estimated by Eq. (4-12). The minimum travel distance of this experiment is the borehole radius ($r_{bw} = 0.1 \text{ m}$), and the maximum travel distance is limited by the size of the tank, which is 9 m. We obtain a longitudinal dispersivity ranging between 0 m and 0.5 m with the resulting transversal dispersivity using the commonly applied 1/10 of α_l .

Table 12 Integral value ranges of hydraulic and thermal parameters for the artificial aquifer of the tank experiment.

| | Value range | |
|---|----------------------|----------------------|
| | Min | Max |
| Hydraulic conductivity K (m s^{-1}) | 8.6×10^{-4} | 1.7×10^{-3} |
| Volumetric heat capacity c_{pm} ($\text{J m}^{-3} \text{K}^{-1}$) | 2.5×10^6 | 3.06×10^6 |
| Thermal conductivity λ_m ($\text{W m}^{-1} \text{K}^{-1}$) | 1.64 | 2.74 |
| Longitudinal dispersivity, α_l (m) | 0 | 0.5 |
| Thermal borehole resistance, R_b (m K W^{-1}) | 0.04 | 0.10 |

4.2.3.2 Field experiment

In addition to the tank experiment, we examine also a field site in the upper Rhine valley at the town of Schwanau in southwest Germany. One vertical borehole of 0.14 m diameter, with double U-tube pipes, was installed to a depth of 100 m (Fig. 22). The length-width ratio of the field scale BHE (length / width = 100 m / 0.2 m = 500) is clearly higher than the one of the tank experiment. It is grouted with thermally enhanced grouting material (ZEO Therm 2.0 from the company Hans G. Hauri KG). Borehole resistance ranges are determined by the multipole based method, analog to the procedure for the tank experiment, considering a shank spacing range from 0 m to 0.108 m. The derived R_b ranges vary between 0.04 and 0.09 m K W^{-1} . The BHE fully penetrates an aquifer with a thickness of 68 m and partially intersects an underlying low permeability formation, which is made up of sandstone and claystone units (Fig. 22). The aquifer is composed of flood plain and low terrace gravel. The low permeability formation consists of one 15 m thick claystone layer embedded in two sandstone layers with a total thickness of 17 m. According to *Junker and Essler* [1980], the hydraulic conductivity, K , of the aquifer, which is allocated to the so-called upper and middle gravel layers of the Rhine valley, varies between 2.3×10^{-3} and $1.2 \times 10^{-2} \text{ m s}^{-1}$. These values were obtained by several sieve curve analyses and hydraulic pumping tests. No specific hydraulic data is available for the low permeability formation. With a typical value range of 10^{-6} - 10^{-9} m s^{-1} for sandstones and $< 10^{-9} \text{ m s}^{-1}$ for clays [*Domenico and Schwartz*, 1998], a parameter range of 10^{-6} - $< 10^{-9} \text{ m s}^{-1}$ is considered here for the hard rocks below the aquifer.

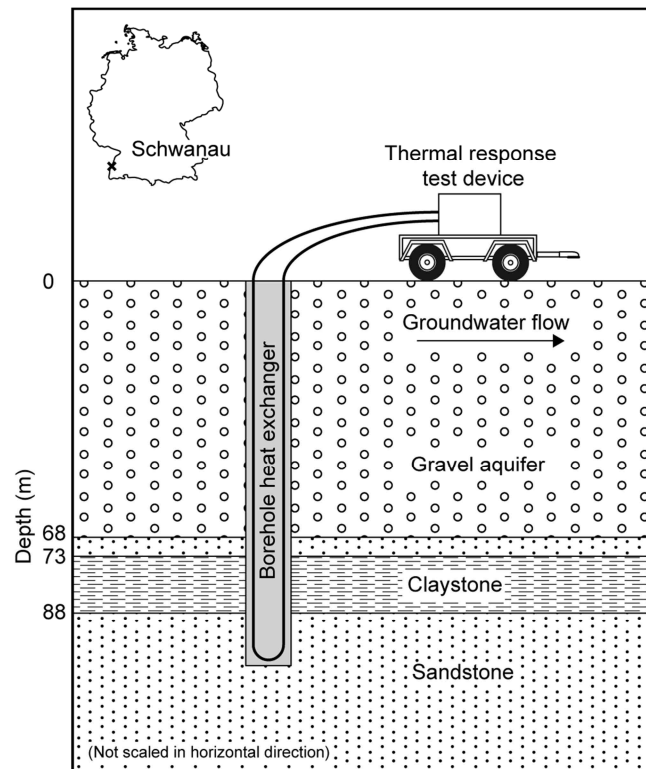


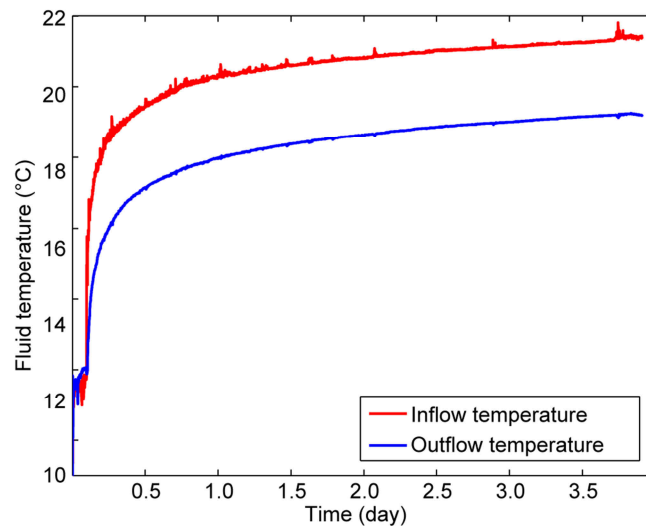
Fig. 22. Schematic cross-section of the studied field experiment in Schwanau (Germany) showing the layered geological units. The individual depths of the layer boundaries are determined based on borehole cuttings. The depth to water table is only 2 m and is therefore, not explicitly shown.

At the field site, thermal parameters are not specifically investigated by additional laboratory experiments. Thus, empirical ranges of the volumetric heat capacity and the thermal conductivity, based on reported data, have to be defined here (Table 13). The volumetric heat capacity of a natural porous aquifer is typically about $2.79 \text{ MJ m}^{-3} \text{ K}^{-1}$, with a variability of $\pm 0.28 \text{ MJ m}^{-3} \text{ K}^{-1}$. A thermal conductivity range from $1.64 \text{ W m}^{-1} \text{ K}^{-1}$ to $2.74 \text{ W m}^{-1} \text{ K}^{-1}$, with a mean value of $2.20 \text{ W m}^{-1} \text{ K}^{-1}$ is assumed for the aquifer material. Volumetric heat capacities of the low permeability formation is estimated based on the study by *Clauser* [2011], and the thermal conductivities of the sandstone and the claystone are extracted from *Domenico and Schwartz* [1998].

Table 13 Properties of the different geological layers for the field site.

| | Aquifer | | Low permeability formation | | | |
|--|----------------------|---------------------|----------------------------|--------------------|----------------------|--------------------|
| | Porous media | | Sandstone | | Claystone | |
| | Min | Max | Min | Max | Min | Max |
| Hydraulic conductivity K (m s^{-1}) | 2.3×10^{-3} | 12×10^{-3} | $< 1 \times 10^{-9}$ | 1×10^{-6} | $< 1 \times 10^{-9}$ | 1×10^{-6} |
| Volumetric heat capacity c_{pm} ($\text{MJ m}^{-3} \text{K}^{-1}$) | 2.51 | 3.07 | 2.05 | 2.05 | 2.30 | 2.30 |
| Thermal conductivity λ_m ($\text{W m}^{-1} \text{K}^{-1}$) | 1.64 | 2.74 | 3.77 | 3.77 | 1.05 | 1.05 |

The TRT started on the 28th of January 2010 and lasted for 4 days. A mobile device was used, which applied power-controlled continuous-flow heaters to reach a constant heat injection rate of 49.3 W m^{-1} during the experiment. The heat carrier fluid was tap water. Flow rates, inlet and outlet temperatures of the fluid in each U-pipe loop were continuously monitored. The testing time can be separated in an initial burn-in phase, where only fluid circulates without any heat injection (0.1 day) and a second constant heating phase. The recorded temperature curves of the fluid at the inlet and outlet of the BHE are shown in Fig. 23. The irregular temperature fluctuations at the inlet fluid temperature are caused by slight instabilities of the chosen fluid flow rate and/or irregularities in the power net supply. In contrast to observations at the tank experiment, atmospheric diurnal temperature fluctuations have no noticeable influence. This is attributed to different measurement devices, as well as to the larger BHE depth and size of the field-scale TRT.


Fig. 23. Measured inflow and outflow temperatures of the heat carrier fluid during TRT at Schwanau field site.

We follow the same procedure as for the tank experiment, and average the hydraulic and thermal values assuming an equivalent homogenous medium. Based on the thicknesses of the

porous aquifer, sandstone and the clay layer, the weighted arithmetic mean of the hydraulic and thermal parameters is calculated. The derived ranges serve as input for Eq. (4-6), except of the hydraulic conductivity, which is utilized for validation (Table 14). Ranges of thermal dispersivity are determined based on Eq. (4-12). The borehole radius of the BHE represents the minimum travel distance for this experiment, which is $r_{bw} = 0.065$ m. The maximum travel distance ($L_s = 5.9$ m) is calculated based on the expected effective heat transport velocity ($v_{th} = 1.7 \times 10^{-5}$ m s⁻¹) and the duration of the TRT ($t = 4$ days). Longitudinal dispersivity values are determined by Eq. (4-12) and the obtained range varies between 0 m and 0.24 m. The transversal dispersivity is set to one tenth of the longitudinal dispersivity.

Table 14 Integral values of thermal and hydraulic parameters at the field site.

| | Value range | |
|--|----------------------|----------------------|
| | Min | Max |
| Hydraulic conductivity K (m s ⁻¹) | 1.6×10^{-3} | 8.3×10^{-3} |
| Volumetric heat capacity c_{pm} (J m ⁻³ K ⁻¹) | 2.40×10^6 | 2.79×10^6 |
| Thermal conductivity λ_m (W m ⁻¹ K ⁻¹) | 1.90 | 2.66 |
| Longitudinal dispersivity, α_l (m) | 0 | 0.24 |
| Thermal borehole resistance, R_b (m K W ⁻¹) | 0.04 | 0.09 |

4.3 Results and discussion

4.3.1 Interpretation of the tank experiment

The undulating inlet and outlet heat carrier fluid temperatures of the tank experiment (Fig. 21) are averaged for TRT interpretation (Fig. 24). By superposition of phases with specific heat loads q_n , Eq. (4-6) facilitates simulations of the two time periods of heating ($q_n = 130$ W m⁻¹, $t = 0$ -3 days) and recovery ($q_n = 0$, $t = 3$ -8 days). The parameter estimation step follows the scheme as illustrated in Fig. 17, and this means that exclusively v_{eff} is iteratively optimized. The evaluation interval considered for the parameter estimation is set to 0.8 to 7.0 days. All other thermal transport parameters λ_m , c_{pm} , α_l and the thermal borehole resistance, R_b , are considered uncertain within the given ranges listed in Table 12. Note that the uncertainty is significant, for instance, within $\pm 40\%$ for R_b . These ranges are discretized in 10 steps for each parameter, and for each of the possible parameters permutations (total number of $(10)^4 = 10,000$), v_{eff} is calibrated. This procedure offers detailed insights into feasible parameter value pairs. Feasibility is defined by a fitting error threshold, which is set here after preliminary visible inspection of fitted curves with RMSE = 0.8°C. This tolerance takes into account that often no unique solution exists or is searched for, and it respects potential measurement errors

and noise. In the tank experiment substantial noise is apparently introduced by the influence of the diurnal atmospheric temperature variability, and the low BHE length-width ratio might also cause some imprecisions. Measurement error by the PT100 sensors is only $\pm 0.1^\circ\text{C}$.

Best fit result is an apparent global optimum, $\text{RMSE} = 0.37^\circ\text{C}$, with $\lambda_m = 2.61 \text{ W m}^{-1} \text{ K}^{-1}$, $c_{pm} = 2.56 \times 10^6 \text{ J m}^{-3} \text{ K}^{-1}$, $\alpha_l = 0.06 \text{ m}$ and with a thermal borehole resistance, $R_b = 0.040 \text{ m K W}^{-1}$. However, Fig. 24a reveals a large number of about 2900 (29% of all trials) of feasible sub-optimal solutions. The simulated temperature trends span the grey shadow surrounding the measured temperatures. As illustrated in Fig. 24a, the threshold of 0.8°C is chosen to encompass the entire undulating curve from the measurement.

Based on the solution-specific thermal conductivity and the determined v_{eff} , the corresponding correction factors (Fig. 16) are selected to derive the (average) Darcy velocity, v . Since the hydraulic gradient of the experiment is known ($i = 0.003$), based on Darcy's law, an integral hydraulic conductivity, K , of the artificial aquifer can be obtained. The values of all possible solutions with their respective fitting errors are shown in Fig. 25. The global optimum of $K = 0.9 \times 10^{-3} \text{ m s}^{-1}$ is close to the mean of the range determined from the sieve analysis with $K = 1.3 \times 10^{-3} \text{ m s}^{-1}$ (Table 12). The point cloud of solutions spans a wide range of resulting hydraulic conductivity values, but this shows an overall best fitting in the range of the sieve curve results and this is the most striking feature. Thus, the TRT based estimation coincides well with the hydraulic characterization based on this hydrogeological standard technique, despite the high uncertainty of the thermal parameters. This indicates that the developed evaluation approach is very robust.

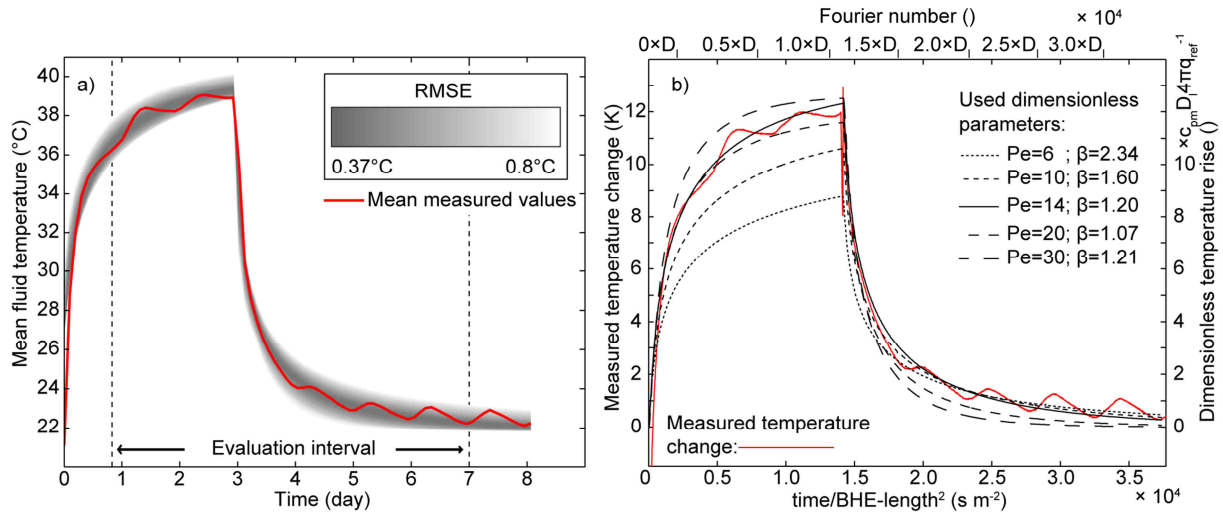


Fig. 24. Fitting results of the tank experiment. a): Comparison of mean measured fluid temperature and results of the parameter estimation approach based on Eq. (4-6). b): Comparison of the measured temperature change and a set of calculated universal temperature response curves based on Eq. (4-7). For straightforward comparison between measured and simulated data, the nondimensionalization is executed by multiplying $t H^{-1}$ with D_l to result in the Fourier number and by multiplying ΔT with $c_{pm} D_l 4 \pi q_{ref}^{-1}$ to determine the dimensionless temperature rise.

For a dimensionless analysis of the results, Eq. (4-7) is applied. Five pairs of the dimensionless variables Pe and β are chosen, consistent with the parameter ranges determined for the tank experiment (Table 12). Pe numbers range from 6 to 30, and β values range from 1.07 to 2.34, which cover the value domain surrounding the best fitted Pe and β combinations. Based on these pairs, a set of five universal thermal response curves are determined and compared to the measured temperature changes of the TRT experiment. This comparison is presented in Fig. 24b for a fixed $R_b = 0.04 \text{ m K W}^{-1}$, which represents the R_b value used to obtain the best fit result of the dimensional formulation of the moving line source.

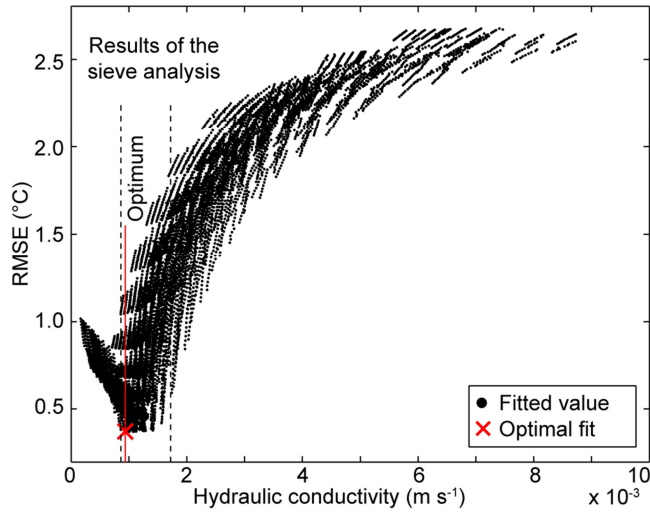


Fig. 25. Hydraulic conductivity values obtained from the determined corrected effective Darcy velocity, and the corresponding RMSE value of the performed parameter estimation approach.

The most suitable pair ($Pe = 14$; $\beta = 1.20$) is also in accordance to the best fit. The dimensionless analysis also reveals the correlation between the four parameters (λ_m , c_{pm} , α_l and v respectively K), suitable to model the observed thermal response of the subsurface. Furthermore, if thermal dispersion is neglected or assumed to be isotropic, i.e. β becomes 1, and the heat transport in the subsurface depends only on Pe . For this simplification, a unique Pe number can be determined and used to derive possible K values based on the predefined thermal parameter ranges, instead of applying a multi-parameter estimation procedure.

4.3.2 Interpretation of the field experiment

The temperature time series measured during the field TRT are employed to validate the introduced parameter estimation approach at the field scale (Fig. 23). First, equivalent to the procedure for the tank experiment, the mean of inlet and outlet heat carrier fluid temperature is computed and plotted in Fig. 26. Then, burn-in phase ($q_n = 0 \text{ W m}^{-1}$, $t = 0 - 0.1$ days) and heating period ($q_n = 49.3 \text{ W m}^{-1}$, $t = 0.1 - 3.9$ days) are superimposed based on Eq. (4-6). The evaluation interval is set from 0.8 to 3.7 days after initiation temperature recording. Again, v_{eff} is iteratively optimized, while the 10 discretization steps within the ranges listed in Table 14 are applied for all other relevant parameters (λ_m , c_{pm} , α_l and R_b). The fitting error threshold is not changed from the tank experiment and kept at 0.8°C .

In comparison to the tank experiment, the influence of diurnal temperature variations is not significant for this experiment; therefore, better agreement between mean measured and

simulated temperatures is achieved. In fact, all parameter variations result in a misfit below the RMSE threshold. This indicates that within the range of noise and measurement error, a large number of acceptable solutions exist. The best result is obtained for a parameter combination of $\lambda_m = 2.66 \text{ W m}^{-1} \text{ K}^{-1}$, $c_{pm} = 2.53 \times 10^6 \text{ J m}^{-3} \text{ K}^{-1}$, $\alpha_l = 0.24 \text{ m}$, and thermal borehole resistance, $R_b = 0.068 \text{ m K W}^{-1}$, with an RMSE value of 0.021°C .

To obtain the integral hydraulic conductivity of the field site, in a first step, the corresponding values of the correction factor are determined. With this factor, the fitted v_{eff} values are transferred to the actual integral Darcy velocity v (Eq. (4-8)). Applying Darcy's law and taking the known hydraulic gradient of 0.001, the integral values of K are determined for all fitting trials. In Fig. 27, the derived K values are plotted versus the fitting errors. The best result, with a misfit of 0.021°C , yields $K = 3.1 \times 10^{-3} \text{ m s}^{-1}$. This value is within the K range determined by sieve analysis and pumping tests for this site, which reaches from 1.6×10^{-3} to $8.3 \times 10^{-3} \text{ m s}^{-1}$ (Table 14). Furthermore, by comparing all obtained results, a distinct optimal interval can be determined, which is also within the range of K values determined from the study of *Junker and Essler* [1980]. This optimal interval, where $\text{RMSE} < 0.05^\circ\text{C}$, reaches from 2.5×10^{-3} to $5.5 \times 10^{-3} \text{ m s}^{-1}$. This demonstrates for the field scale, that the TRT data can also be applied to determine hydraulic conductivity values comparable to the ones obtained from standard hydraulic investigation methods such as hydraulic pumping tests or sieve curve analysis. A premise is that the weighted arithmetic mean is applied to consider a layered structure of the subsurface including penetrated aquifer and low permeability formation. It is noteworthy that the Schwanau experiment was merely conducted to support the design of a larger GSHP system; hence, it clearly demonstrates that the developed procedure can be confidently applied to determine hydraulic parameters.

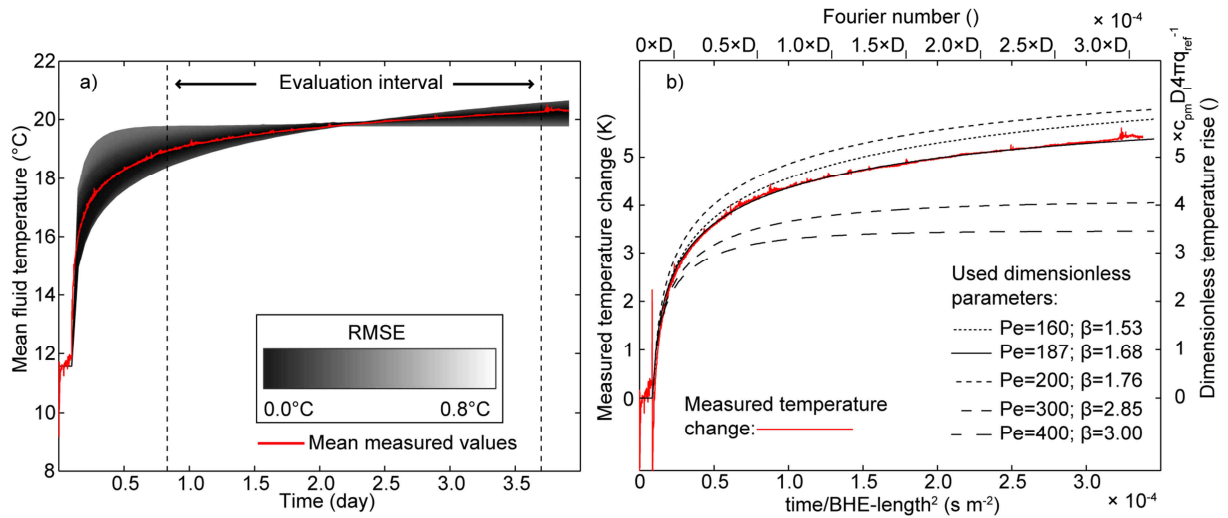


Fig. 26. Fitting results of the field experiment. a): Comparison of the measured mean fluid temperature and the results of the parameter estimation approach based on Eq. (4-6). b): Comparison of the measured temperature change and a set of calculated universal temperature response curves based on Eq. (4-7). For straightforward comparison between measured and simulated data, the nondimensionalization is executed by multiplying $t H^1$ with D_l to result in the Fourier number and by multiplying ΔT with $c_{pm} D_l 4 \pi q_{ref}^{-1}$ to determine the dimensionless temperature rise.

Following the same procedure as for the tank experiment, five pairs of Pe and β are selected for dimensionless analysis of the results. Based on the best-fit result of the dimensional analysis and the specified parameter ranges (Table 14), Pe and β pairs are defined to cover the corresponding dimensionless parameter array. For the field site, these cover the intervals $160 \leq Pe \leq 400$ and $1.53 \leq \beta \leq 3.00$. The R_b is set to 0.068 m K W^{-1} , which represents the value associated with the previously determined best fitted K value.

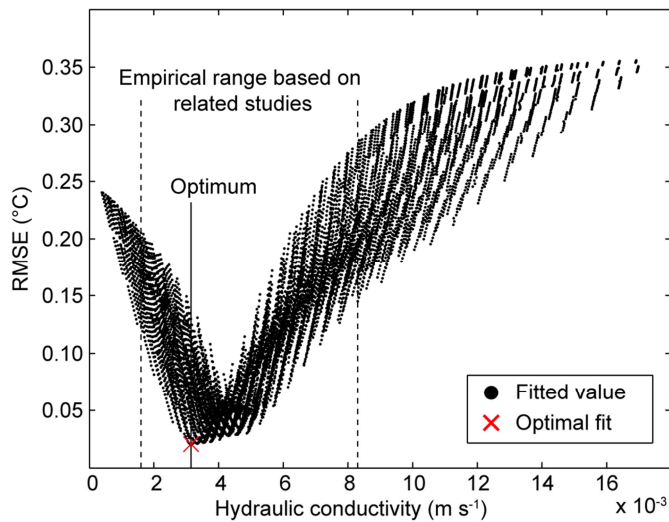


Fig. 27. Hydraulic conductivity, K , values obtained from the determined corrected effective Darcy velocity and the corresponding RMSE value of the performed parameter estimation approach. Empirical range is extracted from Table 14.

As expected, the dimensionless analysis shown in Fig. 26b exhibit the best agreement of the measured and calculated temperature for the parameter pair ($Pe = 187$; $\beta = 1.68$) obtained from the best fit of the dimensional analysis. The dimensionless formulation results in a reduced number of heat transport relevant parameters of the subsurface, two (Pe and β) instead of four (λ_m , c_{pm} , α_l and ν respectively K). Thus, the heat transport behavior can be expressed in a more condensed formulation. Nevertheless, there are still two relevant subsurface parameters, which allow for the determination of one unique Pe number compiling the correlation of the four dimensional heat transport parameters λ_m , c_{pm} , α_l and ν respectively K . Hence, the dimensionless formulation provides a suitable and condensed description of the parameter correlation, but the major objective, to determine the hydraulic conductivity, cannot be further improved by applying a dimensionless formulation.

4.4 Summary and conclusions

Hydraulic characterization of the subsurface is a major task of hydrogeological field methods. This study proposes an advection sensitive TRT evaluation as a potential method to estimate Darcy velocity and integral aquifer hydraulic conductivity. For demonstrating the applicability, the correction term based TRT evaluation by *Wagner et al.* [2013] is integrated in a two-step fitting approach. Two measured TRT temperature time series, from a large-scale tank experiment and one from a standard field TRT are used to validate the new approach. Results for both experiments reveal that temperature time series of a TRT can be assuredly

used to determine hydraulic parameters. This is feasible in spite of (i) the conceptual shortcomings of the simplified line source model, (ii) the high uncertainty in crucial thermal parameter values, and (iii) the noise typically overprinting measurement data.

In principle, the used infinite moving line source model is only applicable to homogeneous conditions, and it does not properly describe the flow and transport processes close to and inside the BHE. As demonstrated, even if heterogeneity cannot be resolved, an integral value of depth averaged Darcy velocity can be obtained. This is a precious insight, comparable to the one obtained by pumping tests. In comparison, however, TRTs are closed applications without mass exchange, with little minor lateral and high axial range. Depth averaging integrates properties of unsaturated zone, aquifer and low permeability formation. An extension to facilitate also depth-dependent evaluation would be a DTS system with an integrated heating wire in the BHE-like enhanced TRT [e.g. *Fujii et al.*, 2009; *Acuña*, 2013]. By the same heat injection in different layers or compartments, the thermal response would allow distinguishing high from low velocity zones.

Simulation of heat transport at the BHE is improved by using superimposed line source equations. The most critical aspect is the lateral heterogeneity due to the discrepancy between grout and ground conductivity. By introducing a versatile correction factor that increases with estimated effective thermal conductivity and decreases with estimated effective Darcy velocity, this hurdle is overcome and robust parameter estimation is developed. Improvement potential lies in the applied line source model. Especially for shorter boreholes, a favorable choice is the finite moving line source model developed by *Molina-Giraldo et al.* (2011b). This variant also considers axial effects, and can be applied at similar computational effort. However, for conditions with substantial axial effects, the correction factor has not been employed, yet, and may need to be adjusted.

Despite the promising results, constructing a BHE and performing a TRT to exclusively characterize hydrogeology is not often favorable, because of the large involved investment costs for constructing a BHE and performance of the TRT. Instead, the potential of the new method is to complement standard interpretation of TRT. This does not only refer to future TRT applications, but we see a high potential in re-interpreting existing temperature time series of the numerous existing TRT applications worldwide, which for example, were

conducted associated with the strong geothermal development in Europe during the last decade.

5 Thermal tracer testing in a heterogeneous sedimentary aquifer: Field experiment and numerical simulation

Reproduced from: Wagner, V., Li, T., Bayer, P., Leven, C., Dietrich, P., Blum, P., (2013): Thermal tracer testing in a heterogeneous sedimentary aquifer. Hydrogeology Journal, 1-13, doi: 10.1007/s10040-013-1059-z. The final publication is available at link.springer.com.

Abstract: An active and short-duration thermal tracer test (TTT) was conducted in a shallow heterogeneous sedimentary aquifer at the Lauswiesen test site near Tübingen, Germany. By injecting 16 m³ of warm water at 22°C, a thermal anomaly was created, which propagated along the local groundwater flow direction. This was comprehensively monitored in five observation wells at a few meters distance. The purpose of this well-controlled experiment was to find out the practicability of such a TTT and its suitability to examine hydraulic characteristics of heterogeneous aquifers. The results showed that the thermal peak arrival times in the observation wells were consistent with previous observations from alternative field testing, such as Direct-Push Injection Logging (DPIL). Combined analysis of depth-dependent temperatures, peak arrival times and comparison with a numerical heat transport model offers valuable insights into the natural flow field and spatial distribution of hydraulic conductivities. We could identify vertical flow focusing and bypassing, which is attributed to preferential flow paths common in such sedimentary sand and gravel aquifers. These findings are fundamental for further development of experimental designs of active and short duration TTTs and provide a basis for a more quantitative analysis of advective and conductive transport processes.

5.1 Introduction

For decades, heat has been considered as a groundwater tracer. However, despite the positive experience from several field tests and a range of different applications, it is still not routinely used in hydrogeology. *Anderson* [2005] and *Saar* [2011] have presented comprehensive reviews of heat as a tracer. Recently, interest has been growing, particularly in using natural temperature variability to characterize surface water-aquifer interactions [*Doussan et al.*, 1994; *Conant*, 2004; *Schmidt et al.*, 2006; *Keery et al.*, 2007; *Constantz*, 2008; *Vogt et al.*, 2010; *Molina-Giraldo et al.*, 2011a], to reveal climate change effects [e.g. *Taniguchi et al.*, 1999; *Brouyère et al.*, 2004], for localization of preferential flow paths or fractures [e.g. *Leaf et al.*, 2012; *Pehme et al.*, 2013], or to trace back direct anthropogenic influences [e.g. *Ferguson and Woodbury*, 2007; *Engelhardt et al.*, 2013; *Menberg et al.*, 2013a]. Further studies concentrated on temperature-depth profiles to estimate vertical heat flux, vertical groundwater flux and thermal aquifers properties [e.g. *Taniguchi et al.*, 2003; *Lowry et al.*, 2007; *Kollet et al.*, 2009].

Natural temperature variability has especially been in focus when pronounced and measurable over long periods of time, for example, as vertical temperature profiles in a streambed, or as observed in seasonal or diurnal temperature fluctuations of groundwater. Such long-term time series can serve as important information to more reliably simulate processes in aquifers on different scales. For example, *Bravo et al.* [2002] applied groundwater temperatures to constrain parameter estimation in a groundwater flow model of a wetland system. *Rath et al.* [2006] and *Jardani and Revil* [2009] used synthetic test cases to demonstrate the usability of temperature measurements for numerical groundwater model inversion.

Significant and abrupt change of temperature in aquifers is less common in nature. In contrast, artificially generated cold or hot temperature anomalies, which can be caused by geothermal energy utilization, often exhibit such a pronounced and abrupt change. In the past, several injection-storage experiments were performed, and mainly deployed to examine the performance of aquifer thermal storage systems [ATES, e.g. *Sauty et al.*, 1982b; *Molz et al.*, 1983; *Xue et al.*, 1990; *Palmer et al.*, 1992; *Kocabas*, 2005; *Wu et al.*, 2008]. Such experiments are commonly conducted with large volume injections of hot water (thousands of m³) and with monitoring of aquifer temperature changes over a relatively long duration (months to years). Main objectives of such field tests are the assessment of hot water storage

capacity and/or recovery efficiencies in the target aquifer and model validation to simulate ATEs [e.g. *Ziagos and Blackwell*, 1986; *Xue et al.*, 1990; *Molson et al.*, 1992].

Sauty et al. [1982a; 1982b] conducted a series of aquifer storage experiments with single and doublet-well configurations and injection volume of 245 to 1680 m³ at the Bonnaud site in France. The temperature measurements were used to calibrate two numerical models. *Palmer et al.* [1992] performed a heat injection experiment at the Borden site in Canada, to investigate the feasibility of storing thermal energy in shallow unconfined aquifers near the water table. In a companion study, *Molson et al.* [1992] successfully validated a three-dimensional (3D) density-dependent numerical flow and transport model using the field data. They demonstrated that processes of heat convection, dispersion, diffusion, retardation, buoyancy and boundary heat loss can be represented by their model. They also emphasized the importance of the vertical surface heat loss mechanism when long-term thermal storage is concerned near the water table. *Shook* [1999; 2001] suggested predicting temperature signals from conservative tracer breakthrough curves (BTC) through variable transformation, for example, by applying thermal retardation factors. This was demonstrated for homogeneous test cases and for heterogeneous conditions when thermal conductivity and dispersion can be neglected as second-order effects.

When using heat as a tracer, there is another type of application, called ‘thermal tracer test’ (TTT) or active TTT [e.g. *Leaf et al.*, 2012]. The utilization of TTT is mainly for aquifer characterization, in which warm (or cold) water is injected as a tracer into the aquifer and then temperature changes are measured in the injection well and/or in nearby observation wells. These tests are different from the above-mentioned studies for thermal storage in injection volume and experimental scale, as well as duration (normally only for a few days in TTT, Table 15). *Keys and Brown* [1978] presented a field study of TTT in the High Plains of Texas, USA. They conducted three artificial recharge experiments with various injection water volumes and rates. The recharged water was supplied from a lake, where the water temperature fluctuated between 13-23°C, and provided thermal pulses recorded in the groundwater temperature logs. By evaluating the thermal pulses they identified contrasts in the horizontal groundwater velocity of the studied area. *Macfalane et al.* [2002] reported an injection/pumping experiment in west-central Kansas, USA. They injected about 360 m³ of heated water (73°C) at one well and then pumped from the other well at about 13 m distance. A distributed optical-fiber temperature-sensing device (DTS) was used for monitoring the

temperature changes under transient conditions, and vertical temperature profiles were recorded from the production well. This study estimated a groundwater velocity from the temperature profiles, which was comparable to that derived from previous pumping tests. DTS was also applied in recent related work by *Leaf et al.* [2012], who examined a porous fractured sandstone aquifer using open-well thermal dilution tests in two wells near Madison, Wisconsin. Their tests only provided information on the borehole flow regimes and not on the spatial heterogeneity of the aquifer. They demonstrated that DTS measurements are a suitable alternative to standard heat pulse methods or spinner flow meters. *Read et al.* [2013] presented a TTT in a fractured aquifer at the Ploemeur site in Brittany, France (Table 15). They determined a pronounced retardation of the BTC in a monitoring well compared to the one of a solute tracer. *Read et al.* [2013] explained this observation by the stronger fracture-matrix interaction of the thermal tracer.

Vandenbohede et al. [2008a; 2008b] reported their experience from two single-well push-pull tests, which they conducted in a deep aquifer in the Belgian coastal plain. The tests were designed to evaluate the performance of a planned ATES, but the data was further interpreted to study the differences between solute and heat transport in *Vandenbohede et al.* [2008a]. The temperature of the injected water for both tests was about 11.5°C, and slightly colder compared to the ambient aquifer temperature of 15.8°C. The tests, including injection, rest and extraction phase were performed in periods of 9 - 22 days, with rates of a few m³ per hour. A numerical model was adopted to simulate the field tests [*Vandenbohede et al.*, 2008a]. After comparing the simulated results on solute (chloride) and heat transport, they concluded that for a push-pull test, the most sensitive parameter in solute transport is solute longitudinal dispersivity and in heat transport it is thermal diffusivity. *Ma et al.* [2012] applied a numerical model of a complex aquifer-river system to discuss the role of variable density and viscosity assumptions on heat transport modeling (Table 15). They observed that up to a maximum temperature difference of 15°C in the model domain, the assumption of constant fluid density and viscosity appears to have only minor effect on the simulated temperature distribution [*Ma and Zheng*, 2010]. They also state that this is valid for any heat transport model and for various field conditions. All studies on TTT successfully demonstrated that aquifer structures and/or properties can be evaluated from monitoring groundwater temperatures. However, active TTT is still not a standard method for aquifer testing.

Table 15 Overview of active, short term (< 12 days) thermal tracer tests reported in the literature.

| Location | Aquifer type | Injected volume (m ³) | Injection rate (m ³ h ⁻¹) | Temperature difference (K) | Injection time (h) | Duration (day) | Observation wells | Remarks | Reference |
|--------------------------|--|-----------------------------------|--|----------------------------|--------------------|----------------|-------------------|--|------------------------------------|
| Stewart site, Texas, USA | Unconsolidated porous aquifer | 32,832 | 3283 | -2.3 to +7.7 | 240 | 10 | 5 | Natural gradient test; variable injection temperature | <i>Keys and Brown</i> [1978] |
| Bonnaud site, France | Confined porous aquifer | 245 to 1680 | 2.9 to 7.5 | ≈+18 to 25 | 72 to 480 | 8 to 184 | 11 | Seven experiments; single-, doublet-, cyclic-type | <i>Sauty et al.</i> [1982a] |
| Kansas, USA | Porous fractured sandstone aquifer | 359.6 | 2.5 | +55 | 173 | 7.2 | 1 | Forced gradient test, one production and one observation well | <i>Macfarlane et al.</i> [2002] |
| Coastal plane, Belgium | Deep fine sand confined porous aquifer | 188 | 3.9 | -4.3 | 48.15 | 9.2 | - | Only short term push and pull test | <i>Vandenboheide et al.</i> [2009] |
| Hanford site, USA | Unconfined and unconsolidated porous aquifer | 156 | 16.3 | -7.8 | 9.75 | 11.8 | 28 | Parallel solute and thermal tracer test | <i>Ma et al.</i> [2012] |
| Wisconsin, USA | Porous fractured sandstone aquifer | Not specified | 0.6 to 0.8 | +2 to 7 | 2.6 to 3 | 0.2 to 0.3 | - | Three open-well thermal dilution tests; wells intersect several aquifers | <i>Leaf et al.</i> [2012] |
| Ploemieur site, France | Fractured basement aquifer | 32.1 | 2.1 | ≈+35 | 11 | 0.67 | 1 | Forced gradient test, one production and one observation well | <i>Read et al.</i> [2013] |
| Lauswiesen site, Germany | Unconfined shallow porous aquifer | 16 | 1.0 | +11 | 8.0 | 4 | 5 | Natural gradient test | This study |

The current study examines viability and usability of the TTT for characterization of a shallow heterogeneous aquifer at the Lauswiesen test site close to Tübingen, Germany. An active, small-scale and short-term TTT was performed with warm water injection in the well-known unconfined porous aquifer (Table 15), and the resulting temperature anomaly was monitored in five downgradient observation wells. For the interpretation, well- and depth-specific temperature time series are evaluated with emphasis on maximum observed temperature changes and peak arrival times. A numerical flow and heat transport model is set up to simulate the experiment and identify effects from aquifer heterogeneity. We ask to what extent spatial hydraulic heterogeneity and density effects influence the thermal tracer propagation. This is complemented by comparison to the findings from an alternative field investigation, the direct-push injection logging (DPIL), at the same site [Lessoff *et al.*, 2010].

5.2 Thermal tracer test set up at Lauswiesen site

5.2.1 Study site

The Lauswiesen test site is located near the city of Tübingen in southwest Germany (Fig. 28), where numerous investigations have previously been performed to study aquifer properties [e.g. Rein *et al.*, 2004; Riva *et al.*, 2006; Lessoff *et al.*, 2010; Händel and Dietrich, 2012]. The test site is part of a heterogeneous alluvial aquifer located close to the Neckar River. The injection well is around 60 m away from the river. The aquifer consists of loosely packed Quaternary sandy gravel, overlain by Quaternary silty clay and clayey gravel. As observed in previous studies by Bou Ghannam [2006] and Schneidewind [2008], the aquifer can be divided into two major zones: The first zone reaches down to 6 m below land surface (bls) and consists of sand and gravel, with a small portion of fines. Based on these studies, it can be assumed that the first layer is more homogeneous than the second layer, which ranges from 6-10 m bls. According to soil sample analyses from Sack-Kühner [1996], the portion of fines increases in the lower part of the aquifer below 7 m bls. This lower part of the aquifer appears to be more heterogeneous with partly lower permeable zones and pronounced local anisotropies. The Lauswiesen aquifer is underlain by Triassic marl and clay stones (Middle Keuper), which form a natural aquitard. The water table at the site is about 4 m below surface, but can vary several decimeters due to the proximity of the Neckar River. The hydraulic gradient of Lauswiesen is estimated to be around 0.2-0.3%. The hydraulic conductivity of the aquifer was measured in several field campaigns using a variety of techniques, yielding average values in the range of $K = 2-3 \times 10^{-3} \text{ m s}^{-1}$ [Sack-Kühner, 1996; Lessoff *et al.*, 2010].

Using a multilevel-multi-tracer field experiment, *Riva et al.* [2006] determined an average effective porosity of 9.8% for the test site. Thus, the average and natural groundwater flow velocity towards the Neckar River is around 5.5 m day^{-1} at the site.

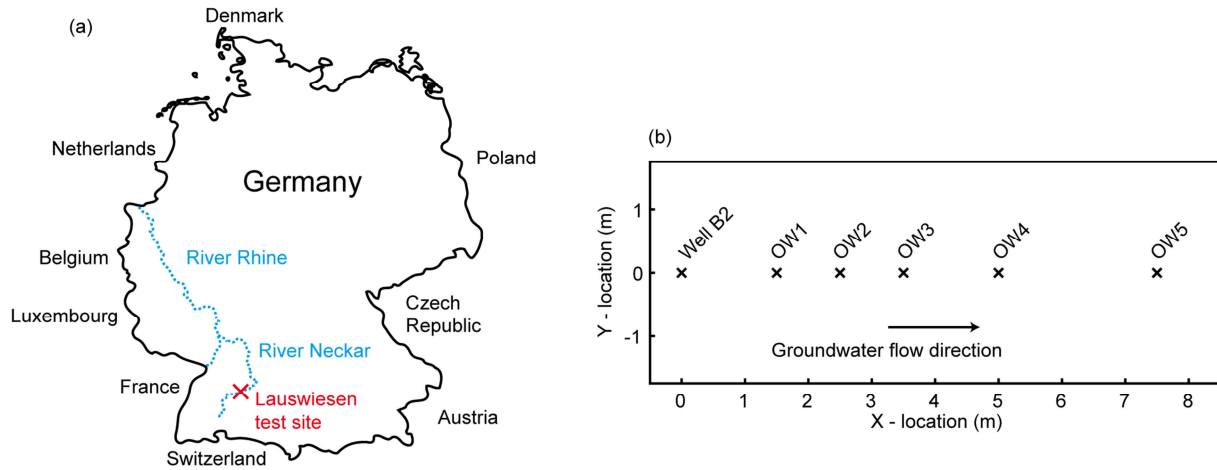


Fig. 28. a) Location of the Lauswiesen test site, close to Tübingen, SW Germany. (b) Plan view of setup of the thermal tracer test. Well B2 ($x = 0$, $y = 0$) was used as injection well and OW1 – OW5 served as observation wells during the test.

5.2.2 Thermal tracer test

The main groundwater flow axis through the chosen experimental area was determined from groundwater contour maps based on water level measurements done over a two-month period in existing monitoring wells, before the installation of the observation wells. The configuration of the wells for the TTT at the Lauswiesen site is outlined in Fig. 28. Thermal tracer injection was performed in a fully penetrating well, B2 (Table 16). For the tracer monitoring, five fully penetrating observation wells OW1-OW5 (1" diameter) were installed along the pre-determined main groundwater flow axis with various spacing (Table 16). The reason of using small diameter observation wells for TTT was to minimize the effect of free convection within the well column, so that the measured fluid temperature in the observation wells could more accurately represent the temperature in the surrounding solid/fluid matrix [*Leaf et al.*, 2012].

Table 16 Information on the wells used for the thermal tracer test at the Lauswiesen site.

| Well | Distance from the injection well B2 (m) | Screen length (m) | Inner well diameter (mm) | Material |
|------|---|-------------------|--------------------------|--------------------|
| B2 | 0.0 | Fully screened | 150 | PVC ¹⁾ |
| OW1 | 1.5 | 6 | 25 | HDPE ²⁾ |
| OW2 | 2.5 | 4 | 25 | HDPE ²⁾ |
| OW3 | 3.75 | 4 | 25 | HDPE ²⁾ |
| OW4 | 5.0 | 4 | 25 | HDPE ²⁾ |
| OW5 | 7.5 | 4 | 25 | HDPE ²⁾ |

¹⁾ Polyvinylchloride; ²⁾ High density polyethylene

For the preparation of the thermal tracer approximately 16 m³ of groundwater were pumped out from the aquifer and then stored in a basin. As the experiment was conducted in summer time, during a warm weather period, the extracted water could be heated in the sun to about 22°C. Groundwater temperatures in the aquifer were continually monitored before the injection in every installed observation well and recorded showing an average initial temperature T_0 of $11.02 \pm 0.30^\circ\text{C}$. Temperature measurements were acquired using chains of PT-100 thermistors (Platinum Thermometer, resolution 0.01°C): For each temperature chain ten PT-100 sensors are attached with a spacing of 0.5 m to a transmission cable which is connected to a data reading unit (Fig. 29). Two temperature sensors (OW4; 7.2 m bls and OW5; 8.2 m bls) were damaged during the installation and therefore, both sensors were omitted for the experiment. During operation, measurements from each sensor are transmitted to a reading device at the land surface and recorded manually. The induced head changes from the injection were manually recorded in irregular time steps. The constant injection resulted in 3 cm of increase in hydraulic head at the injection well during the whole injection period.

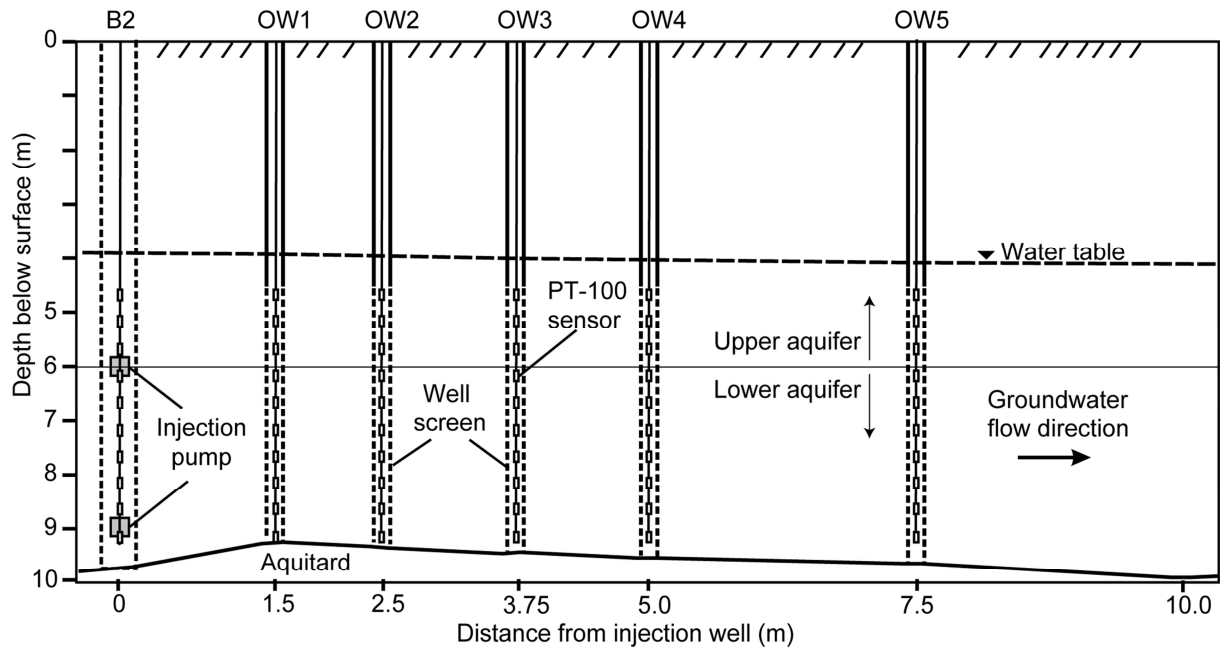


Fig. 29. Vertical cross-section along the well axis (x) showing positions of wells (B2, OW1 – OW5), water table, aquifer and aquitard.

During the injection period, the heated water was introduced as a thermal tracer from two injection units in B2 at 6 m and 9 m bls, both with constant rates of $2 \times 1 \text{ m}^3 \text{ h}^{-1}$ using two Grundfos MP1 pumps. Temperature changes were then monitored simultaneously in all observation wells and in the injection well B2. At the early phase of the experiment, measurements were taken more frequently (every 30 minutes). The injection ended after 8 hours (0.33 days), while the temperature monitoring was continued until the end of experiment, which was terminated after about 100 hours (4.2 days) after the start of injection.

5.2.3 Direct-push injection logging

Lessoff et al. [2010] applied the direct-push injection logging (DPIL, [*Dietrich et al.*, 2008]) and direct-push slug test (DPST, [*Butler et al.*, 2002]) for characterizing the spatial structure of hydraulic conductivity (K) at the Lauswiesen site test. They could demonstrate that the 258 measurements of relative conductivity (K_r) using DPIL are compatible with results from other more conventional methods performed at the site. All recorded DPIL-profiles (Fig. 30) are within a radius of 15 m around the injection well of the TTT. One DPIL-profile was directly obtained at the injection well and two profiles at the observation wells OW4 and OW5, which were also used for the TTT. The profiles are highlighted in Fig. 30 and will be compared to the TTT results of this study. All measured K_r values indicate that there is a significant difference in the hydraulic conductivities of the upper and lower part of the aquifer. A more

detailed inspection of the profiles from B2, OW4 and OW5 reveals that the transition between the upper and the lower part of the aquifer is not at constant depth. *Lessoff et al.* [2010] deduced from the DPIL-profiles, that the upper part of the aquifer is more conductive and more homogenous than the lower part. Moreover, all three profiles show local maxima of K_r at certain depths (e.g. OW4 at a depth of 6.4 m bls, OW5 at a depth of 7.4 m bls).

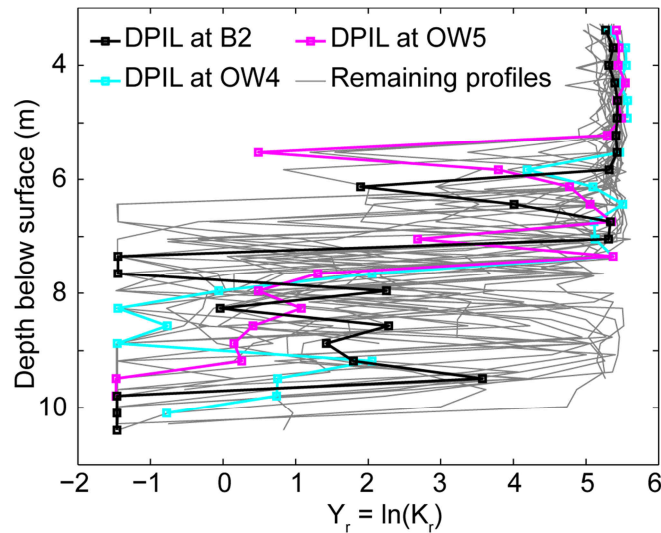


Fig. 30. Compound profiles of $Y_r = \ln(K_r)$ obtained from DPIL measurements within a radius of 15 m around the injection well of the TTT. The three DPIL profiles that are taken from observation wells also monitored during the TTT are highlighted. The DPIL measurements are extracted from the study of *Lessoff et al.* [2010].

5.2.4 Numerical model

Based on the existing knowledge of the Lauswiesen site, it is assumed that the subsurface can be represented by a layered unconfined aquifer with an underlying aquitard. A numerical model was set up using FEFLOW [Diersch, 2009a] to simulate the TTT with the injection of warm water in the aquifer and the transport of the heated groundwater through the sedimentary strata. Analogous to the TTT at the Lauswiesen site, the model contains 5 observation wells (Fig. 31). These are positioned in the centre of the model domain, where the TTT is simulated. The total size of the numerical model is 130 m \times 26 m \times 15 m (width \times height \times depth). This size is considered large enough to minimize boundary effects at the injection and observation wells. The total area is discretized with 30,656 triangle prismatic elements with an increasing resolution of the numerical mesh towards the well transect. The distance between the numerical nodes decreases from the model boundary to the well transect by a factor of 40.

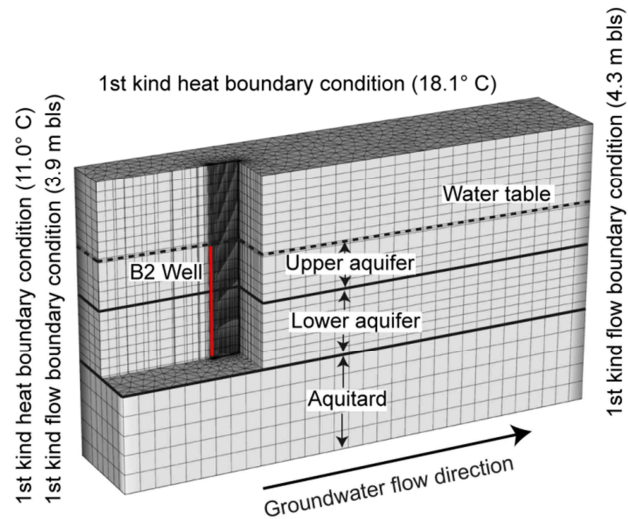


Fig. 31. Three-dimensional sketch of the model domain, numerical mesh, hydraulic and thermal boundary conditions. Values used as hydraulic and thermal boundary condition are specified in brackets.

The simulated stratified aquifer is separated in an upper and a lower part as suggested by the results of *Lessoff et al.* [2010]. In the upper part of the aquifer, a free water table is simulated to account for a potential mound of the water table due to injection of water. This groundwater mound may affect the flow field, especially close to the injection well. Unsaturated flow is calculated by applying the Richards equation, and the model allows for heat exchange between aquifer and unsaturated zone.

Fixed hydraulic heads are assigned at the inflow and outflow boundary of the model, and no flow at the remaining boundaries. The fixed heads are set to ensure a horizontal hydraulic gradient of 0.003 along the well transect and a height of the water table of 4.0 m bls at B2 as measured before the TTT. On the upstream model boundary, a hydraulic head of 3.9 m bls is assigned and on the opposing site a value of 4.3 m bls. The temperatures of the inflowing groundwater and at the surface are similarly controlled by Dirichlet boundary conditions. The temperature of the inflowing groundwater and at all aquifer model edges is set to 11.0°C. This value was obtained from groundwater measurements before the TTT started. At the top of the model, the temperature is set fixed at 18.1°C, gradually declining to the groundwater temperature at the lateral unsaturated boundaries. This value was derived from linear extrapolation of temperature values obtained before the tracer injection in the section of the unsaturated zone (from the water table to 2.2 m bls).

The injection well, B2, is represented by a well module integrated in FEFLOW, which assigns a given extraction or injection rate to all nodes of the well. To realistically reproduce the conditions of the heated water injection, a combination of a temperature and the described well boundary condition is applied. For the injection phase (0 to 8 h) water is injected in the aquifer at a constant rate along the well screen. The temperature of the injected water is stated by a Dirichlet boundary condition. After the injection phase (> 8 h after start of the injection), both boundary conditions referring to the injection well are deactivated.

Hydraulic and thermal parameters for the three model layers are subsequently calibrated by fitting simulated to measured temperatures during the TTT. The possible ranges of hydraulic conductivities of the three layers are derived from previous studies at this site. *Lessoff et al.* [2010] suggest an integral hydraulic conductivity of $3 \times 10^{-3} \text{ m s}^{-1}$. *Riva et al.* [2006] compiled the results of several sieve analyses and determined different cluster groups with hydraulic conductivity values, K , between $3 \times 10^{-4} \text{ m s}^{-1}$ and $5.9 \times 10^{-3} \text{ m s}^{-1}$. We selected these two values as initial assumptions for the two layers, with the upper aquifer layer being more conductive as the integral parameter suggested by *Lessoff et al.* [2010]. A range of $\pm 50\%$ uncertainty is then defined for the calibration. Furthermore, we assume that the aquitard has a significantly lower hydraulic conductivity of $1.0 \times 10^{-9} \text{ m s}^{-1}$. A constant effective porosity of 9.8%, as suggested by *Riva et al.* [2006], is set for the entire aquifer.

No measurements of the thermal conductivity and the heat capacity exist for the Lauswiesen test site. However, these parameters only show a small variability in sedimentary aquifers and may be well estimated by adopting values from other work: *Parr et al.* [1983], *Palmer et al.* [1992] and *Markle et al.* [2006] examined thermal properties of porous aquifers similar to the one at the Lauswiesen site. Based on the values and ranges reported therein, we chose $c_{pm} = 2.8 \pm 0.3 \times 10^6 \text{ J m}^{-3} \text{ K}^{-1}$ and $\lambda_m = 2.2 \pm 0.5 \text{ W m}^{-1} \text{ K}^{-1}$. The thermal properties of the aquitard are estimated assuming a pure clay stone layer (Table 17). Volumetric heat capacities are derived from the study by *Clauser* [2011], and the corresponding thermal conductivity values are extracted from *Domenico and Schwartz* [1998]. The longitudinal thermal dispersivity is estimated based on the empirical relationship by *Neuman* [1990]:

$$\alpha_l = 0.017L_s^{1.5} \tag{5-1}$$

where the travel distance L_s is considered to be the maximum distance between the source and the most distant observation well. The transversal dispersivity is set to one tenth of the

longitudinal one [e.g. *Molina-Giraldo et al.*, 2011a]. For this TTT experiment, L_s , is 7.5 m and thus we derive a first estimate of $\alpha_l = 0.34$ m. Due to the substantial uncertainty in this parameter value, for the calibration feasible ranges from 0 to 0.68 m are defined. Since mechanical thermal dispersion is not expected to be relevant for the diffusion-dominated transport in the Aquitard, a small fixed value of $\alpha_l = 0.01$ m is set in the numerical model.

5.2.5 Evaluation methodology

The analysis of the recorded TTT data focuses on the development of the thermal plume and the governing transport processes in the porous aquifer. Injection of warm water induces a dynamically evolving thermal anomaly in the aquifer. We focus on the temperature change ΔT , which is determined by the difference between initial temperature and measured temperature values. Propagation of the warm water is seen in the wells by recorded thermal breakthrough curves (BTC). As diagnostics of the BTC, we choose the maximal observed temperature change ΔT_{peak} and the peak arrival time t_{peak} . The ΔT_{peak} values are determined by scanning each measured temperature curve for the global temperature maximum. Thus, the peak arrival time t_{peak} is the corresponding point of time for which the temperature maximum is detected. According to *Bellin and Rubin* [2004], evaluation of t_{peak} has several advantages to examine tracer BTCs. It is not so much interfered by infrequent sampling, and missing of early or late parts of the signal or measurements below the detection level is not as problematic as it is for the analysis of moments of the BTC. These interferences, which could hamper BTC interpretation, are also seen as critical for the TTT at the Lauswiesen site.

The influence of different transport processes can be quantified by dimensionless numbers. To analyze the ratio between advection and thermal conduction, the macroscopic Peclet number is defined as [e.g. *Ma et al.*, 2012]

$$Pe = \frac{c_{pw} v_D l}{\lambda_m} \quad (5-2)$$

where c_{pw} is the volumetric heat capacity of water ($c_{pw} = 4.2 \times 10^6 \text{ J m}^{-3} \text{ K}^{-1}$), v_D the Darcy velocity and l the characteristic length, which is a length specifying changes in the temperature (e.g. here total length of the observation well transect with 7.5 m).

The importance of considering density effects can be evaluated by calculating the ratio between the vertical buoyancy force and the horizontal friction force from regional groundwater flow. *Oostrom et al.* [1992] defined a stability number G as

$$G = \frac{K \frac{\Delta\rho}{\rho_0}}{v_D} = \frac{\Delta\rho}{i\rho_0} \quad (5-3)$$

where i is the hydraulic gradient, ρ_0 is the reference density of the thermally undisturbed aquifer and $\Delta\rho$ is the induced density difference. *Oostrom et al.* [1992] experimentally determined a critical value of $G_c = 0.3$, where the transition from a stable to an unstable plume set in.

5.3 Results and discussion

During the TTT the vertical temperature profiles were recorded for four days in the injection well B2 and in the five downgradient observations wells (OW1-5). The measurements are shown in Fig. 32 as thermoisopleth graphs, which visualize the time-dependent evolution of the temperatures in the Lauswiesen aquifer cross-sections. In the same manner the results of the numerical simulation are presented in Fig. 33. In the following, first the calibration of the numerical model is presented and then the temperature development at the injection well is discussed. Next, the effects of hydraulic heterogeneity and induced density differences are examined. Then the heat transport in the down gradient observation wells is discussed in more detail. Finally the findings of the TTT are compared to those from previous DPIL measurements.

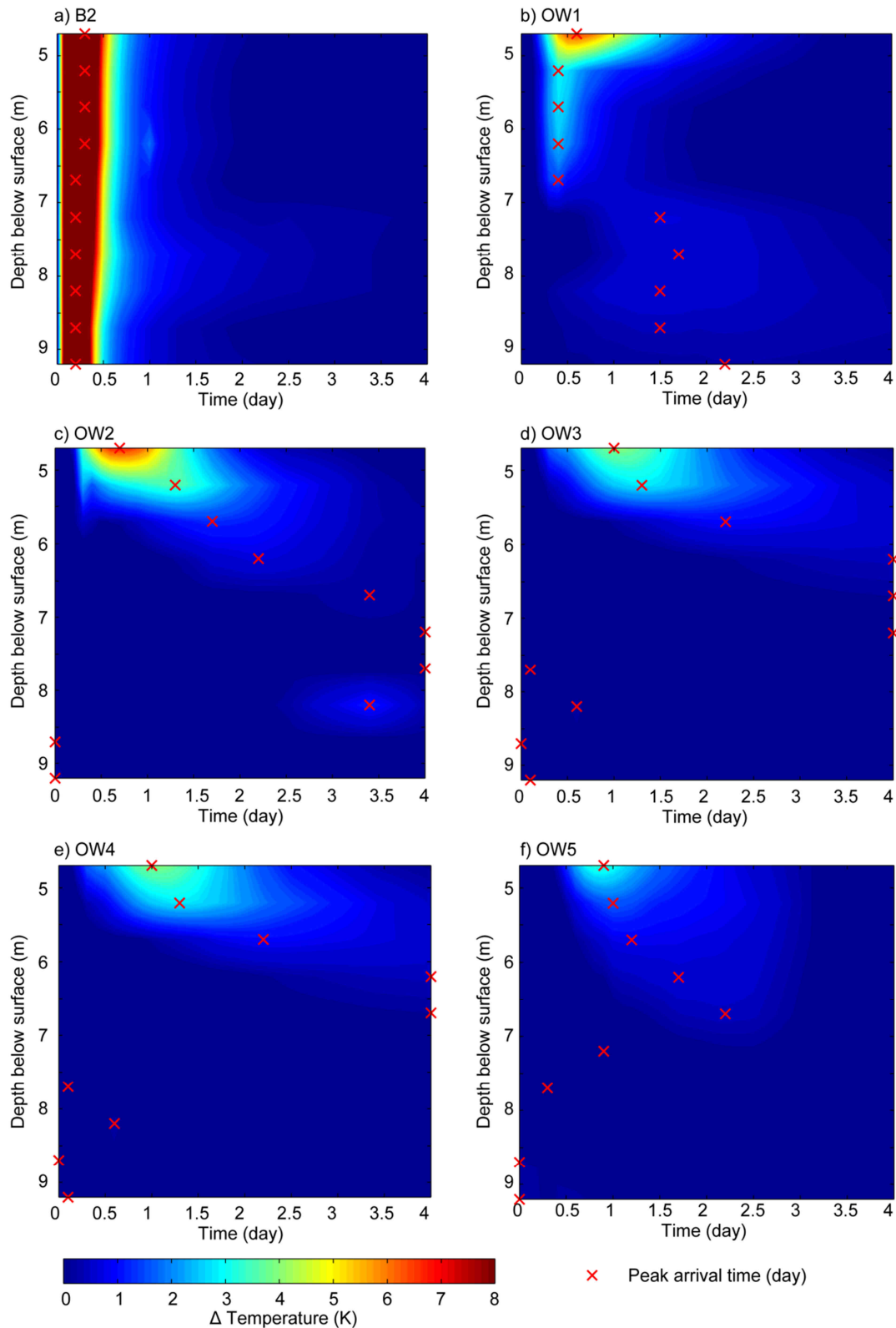


Fig. 32. Measured depth related temperature development over the entire experimental period. The temperature change is calculated based on the initial temperature at the start of the experiment. Additionally, temperature peak arrival times for every measurement location are emphasized; a) injection well B2; b)-f) observation wells OW1-5. For interpolation the MATLAB[®]-function `contourc` is used.

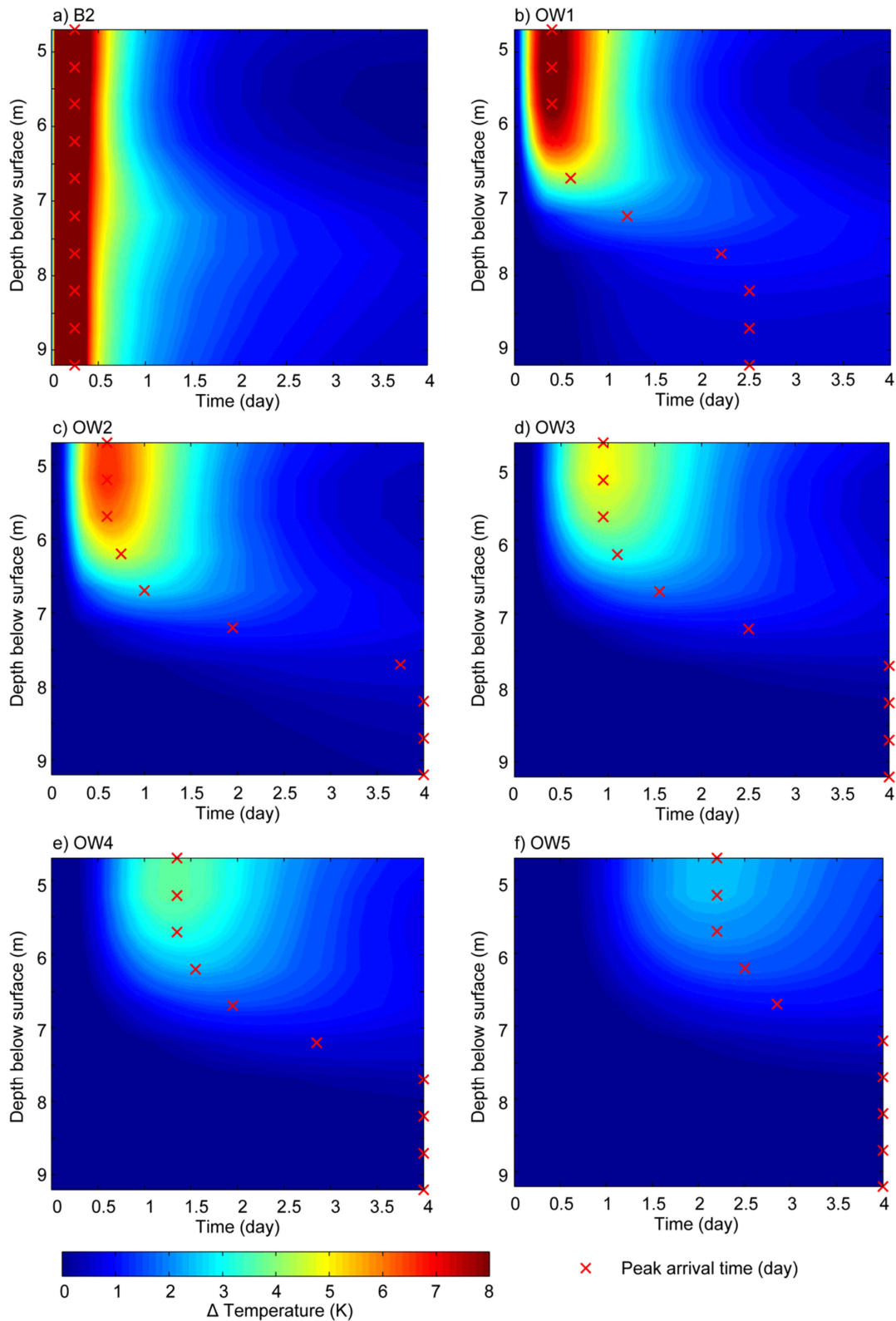


Fig. 33. Simulated depth related temperature development over the entire experimental period using the numerical heat transport model. The temperature change is calculated based on the initial temperature at the start of the experiment. Additionally, temperature peak arrival times for every measurement location are emphasized; a) injection well B2; b)-f) observation wells OW1-5. For interpolation the MATLAB[®]-function `contourc` is used.

5.3.1 Calibration of the numerical model

For the calibration, we considered mean, minimal and maximal values of the uncertain flow and transport parameters of the two aquifer layers K , λ_m , c_{pm} , and α_l . Preliminary testing revealed that simulated results are least sensitive to the thermal properties and strongly controlled by the hydraulic conductivity. Consequently, thermal properties and dispersivity, which are not expected to substantially vary in the aquifer, were assumed to be the same for both aquifer layers. The hydraulic conductivities were individually calibrated for each layer. Thus, $3^4 = 81$ value combinations were tested, and the best fit between simulated and measured groundwater temperatures at injection and observation wells during the TTT is chosen for further analysis (Table 17).

For the thermal transport parameters of the aquifer we derived $\alpha_l = 0.68$ m; $c_{pm} = 2.5 \times 10^6$ MJ $m^{-3} K^{-1}$; $\lambda_m = 2.7$ W $m^{-1} K^{-1}$. The obtained hydraulic conductivity of the more conductive upper aquifer layer is 8.9×10^{-3} m s^{-1} and the value of the lower one is 4.5×10^{-4} m s^{-1} . The model with this parameter set results in a root mean squared error (RMSE) between all simulated and measured BTCs of $0.65^\circ C$. This misfit highlights that the numerical model may capture the main thermal transport processes in the aquifer, but is not capable of fully reproducing the observed temperature evolution, which is comprehensively discussed in the following chapters.

Table 17 Hydraulic and thermal parameter ranges applied for the numerical simulation. Values in **bold** are used to generate the numerical results which are further analyzed.

| | | Hydraulic conductivity K (m s^{-1}) | | Volumetric heat capacity c_{pm} (MJ $m^{-3} K^{-1}$) | Thermal conductivity λ_m (W $m^{-1} K^{-1}$) | Longitudinal dispersivity α_l (m) |
|--------------------------|--------|---|--|--|--|---|
| | | Lower part | Upper part | | | |
| Aquifer (and gravel) | Min | 1.5×10^{-4} | 3.0×10^{-3} | 2.5×10^6 | 1.7 | 0.01 |
| | Median | 3.0×10^{-4} | 5.9×10^{-3} | 2.8×10^6 | 2.2 | 0.34 |
| | Max | 4.5×10^{-4} | 8.9×10^{-3} | 3.1×10^6 | 2.7 | 0.68 |
| | | | | | | |
| Aquitard (clay stone) | Min | 1.0×10^{-9} | | 2.3×10^6 | 1.1 | 0.01 |
| | Median | 1.0×10^{-9} | | 2.3×10^6 | 1.1 | 0.01 |
| | Max | 1.0×10^{-9} | | 2.3×10^6 | 1.1 | 0.01 |

5.3.2 Temperature evolution at injection well

First the temperature evolution at the injection well B2 is inspected. The temperature changes measured are illustrated in Fig. 32a. Small vertical variability indicates that a homogenized line-source with a temperature of $22.4 \pm 0.5^\circ C$ ($\Delta T = 11.4$ K) was created below the water table during the injection experiment ($t < 0.33$ d). Proper mixing of the injected thermal tracer and the groundwater in and around the well was achieved, and after the warm water injection,

only a slight vertical variability in the temperature is observed. Even if this variability is only marginal, it can be seen that long-term cooling is most pronounced at the bottom and highest temperatures appear in the lower section at about 7.2 m bls. This pattern of the temperature signal could be interpreted as a first indication of non-uniform horizontal groundwater movement with lower advective flow velocity in the lower part of the aquifer. Minor long-term cooling at the bottom may be attributed to slight vertical heat loss due to conduction into the aquitard beneath.

The numerical simulation for B2 shows a very similar development of the temperature in the injection well (Fig. 33a). However, a closer look reveals that after the injection, the thermal anomaly is more persistent. A possible explanation for this observation is that the assumption of a thermal equilibrium between solid and fluid phase in the numerical model, is not instantaneous in the vicinity of the injection well. Hence, less heat is stored in the subsurface than expected based on the simulation, particularly during the fast injection of the warm water. As a consequence, after the injection period also faster cooling rates are measured than observed for thermally equilibrated conditions in the numerical simulation (Fig. 33a). After one day, increased temperatures are still apparent in the model, especially at the central and lower profiles. There is a temperature maximum in the injection well at a depth of around 7.2 to 7.7 m bls (Fig. 33a). Apparently, as observed in the field and in the model, the aquitard (and lower aquifer layer) temporally stores and slowly releases thermal energy at the injection well.

5.3.3 Density effects vs. hydraulic heterogeneity

Due to layering of the aquifer, advective forces in the more permeable layer dictate and focus thermal breakthrough in the upper part of the aquifer. This is confirmed by applying the values used for the calibrated numerical model to calculate the layer-specific Peclet numbers, Pe (Table 17, Eq. 5-2). For the upper part of the aquifer $Pe = 420$ and for the lower part $Pe = 21$. Therefore, heat transport in both parts of the aquifer is dominated by advection, however, it is more pronounced in the upper part. In comparison, for the aquitard Pe is only 9×10^{-5} , indicating conduction dominated conditions in the aquitard.

The next observation well in the regional groundwater flow direction, OW1, positioned just 1.5 m downgradient of the injection well, reveals that the moving warm water only leaves a trace in the upper layer of the aquifer with a peak value of $\Delta T_{peak} = 6.6$ K (Fig. 32b). In

comparison with the numerical model (Fig. 33b), significant temperature changes are only detected in the upper most part of the aquifer. At first sight, this observation may be a sign of density effects, however, for example, following previous studies by *Hecht-Méndez et al.* [2010], *Ma and Zheng* [2010], *Ma et al.* [2012] and *Leaf et al.* [2012], such effects are expected to be negligible given the small temperature range and the short duration of the performed TTT experiment. Hence, a more plausible reason could be hydraulic heterogeneities within the upper layer with highest advection on top of the profile.

Further insight provides the stability criterion, G_c , according to *Oostrom et al.* [1992]. Based on a groundwater density of 999.6 kg m^{-3} for 11°C , and an undisturbed hydraulic gradient of $i = 0.003$, a maximum possible density change of 0.9 kg m^{-3} would be acceptable to avoid buoyancy effects ($G \leq G_c = 0.3$). During the TTT at the Lauswiesen site, the maximal density change by temperature increase from 11°C to 17°C is $\Delta\rho = 0.9 \text{ kg m}^{-3}$. Consequently, the resulting value of $G = 0.3$ indicates that density effects could not be completely ruled out (Eq. 5-3). However, temporary warm water infiltration yields transient conditions with a head build up at the injection well, and thus during injection the local hydraulic gradient is increased at the injection well B2 ($i > 0.003$). As a result, the maximum ΔT can be expected to be higher than the limit of $\Delta T = 6 \text{ K}$ obtained from a calculated density difference based by Eq. 5-3 for undisturbed flow conditions. Furthermore flow field changes are most pronounced very close to the injection well and even under well-controlled experiments, induced small-scale lateral and vertical flow components may be significant. Since hydraulic heads have not been continuously monitored during the experiment, clear quantitative evidence from the field cannot be provided.

5.3.4 Downgradient propagation of the thermal plume

The focus of the thermal plume in the uppermost part of the well is also observed in the more downgradient observation wells. Accordingly, the numerical model overestimates the vertical extension of the plume throughout the experiment. These observations may be influenced by measurement inaccuracies: The experiment is possibly prone to technical artifacts, like intra borehole convection, which is not considered in the numerical simulation either. Slight vertical warm water flow in the wells could have smeared the plume. Therefore, caution is given when interpreting the measured temperature trends at the wells. In further analysis, we favor the peak arrival time as a potentially more robust criterion. The values of t_{peak} are marked as red crosses in Fig. 32 and Fig. 33 for each sensor position.

The lower aquifer has a lower hydraulic conductivity, assuming that differences in pronounced t_{peak} are mainly controlled by different horizontal advective flow velocities. Thermal effects are minimal in the lower part of the aquifer (6 – 10 m bls). As a consequence of the small signal to noise ratio, the t_{peak} in the lower part the aquifer cannot be well determined. This is in line with the simulated results. The model predicts (Figure 6) here that during the TTT no thermal peak passes OW2-5, because obtained t_{peak} values are at the end of the experiment.

Under ideal conditions, the result of a TTT would show later t_{peak} values for the more downgradient wells with a decrease of ΔT_{peak} . Advection would move the peaks in the upper layer in flow direction from OW1 to OW5, and diffusion and mechanical dispersion would lead to a longitudinal thermal plume spreading and transversal heat loss. This ideal transport behavior can be seen in the numerical simulation (Fig. 33). There is a gradual decline of the numerically obtained peak temperatures with increasing distance of observation well from injection well. For example, the temperature differences at a depth 4.7 m bls are $\Delta T = 8.5$ K (OW1) to 6.6 K (OW2), 4.9 K (OW3), 3.8 K (OW4), and 2.5 K (OW5).

The measured temperature values follow a similar trend as those simulated by the model, but with some deviations. As expected, temperature differences are least pronounced at the most distant observation well OW5 (Fig. 32f). Measured and simulated t_{peak} agree well in the closest OW1. However, there is no gradual decline in the wells closer to the injection well. Peak temperatures on top of the screened section (4.7 m bls) change from $\Delta T = 6.6$ K (OW1) to 6.8 K (OW2), 4.0 K (OW3), 4.7 K (OW4), and 3.3 K (OW5). Furthermore, peak arrival times recorded at the upper sensor do not increase with distance.

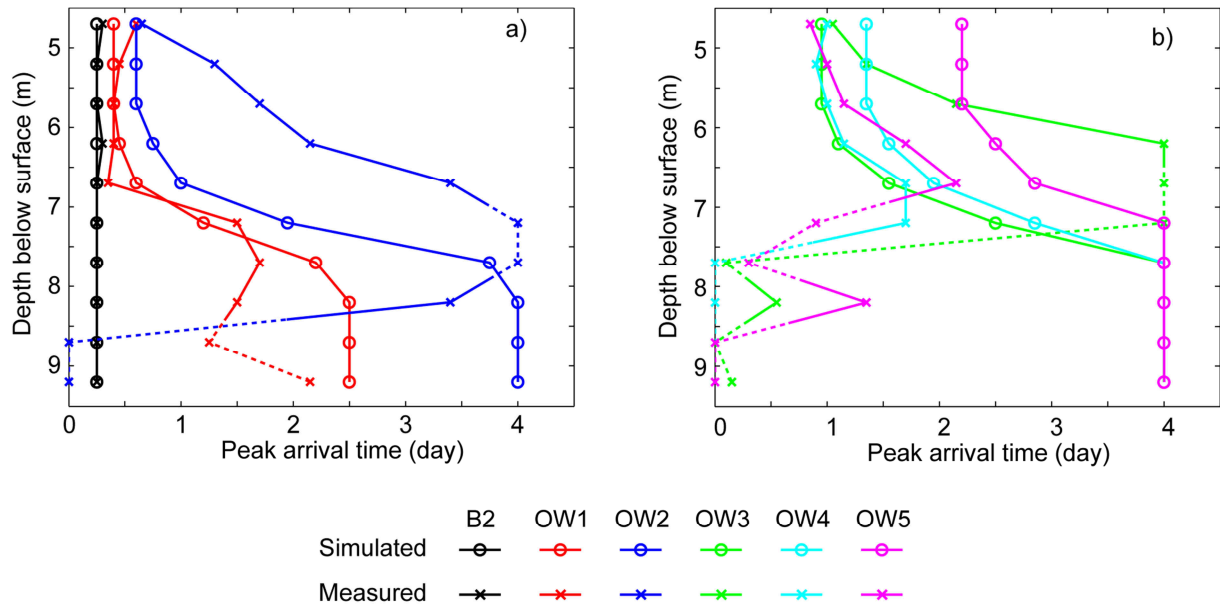


Fig. 34. Comparison of the peak arrival times (t_{peak}) measured and simulated for the TTT experiment. a) B2, OW1 and OW2; b) OW3-5. Dashed lines indicate uncertain sections, influenced by measurement inaccuracies or data noise ($\Delta T_{peak} < 0.3$ K).

The evolution of the thermal plume measured during the TTT and values of t_{peak} provide crucial hints that substantial spatial heterogeneity are present in the aquifer, which is insufficiently reproduced in the model by two horizontal and laterally persistent layers. Small-scale, vertical heterogeneity has already been identified as a potential reason that the plume is detected only in the uppermost well screens. In the upper part of the aquifer, at OW2 and OW3, t_{peak} trends would compare better by simple shifting along the vertical axis. This shift could be an indication that the boundary between the upper and the lower aquifer part is declined or displaced relative to the assumptions in the model. The inconsistencies in t_{peak} between model and field of OW4 and OW5 are a sign of lateral heterogeneities in the direction of the well transect, as well as perpendicular. The thermal plume appears locally deviated from the suspected centerline, potentially with meandering. Thus, the measured temperatures may originate from the fringe of the thermal plume. This conclusion is supported by the measured t_{peak} values at OW4 and OW5, which are smaller than those at OW3, meaning that the thermal peak arrives at OW4 and OW5 before it passes OW3.

5.3.5 Comparison to DPIL

Finally, t_{peak} values are compared to the DPIL profiles (Fig. 30 and Fig. 34). The overall patterns are comparable, and both field experiments are obviously consistent with higher relative hydraulic conductivities and smaller t_{peak} values in the upper part of the aquifer. The 6

m bls boundary between both aquifer parts in the DPIL-profile of B2 is well reproduced by the model. The DPIL-profiles of OW4 and OW5 indicate that this boundary could be at a more shallow depth, which corresponds to the interpretation from trends in the t_{peak} values. Due to the substantial influence of noise on the small values shown on logarithmic scale, the DPIL-based characterization of the lower section is as unsatisfactory as from the TTT. Further insights in the heat transport characteristics of the studied aquifer would mandate an even denser measurement network and a longer duration of TTT observation to assure the monitoring of the passage of the thermal peak.

5.4 Conclusions

The main objective of the TTT at the Lauswiesen site was to improve our understanding from the experiment and with the obtained experience, identify implications for future TTT designs. By numerical simulation of the TTT, the governing transport processes could be identified, and high-conductivity regions at the top of the aquifer could also be confirmed. The heterogeneous hydraulic properties of the studied shallow aquifer, which is generally well known and has already served as hydrogeological test case for decades, have substantial effects on the heat transport behavior. It is shown that macrodispersion and flow-focusing occurred, and that complex flow patterns result in thermal breakthrough curves (shown as thermoisopleth graphs) that are substantially distinct from what would be expected under ideal conditions in a layered aquifer. Accordingly, the capability of the presented model to simulate the measured propagation of the thermal plume is limited. For more comprehensive flow and transport simulations, however, the data collected during our experiment is insufficient. A main obstacle is that the induced transient hydraulic head change at injection well and in the observation wells were not continuously monitored during the experiment. Hence, piezometers have to be added to the experimental design, especially, when the injected water volume per time is significant in comparison to the anticipated natural groundwater flow.

Considering that lateral and even vertical flow and transport components may be significant in such highly heterogeneous systems, it is also recommended to prefer a more distributed and space filling arrangement of observation wells (e.g. several observation well transects) to the linear one chosen in the performed TTT. Such wells, which also reveal the thermal evolution aside from the expected dominant flow direction, show valuable insights in the 3D characteristics of the transport mechanisms. Furthermore, particularly in the case of long-

duration experiments, sensors are needed that monitor potential vertical conductive heat losses, such as into the underlying aquitard and the unsaturated zone above.

Ideally, the TTT is complemented by additional field experiments, such as near surface geophysics [e.g. *Slater, 2007*] or hydraulic tomography [e.g. *Brauchler et al., 2013*], which are able to identify the main structural build-up of the aquifer. For example, at the Lauswiesen site, DPIL field tests have been performed before the TTT. It is demonstrated that the monitored thermal transport along the local hydraulic gradient is consistent with the findings from the DPIL campaign. In addition, as reported by *Ma et al. [2012]*, injection of both thermal and dye tracers, is an appealing combination, which should be considered for future active and short-term TTT. Thus, coupled parameter estimation for determining both thermal and solute transport parameters would be possible [*Rau et al., 2012*], which would better constrain the inversion problem than by separate interpretation of individual tracer tests. Although, heat appears to be a favourable tracer for studying aquifer properties, care has to be taken to interpret the acquired data. Hence, more studies on active and short-term TTT are required to establish such tests as a standard hydrogeological investigation technique.

6 Summary and conclusions

Anderson [2005] designated inverse problems as the most powerful application of temperature data in hydrogeology. She also suggest that temperature signal analyses should become a standard tool in hydrogeology. The studies enclosed in this thesis rely on this suggestion. Therefore, the main objective is to further improve the interpretation of artificially generated temperature signals and to extract as much information as possible about the subsurface from those signals. All four individual studies of this thesis apply time series of artificially disturbed subsurface temperature for the characterization of hydraulic and thermal parameters. The first three studies (chapter 2 to 4), which are closely related, analyze and develop innovative methodologies to interpret temperature signals from TRTs. The fourth study (chapter 5) interprets the temperature signals of a TTT to further characterize the subsurface.

The first study (chapter 2) analyses potential shortcomings of the standard TRT evaluation. The second study (chapter 3) develops a new TRT evaluation to overcome the most important shortcoming detected in chapter 2. The third study (chapter 4) is directly connected to the previous study and validates this new methodology. This study further lifts the TRT beyond the classical geothermal application area and introduces it as a hydrogeological investigation method comparable to a pumping test.

The first study reveals, on the one hand, that there are shortcomings based on the ill-posed character of the standard TRT evaluation by performing a rigorous two-variable parameter estimation. Hence, there is no distinct λ_{eff} and R_b pair as a parameter estimation result, but a range of parameter combinations of equal quality. On the other hand, this study systematically analyzes the distorting potential of pipe positions, non-uniform initial temperature distributions and thermal dispersion in an advection influenced environment on the TRT evaluation. The analyses exhibit significant tampering effects only for thermal dispersion in an advection influenced environment. For a constant Darcy velocity of 0.1 m day^{-1} and considering longitudinal thermal dispersivity values between 0 and 2 m, an overestimation of the actual thermal conductivity by the TRT result from 0.5 to $3.9 \text{ W m}^{-1} \text{ K}^{-1}$ is determined. These findings confirm the assumption of *Raymond et al.* [2011b] that thermal dispersion might influence the TRT and are therefore taken up by the scientific community [*Dehkordi and Schincariol*, 2013; *Witte*, 2013; *Casasso and Sethi*, 2014]. Furthermore, the potential

overestimation of λ_{eff} compared to λ_m clarifies the need of an advection sensitive TRT evaluation approach, which also considers the influence of thermal dispersion.

In line with this need, the second study (chapter 3) introduces an advection sensitive TRT evaluation approach by using the moving line source equation [e.g. *Molina-Giraldo et al.*, 2011a]. Here, it is demonstrated by detailed comparisons of analytical and numerical results that the hydraulic conductivity discrepancy of the aquifer and the BHE cause a non-uniform groundwater velocity field in the vicinity of the BHE. This provokes a considerable difference between both solutions. Therefore, for most of the analyzed aquifer settings, the application of the unimproved moving line source based evaluation would result in underestimated groundwater flow velocities. For instance, such an unimproved evaluation in an aquifer ($v = 1.8 \text{ m day}^{-1}$ and $\lambda_m = 2.2 \text{ W m}^{-1} \text{ K}^{-1}$) would underestimate the Darcy velocity by a factor of two. To overcome this tampering effect a correction term is developed which is derived from the analytical and numerical comparison. This entire evaluation approach using an improved version of the moving line source model is successfully tested on three different literature based TRT datasets. The newly developed parameter estimation procedure is applied to determine the thermal conductivity and the groundwater flow velocity of the three test cases. Comparable to the standard TRT evaluation (chapter 2), this is also an ill-posed problem and it is not possible to determine a distinct parameter combination. Instead all three test evaluations result in an array of equally suitable parameter combinations with a definitely negative correlation. This clear correlation and the fact that the variability of the thermal conductivity is considerably smaller than the variability of naturally occurring hydraulic conductivity values are the starting point of the third study.

The third TRT related study achieves two objectives. First, the validation of the evaluation approach presented in chapter 3, which is already accepted by the scientific community [*Sharqawy et al.*, 2013; *Casasso and Sethi*, 2014]. Secondly, it successfully demonstrates that an integral Darcy velocity or an integral hydraulic conductivity, respectively, can be determined using the new evaluation approach on temperature time series from a TRT. Both objectives are fulfilled by evaluating TRT datasets from two different locations. Assuming realistic ranges for the thermal properties of a porous aquifer, i.e. thermal conductivity, volumetric heat capacity and longitudinal thermal dispersivity, and the thermal borehole resistance of the BHE, the new evaluation approach results in correct hydraulic conductivity ranges of the aquifers sampled by the two TRT experiments. The subsurfaces of both test sites

are also investigated by classical hydrogeological investigation techniques, like a sieve curve analysis or a pumping tests. The hydraulic conductivity ranges obtained from the TRT and from the classical methods are nearly the same for the tank experiment. The TRT based hydraulic conductivity range of the field experiment (2.5×10^{-3} to $5.5 \times 10^{-3} \text{ m s}^{-1}$) is not only within the ranges from classical methods, but also further specifies this range (1.6×10^{-3} to $8.3 \times 10^{-3} \text{ m s}^{-1}$). The successful validation of the moving line source based evaluation method presented in chapter 2 also demonstrates that the TRT can be employed as a hydrogeological characterization method. The developed and validated approach (chapter 3 and 4) certainly improves and extends the current applicability of the TRT. Temperature signals recorded from TRTs can now be used to provide suitable subsurface parameters for advanced numerical simulation codes, which implement advection and conduction heat transport.

The fourth study (chapter 5) interprets temperature time series of a TTT. During the TTT experiment, 16 m^3 of 22°C hot water is injected into the subsurface and the heat transport is observed along one transect containing five observation wells. The location of the TTT is the well characterized Lauswiesen test site. Based on the existing knowledge of the test site, a numerical model is set up to distinguish the governing heat transport processes by comparing measured and simulated results. The separation of the aquifer into a high conductive upper part and an underlying low conductive part, which is known from previous studies [e.g. *Lessoff et al.*, 2010], can be clearly detected from the measured and simulated thermoisopleth graphs from all observation wells along the entire well transect. However, a more detailed interpretation of the measured thermal breakthrough curves and comparisons with the numerical results illustrate that there is a significant deviation from the ideal heat transport behavior observed in the numerical simulation. For instance, peak arrival times measured at the observation wells OW3 to OW5 of the upper aquifer decrease with increasing distance from the well. This effect, which deviates from the ideal model assumption, is an indication for the likely occurrence of flow focusing zones. Further, the comparison of the thermoisopleth graphs demonstrates that the boundary depth between the upper and the lower aquifer part is not uniform. Beside from improving the process understanding of a TTT, the second objective of this study is to identify implications to further improve the TTT experimental design. This study provides fundamental evidence that the temperature signal is very sensitive to the actual flow paths in the porous media.

To be able to measure the effects of the existent flow paths, a wider distributed temperature sensor network is mandatory. In addition, complementary field investigation techniques should be performed in order to avoid significant uncertainties caused by the geological structure.

The investigations described in the present thesis demonstrate the capabilities of using standard field investigation techniques such as TRTs and TTTs, commonly applied in the area of geothermics, in a broader manner. In summary, the studies enclosed in this thesis help to achieve a further step to establish the TTT as a standard tool in hydrogeology. In addition, studies enclosed in this thesis introduces the first time a new evaluation approach for the TRT, which accesses to a novel correction factor, to be able to determine simultaneously advective and conductive heat transport parameters. Applying this novel evaluation procedure, the first time, TRT temperature time series are used to determine the hydraulic conductivity of an aquifer. Therefore the TRT is introduced as a completely new temperature related tool in the toolbox of hydrogeologists.

7 Perspectives

In this section future research questions are compiled, which arise from the results presented in this thesis. First the major research perspectives related to the new TRT evaluation are presented, then the ones related to the TTT evaluation and at last perspectives to thermal field test in general are introduced.

Future research should focus on the extension of the new application area for TRT datasets beyond the classical shallow geothermal background. Existing TRT datasets of advection influenced test sites can be reevaluated in order to obtain an integral hydraulic conductivity value instead of tampered λ_{eff} value. It should be further evaluated whether it is possible to apply this approach to enhanced TRT datasets [Acuña, 2013] in order to interpret the temperature signals at various depths during a TRT. Using such a dataset, the determination of depth depending hydraulic conductivities might be possible. This new evaluation approach should also be applied on TRT datasets from fractured or karstic rocks to inspect the applicability for subsurfaces, which are not a porous media. Future work should also analyze the sensitivity of the determined correction term and the parameter estimation result itself on the chosen length of the evaluation interval.

The results of this thesis, which are related to the TTT, indicate that the transient head changes caused by the tracer injection tamper the result of the experiment. Future TTT experiments should analyze, if it is necessary to inject the heat as hot water into the aquifer or if it is sufficient to install heating devices directly into the well. This new position of the heat source would avoid a significant change of the local hydraulic gradients and the influences by this latter effect. Furthermore, future studies should analyze the benefit of extending the temperature sensor network not only in horizontal but also in vertical direction, especially additional temperature measurements in the unsaturated zone and the underlying aquitard.

The studies enclosed in this thesis focus on the hydraulic and thermal characterization of the subsurface by TRT or TTT. The recent work of *Bons et al.* [2013] presents a unifying expression for heat and solute dispersion coefficients. Applying this new expression and the associated transferability of the suggested formulation of the dispersion coefficients, the obtained results from TRTs or TTTs can be also used to get further insights in the solute transport properties of the subsurface. Or vice versa, solute dispersion coefficients can be applied to further constrain the TRT or TTT evaluation, respectively.

8 References

Acuña, J., and B. Palm (2009), Local Conduction Heat Transfer in U-pipe Borehole Heat Exchangers, in *COMSOL Conference*, edited, Milan, Italy.

Acuña, J. (2013), Distributed thermal response tests – New insights on U-pipe and Coaxial heat exchangers in groundwater-filled boreholes, KTH School of Industrial Engineering and Management, Stockholm, Sweden.

Anderson, M. P. (2005), Heat as a ground water tracer, *Ground Water*, 43(6), 951-968.

Angermann, L., S. Krause, and J. Lewandowski (2012), Application of heat pulse injections for investigating shallow hyporheic flow in a lowland river, *Water Resour. Res.*, 48, W00P02, doi: 10.1029/2012wr012564.

Bandos, T. V., Á. Montero, E. Fernández, J. L. G. Santander, J. M. Isidro, J. Pérez, P. J. F. d. Córdoba, and J. F. Urchueguía (2009), Finite line-source model for borehole heat exchangers: effect of vertical temperature variations, *Geothermics*, 38(2), 263-270, doi: 10.1016/j.geothermics.2009.01.003.

Bandos, T. V., Á. Montero, P. Fernández de Córdoba, and J. F. Urchueguía (2011), Improving parameter estimates obtained from thermal response tests: Effect of ambient air temperature variations, *Geothermics*, 40(2), 136-143, doi: 10.1016/j.geothermics.2011.02.003.

Banks, D. (2008), An introduction to thermogeology: ground source heating and cooling, Blackwell Pub.

Barcenilla, J. R., D. W. Nutter, and R. J. Couvillion (2005), Effective thermal conductivity for single-bore vertical heat exchangers with groundwater flow, *Ashrae Tran*, 111(2), 258-263.

Bauer, D., W. Heidemann, H. Muller-Steinhagen, and H. J. G. Diersch (2011), Thermal resistance and capacity models for borehole heat exchangers, *Int J Energ Res*, 35(4), 312-320, doi: 10.1002/Er.1689.

Bayer, P., and M. Finkel (2007), Optimization of concentration control by evolution strategies: Formulation, application, and assessment of remedial solutions, *Water Resources Research*, 43(2), W02410, doi: 10.1029/2005wr004753.

Bayer, P., D. Saner, S. Bolay, L. Rybach, and P. Blum (2012), Greenhouse gas emission savings of ground source heat pump systems in Europe: A review, *Renewable and Sustainable Energy Reviews*, 16(2), 1256-1267, doi: 10.1016/j.rser.2011.09.027.

Bear, J. (1988), *Dynamics of Fluids in Porous Media*, Dover Publications, Mineola, NY, USA.

Bear, J., and A. Cheng (2010), *Modeling Groundwater Flow and Contaminant Transport*, Springer Science+Business Media B.V., Dordrecht.

Beier, R. A., M. D. Smith, and J. D. Spitler (2011), Reference data sets for vertical borehole ground heat exchanger models and thermal response test analysis, *Geothermics*, 40(1), 79-85, doi: 10.1016/j.geothermics.2010.12.007.

Bellin, A., and Y. Rubin (2004), On the use of peak concentration arrival times for the inference of hydrogeological parameters, *Water Resources Research*, 40(7), 1-13, doi: 10.1029/2003wr002179.

Bennet, J., J. Claesson, and G. Hellström (1987), Multipole method to compute the conductive heat flows to and between pipes in a composite cylinder, Department of Building Technology and Department of Mathematical Physics, Lund Institute of Technology.

Beyer, W. (1964), Zur Bestimmung der Wasserdurchlässigkeit von Kiesen und Sanden aus der Kornverteilung, *Wasserwirtschaft-Wassertechnik (WWT)*, 165 - 169.

Blackwell, J. H. (1954), A transient-flow method for determination of thermal constants of insulating materials in bulk part I - Theory, *Journal of Applied Physics*, 25(2), 137-144.

Blum, P., G. Campillo, W. Münch, and T. Kölbl (2010), CO₂ savings of ground source heat pump systems – A regional analysis, *Renewable Energy*, 35(1), 122-127, doi: 10.1016/j.renene.2009.03.034.

Blum, P., G. Campillo, and T. Kölbl (2011), Techno-economic and spatial analysis of vertical ground source heat pump systems in Germany, *Energy*, 36(5), 3002-3011, doi: 10.1016/j.energy.2011.02.044.

Bons, P. D., B. P. van Milligen, and P. Blum (2013), A general unified expression for solute and heat dispersion in homogeneous porous media, *Water Resources Research*, 1-13, doi: 10.1002/wrcr.20488.

Bou Ghannam, O. (2006), Determination of the Hydraulic Conductivity using Direct-Push Methods, Master thesis, University of Tübingen, Germany, Tübingen, Germany.

Bozdog, S., B. Turgut, H. Paksoy, D. Dikici, M. Mazman, and H. Evliya (2008), Ground water level influence on thermal response test in Adana, Turkey, *Int J Energ Res*, 32(7), 629-633, doi: 10.1002/Er.1378.

Brauchler, R., R. Hu, L. Hu, S. Jiménez, P. Bayer, P. Dietrich, and T. Ptak (2013), Rapid field application of hydraulic tomography for resolving aquifer heterogeneity in unconsolidated sediments, *Water Resources Research*, 49(4), 2013-2024, doi: 10.1002/wrcr.20181.

Bravo, H. R., F. Jiang, and R. J. Hunt (2002), Using groundwater temperature data to constrain parameter estimation in a groundwater flow model of a wetland system, *Water Resour. Res.*, 38(8), 1153, doi: 10.1029/2000wr000172.

Bromley, C. J., M. Mongillo, G. Hiriart, B. Goldstein, R. Bertani, E. Huenges, A. Ragnarsson, J. Tester, H. Muraoka, and V. Zui (2010), Contribution of geothermal energy to climate change mitigation: the IPCC renewable energy report, paper presented at Proceedings of the World Geothermal Congress.

Brouyère, S., G. Carabin, and A. Dassargues (2004), Climate change impacts on groundwater resources: modelled deficits in a chalky aquifer, Geer basin, Belgium, *Hydrogeology Journal*, 12(2), 123-134, doi: 10.1007/s10040-003-0293-1.

Butler, J. J., J. M. Healey, G. W. McCall, E. J. Garnett, and S. P. Loheide (2002), Hydraulic Tests with Direct-Push Equipment, *Ground Water*, 40(1), 25-36, doi: 10.1111/j.1745-6584.2002.tb02488.x.

Byrne, G. F., J. E. Drummond, and C. W. Rose (1967), A sensor for water flux in soil. "Point source" instrument, *Water Resour. Res.*, 3(4), 1073-1078, doi: 10.1029/WR003i004p01073.

Cardenas, M. B. (2010), Thermal skin effect of pipes in streambeds and its implications on groundwater flux estimation using diurnal temperature signals, *Water Resour. Res.*, 46(3), W03536, doi: 10.1029/2009wr008528.

Carslaw, H. S., and J. C. Jaeger (1959), *Conduction of heat in solids*, 2d ed., 510 pp., Clarendon Press, Oxford.

Casasso, A., and R. Sethi (2014), Efficiency of closed loop geothermal heat pumps: A sensitivity analysis, *Renewable Energy*, 62(0), 737-746, doi: 10.1016/j.renene.2013.08.019.

Chiasson, A., and A. O'Connell (2011), New analytical solution for sizing vertical borehole ground heat exchangers in environments with significant groundwater flow: Parameter estimation from thermal response test data, *HVAC&R Research*, 17(6), 1000-1011.

Chiasson, A. C., S. J. Rees, and J. D. Spitler (2000), A Preliminary Assessment Of The Effects Of Ground-Water Flow On Closed-Loop Ground-Source Heat Pump Systems, *ASHRAE Transactions*, 106(1), 380-393.

Clausen, H. (2008), Durchführung von Simulationsrechnungen zum Einfluss verschiedener Randbedingungen auf die thermische Leistungsfähigkeit von Erdwärmesonden, Diploma thesis, Universität Stuttgart, Stuttgart.

Clauser, C. (2011), Thermal Storage and Transport Properties of Rocks, I: Heat Capacity and Latent Heat, in *Encyclopedia of Solid Earth Geophysics*, edited by H. Gupta, pp. 1423-1431, Springer Netherlands.

Conant, B. (2004), Delineating and Quantifying Ground Water Discharge Zones Using Streambed Temperatures, *Ground Water*, 42(2), 243-257, doi: 10.1111/j.1745-6584.2004.tb02671.x.

Constantz, J. (2008), Heat as a tracer to determine streambed water exchanges, *Water Resources Research*, 44(4), 1-20, doi: 10.1029/2008wr006996.

De Carli, M., M. Tonon, A. Zarrella, and R. Zecchin (2010), A computational capacity resistance model (CaRM) for vertical ground-coupled heat exchangers, *Renewable Energy*, 35(7), 1537-1550, doi: 10.1016/j.renene.2009.11.034.

de Marsily, G. (1986), *Quantitative hydrogeology: groundwater hydrology for engineers*, Academic Press.

de Vries, D. (1963), Thermal Properties of Soils, Chapter in *Physics of the Plant Environment*, WR Van Wijk, Editor, edited, North Holland Publishing Co., Amsterdam, Netherlands.

Dehkordi, S. E., and R. Schincariol (2013), Effect of thermal-hydrogeological and borehole heat exchanger properties on performance and impact of vertical closed-loop geothermal heat pump systems, *Hydrogeology Journal*, 1-15, doi: 10.1007/s10040-013-1060-6.

Diao, N., Q. Li, and Z. Fang (2004), Heat transfer in ground heat exchangers with groundwater advection, *Int J Therm Sci*, 43(12), 1203-1211, doi: 10.1016/j.ijthermalsci.2004.04.009.

Diersch, H.-J. G. (2009a), *FEFLOW Reference Manual*, WASY GmbH, Berlin, Germany.

Diersch, H. (2005), Discrete feature modeling of flow, mass and heat transport processes by using FEFLOW, *WASY Software FEFLOW White Paper, 1*, 151-198.

Diersch, H. (2006), FEFLOW 5.3 User's Manual, Berlin.

Diersch, H., D. Bauer, W. Heidemann, W. Rühaak, and P. Schätzl (2010), Finite element formulation for borehole heat exchangers in modeling geothermal heating systems by FEFLOW, *WASY Software FEFLOW White Paper, 5*, 5-96.

Diersch, H. J. G. (2009b), FEFLOW User's Manual, edited, WASY GmbH, Berlin, Germany.

Diersch, H. J. G., D. Bauer, W. Heidemann, W. Rühaak, and P. Schätzl (2011a), Finite element modeling of borehole heat exchanger systems: Part 1. Fundamentals, *Computers & Geosciences*, 37(8), 1122-1135, doi: 10.1016/j.cageo.2010.08.003.

Diersch, H. J. G., D. Bauer, W. Heidemann, W. Rühaak, and P. Schätzl (2011b), Finite element modeling of borehole heat exchanger systems: Part 2. Numerical simulation, *Computers & Geosciences*, 37(8), 1136-1147, doi: 10.1016/j.cageo.2010.08.002.

Dietrich, P., J. J. Butler, and K. Faiß (2008), A Rapid Method for Hydraulic Profiling in Unconsolidated Formations, *Ground Water*, 46(2), 323-328, doi: 10.1111/j.1745-6584.2007.00377.x.

Domenico, P. A., and V. V. Palciauskas (1973), Theoretical Analysis of Forced Convective Heat Transfer in Regional Ground-Water Flow, *Geological Society of America Bulletin*, 84(12), 3803-3814, doi: 10.1130/0016-7606(1973)84<3803:taofch>2.0.co;2.

Domenico, P. A., and F. W. Schwartz (1998), Physical and Chemical Hydrogeology (2nd Edition), John Wiley & Sons, Chichester, United Kingdom.

Dornstädter, J., P. Heidinger, and B. Heinemann-Glutsch (2008), Erfahrungen aus der Praxis mit dem Enhanced Geothermal Response Test (EGRT), in *Der Geothermiekongress 2008*, edited, pp. 271-279, Karlsruhe.

Doussan, C., A. Toma, B. Paris, G. Poitevin, E. Ledoux, and M. Detay (1994), Coupled use of thermal and hydraulic head data to characterize river-groundwater exchanges, *J Hydrol*, 153(1-4), 215-229, doi: 10.1016/0022-1694(94)90192-9.

Engelhardt, I., H. Prommer, C. Moore, M. Schulz, C. Schüth, and T. A. Ternes (2013), Suitability of temperature, hydraulic heads, and acesulfame to quantify wastewater-related

fluxes in the hyporheic and riparian zone, *Water Resources Research*, 49(), 1-15, doi: 10.1029/2012wr012604.

Esen, H., and M. Inalli (2009), In-situ thermal response test for ground source heat pump system in Elazığ, Turkey, *Energy and Buildings*, 41(4), 395-401, doi: 10.1016/j.enbuild.2008.11.004.

Esen, H., M. Inalli, and Y. Esen (2009), Temperature distributions in boreholes of a vertical ground-coupled heat pump system, *Renewable Energy*, 34(12), 2672-2679, doi: 10.1016/j.renene.2009.04.032.

Eugster, W. (2002), *Angewandte Forschung: Workshop zur Qualitätssicherung von geothermischen Response Tests Rep.*, Swiss federal office of energy, Bern, Switzerland.

Ferguson, G., and A. D. Woodbury (2007), Urban heat island in the subsurface, *Geophysical Research Letters*, 34(23), 1-4, doi: 10.1029/2007gl032324.

Fetter, C. W. (2001), *Applied Hydrogeology*, Prentice Hall PTR.

Fujii, H., H. Okubo, K. Nishi, R. Itoi, K. Ohyama, and K. Shibata (2009), An improved thermal response test for U-tube ground heat exchanger based on optical fiber thermometers, *Geothermics*, 38(4), 399-406, doi: 10.1016/j.geothermics.2009.06.002.

Gao, J., T. Ren, and Y. Gong (2006), Correcting Wall Flow Effect Improves the Heat-Pulse Technique for Determining Water Flux in Saturated Soils, *Soil Sci. Soc. Am. J.*, 70(3), 711-717, doi: 10.2136/sssaj2005.0174.

Gauthier, C., M. Lacroix, and H. Bernier (1997), Numerical simulation of soil heat exchanger-storage systems for greenhouses, *Sol Energy*, 60(6), 333-346.

Gehlin, S. (1998), Thermal response test: in situ measurements of thermal properties in hard rock, Licentiate thesis, Lulea University of Technology, Lulea.

Gehlin, S. (2002), Thermal Response Test Method Development and Evaluation, Phd thesis, Luleå University of Technology, Luleå.

Gehlin, S., and G. Hellström (2003), Influence on thermal response test by groundwater flow in vertical fractures in hard rock, *Renewable Energy*, 28(14), 2221-2238, doi: 10.1016/s0960-1481(03)00128-9.

-
- Gehlin, S. E. A., G. Hellström, and B. Nordell (2003), The influence of the thermosiphon effect on the thermal response test, *Renewable Energy*, 28(14), 2239-2254, doi: 10.1016/s0960-1481(03)00129-0.
- Gelhar, L. W., C. Welty, and K. R. Rehfeldt (1992), A critical review of data on field-scale dispersion in aquifers, *Water Resour. Res.*, 28(7), 1955-1974, doi: 10.1029/92wr00607.
- Greswell, R. B., M. S. Riley, P. F. Alves, and J. H. Tellam (2009), A heat perturbation flow meter for application in soft sediments, *J Hydrol*, 370(1-4), 73-82, doi: 10.1016/j.jhydrol.2009.02.054.
- Gustafsson, A. M., and S. Gehlin (2008), Influence of natural convection in water-filled boreholes for GCHP.
- Gustafsson, A. M., and L. Westerlund (2010), Multi-injection rate thermal response test in groundwater filled borehole heat exchanger, *Renewable Energy*, 35(5), 1061-1070, doi: 10.1016/j.renene.2009.09.012.
- Gustafsson, A. M., and L. Westerlund (2011), Heat extraction thermal response test in groundwater-filled borehole heat exchanger – Investigation of the borehole thermal resistance, *Renewable Energy*, 36(9), 2388-2394, doi: 10.1016/j.renene.2010.12.023.
- Hähnlein, S., N. Molina-Giraldo, P. Blum, P. Bayer, and P. Grathwohl (2010), Ausbreitung von Kältefahnen im Grundwasser bei Erdwärmesonden (Cold plumes in groundwater for ground source heat pump systems), *Grundwasser*, 15(2), 123-133, doi: 10.1007/s00767-009-0125-x.
- Händel, F., and P. Dietrich (2012), Relevance of Deterministic Structures for Modeling of Transport: The Lauswiesen Case Study, *Ground Water*, 50(6), 935-942, doi: 10.1111/j.1745-6584.2012.00948.x.
- Hazen, A. (1893), Some physical properties of sand and gravels with special reference to their use in filtration *Rep.*, 539-556 pp, Massachusetts State Board of Health, Boston.
- Hecht-Méndez, J., N. Molina-Giraldo, P. Blum, and P. Bayer (2010), Evaluating MT3DMS for Heat Transport Simulation of Closed Geothermal Systems, *Ground Water*, 48(5), 741-756, doi: 10.1111/j.1745-6584.2010.00678.x.
- Hellström, G. (1991), Ground Heat Storage, Thermal Analyses of Duct Storage Systems, Doctoral thesis, Luleå University of Technology, Luleå.
-

Hellström, G., and B. Sanner (2000), Earth Energy Designer-EED, Version 2.0.

Herrmann, J. (2008), Ingenieurgeologische Untersuchungen zur Hinterfüllung von Geothermie-Bohrungen mit Erdwärmesonden, Doctoral thesis, Fridericiana University of Karlsruhe, Karlsruhe.

Hopmans, J. W., J. Šimunek, and K. L. Bristow (2002), Indirect estimation of soil thermal properties and water flux using heat pulse probe measurements: Geometry and dispersion effects, *Water Resour. Res.*, 38(1), 1006, doi: 10.1029/2000wr000071.

Hurtig, E., S. Großwig, M. Jobmann, K. Kühn, and P. Marschall (1994), Fibre-optic temperature measurements in shallow boreholes: experimental application for fluid logging, *Geothermics*, 23(4), 355-364, doi: 10.1016/0375-6505(94)90030-2.

Jardani, A., and A. Revil (2009), Stochastic joint inversion of temperature and self-potential data, *Geophysical Journal International*, 179(1), 640-654, doi: 10.1111/j.1365-246X.2009.04295.x.

Junker, B., and H. Essler (1980), Hydrogeologische Karte von Baden-Württemberg 1 : 50 000 (dHGK). HGK Lahr. 8 Karten/Beilagen. Erläuterungen: 63 S., 25 Abb., 7 Tab., (CD-ROM mit Karten und Texten im PDF-Format und georeferenzierten Rasterdaten/Scans).

Katsura, T., K. Nagano, S. Takeda, and K. Shimakura (2006), Heat transfer experiment in the ground with ground water advection, in *The IEA 10th Energy Conservation Thermal Energy Storage Conference* edited, New Jersey, USA.

Keery, J., A. Binley, N. Crook, and J. W. N. Smith (2007), Temporal and spatial variability of groundwater–surface water fluxes: Development and application of an analytical method using temperature time series, *J Hydrol*, 336(1–2), 1-16, doi: 10.1016/j.jhydrol.2006.12.003.

Keys, W. S., and R. F. Brown (1978), The Use of Temperature Logs to Trace the Movement of Injected Water, *Ground Water*, 16(1), 32-48, doi: 10.1111/j.1745-6584.1978.tb03201.x.

Kocabas, I. (2005), Geothermal reservoir characterization via thermal injection backflow and interwell tracer testing, *Geothermics*, 34(1), 27-46, doi: 10.1016/j.geothermics.2004.09.003.

Koenigsdorff, R. (2011), Oberflächennahe Geothermie für Gebäude: Grundlagen und Anwendungen zukunftsfähiger Heizung und Kühlung, Fraunhofer Irb Stuttgart.

Kollet, S. J., I. Cvijanovic, D. Schüttemeyer, R. M. Maxwell, A. F. Moene, and P. Bayer (2009), The Influence of Rain Sensible Heat and Subsurface Energy Transport on the Energy Balance at the Land Surface, *Vadose Zone Journal*, 8(4), 846-857.

Kübert, M., S. Walker-Hertkorn, and A. Voutta (2009), Temperaturtiefenprofile stärken die Aussagekraft von Thermal Response Tests, *bbr-Fachmagazin für Brunnen und Leitungsbau oberflächennahe Geothermie*, 60(9), 38-43.

Lagarias, J. C., J. A. Reeds, M. H. Wright, and P. E. Wright (1998), Convergence properties of the Nelder-Mead simplex method in low dimensions, *Siam J Optimiz.*, 9(1), 112-147.

Lamarche, L., S. Kajl, and B. Beauchamp (2010), A review of methods to evaluate borehole thermal resistances in geothermal heat-pump systems, *Geothermics*, 39(2), 187-200, doi: 10.1016/j.geothermics.2010.03.003.

Lautz, L. K. (2010), Impacts of nonideal field conditions on vertical water velocity estimates from streambed temperature time series, *Water Resour. Res.*, 46(1), W01509, doi: 10.1029/2009wr007917.

Leaf, A. T., D. J. Hart, and J. M. Bahr (2012), Active Thermal Tracer Tests for Improved Hydrostratigraphic Characterization, *Ground Water*, 50(5), 726-735, doi: 10.1111/j.1745-6584.2012.00913.x.

Lessoff, S. C., U. Schneidewind, C. Leven, P. Blum, P. Dietrich, and G. Dagan (2010), Spatial characterization of the hydraulic conductivity using direct-push injection logging, *Water Resources Research*, 46(12), 1-9, doi: 10.1029/2009wr008949.

Loague, K., and R. E. Green (1991), Statistical and graphical methods for evaluating solute transport models: Overview and application, *J. Contam. Hydrol.*, 7(1-2), 51-73, doi: 10.1016/0169-7722(91)90038-3.

Lowry, C. S., J. F. Walker, R. J. Hunt, and M. P. Anderson (2007), Identifying spatial variability of groundwater discharge in a wetland stream using a distributed temperature sensor, *Water Resources Research*, 43(10), 1-9, doi: 10.1029/2007wr006145.

Lund, J. W., D. H. Freeston, and T. L. Boyd (2011), Direct utilization of geothermal energy 2010 worldwide review, *Geothermics*, 40(3), 159-180, doi: 10.1016/j.geothermics.2011.07.004.

Ma, R., and C. Zheng (2010), Effects of Density and Viscosity in Modeling Heat as a Groundwater Tracer, *Ground Water*, 48(3), 380-389, doi: 10.1111/j.1745-6584.2009.00660.x.

Ma, R., C. Zheng, J. M. Zachara, and M. Tonkin (2012), Utility of bromide and heat tracers for aquifer characterization affected by highly transient flow conditions, *Water Resources Research*, 48(8), 1-18, doi: 10.1029/2011wr011281.

Macfarlane, A., A. Förster, D. Merriam, J. Schrötter, and J. Healey (2002), Monitoring artificially stimulated fluid movement in the Cretaceous Dakota aquifer, western Kansas, *Hydrogeology Journal*, 10(6), 662-673, doi: 10.1007/s10040-002-0223-7.

Maier, U., C. DeBiase, O. Baeder-Bederski, and P. Bayer (2009), Calibration of hydraulic parameters for large-scale vertical flow constructed wetlands, *J Hydrol*, 369(3-4), 260-273, doi: 10.1016/j.jhydrol.2009.02.032.

Marcotte, D., and P. Pasquier (2008), On the estimation of thermal resistance in borehole thermal conductivity test, *Renewable Energy*, 33(11), 2407-2415, doi: 10.1016/j.renene.2008.01.021.

Markle, J. M., R. A. Schincariol, J. H. Sass, and J. W. Molson (2006), Characterizing the Two-Dimensional Thermal Conductivity Distribution in a Sand and Gravel Aquifer, *Soil Sci. Soc. Am. J.*, 70(4), 1281-1294, doi: 10.2136/sssaj2005.0293.

Menberg, K., P. Bayer, K. Zosseder, S. Rumohr, and P. Blum (2013a), Subsurface urban heat islands in German cities, *Science of The Total Environment*, 442(0), 123-133, doi: 10.1016/j.scitotenv.2012.10.043.

Menberg, K., H. Steger, R. Zorn, M. Reuß, M. Pröll, P. Bayer, and P. Blum (2013b), Bestimmung der Wärmeleitfähigkeit im Untergrund durch Labor- und Feldversuche und anhand theoretischer Modelle, *Grundwasser*, 18(2), 103-116, doi: 10.1007/s00767-012-0217-x.

Metzger, T., S. Didierjean, and D. Maillet (2004), Optimal experimental estimation of thermal dispersion coefficients in porous media, *International Journal of Heat and Mass Transfer*, 47(14-16), 3341-3353, doi: 10.1016/j.ijheatmasstransfer.2004.02.024.

Mogensen, P. (1983), Fluid to duct wall heat transfer in duct system heat storage, paper presented at Proceedings of the International Conference on Surface Heat Storage in Theory and Practice, Stockholm, Sweden.

Mohrlok, U. (2008), Bilanzmodelle in der Grundwasserhydraulik: quantitative Beschreibung von Strömung und Transport im Untergrund, Univ.-Verlag Karlsruhe.

-
- Molina-Giraldo, N., P. Bayer, and P. Blum (2011a), Evaluating the influence of thermal dispersion on temperature plumes from geothermal systems using analytical solutions, *Int J Therm Sci*, 50(7), 1223-1231, doi: 10.1016/j.ijthermalsci.2011.02.004.
- Molina-Giraldo, N., P. Blum, K. Zhu, P. Bayer, and Z. Fang (2011b), A moving finite line source model to simulate borehole heat exchangers with groundwater advection, *Int J Therm Sci*, 50(12), 2506-2513, doi: 10.1016/j.ijthermalsci.2011.06.012.
- Molson, J. W., E. O. Frind, and C. D. Palmer (1992), Thermal energy storage in an unconfined aquifer: 2. Model development, validation, and application, *Water Resources Research*, 28(10), 2857-2867, doi: 10.1029/92wr01472.
- Molz, F. J., J. G. Melville, A. D. Parr, D. A. King, and M. T. Hopf (1983), Aquifer thermal energy storage : A well doublet experiment at increased temperatures, *Water Resources Research*, 19(1), 149-160, doi: 10.1029/WR019i001p00149.
- Morgensen, P. (1983), Fluid to duct wall heat transfer in duct system heat storage, paper presented at Proceedings of the International Conference on Surface Heat Storage in Theory and Practice, Stockholm, Sweden.
- Nelder, J. A., and R. Mead (1965), A Simplex Method for Function Minimization, *The Computer Journal*, 7(4), 308-313, doi: 10.1093/comjnl/7.4.308.
- Neuman, S. P. (1990), Universal scaling of hydraulic conductivities and dispersivities in geologic media, *Water Resources Research*, 26(8), 1749-1758, doi: 10.1029/WR026i008p01749.
- Niekamp, A., K. Unklesbay, N. Unklesbay, and M. Ellersieck (1984), Thermal-Properties of Bentonite-Water Dispersions Used for Modeling Foods, *J Food Sci*, 49(1), 28-31.
- Ochsner, T. E., R. Horton, G. J. Kluitenberg, and Q. Wang (2005), Evaluation of the Heat Pulse Ratio Method for Measuring Soil Water Flux, *Soil Sci. Soc. Am. J.*, 69(3), 757-765, doi: 10.2136/sssaj2004.0278.
- Ostrom, M., J. S. Hayworth, J. H. Dane, and O. Güven (1992), Behavior of dense aqueous phase leachate plumes in homogeneous porous media, *Water Resources Research*, 28(8), 2123-2134, doi: 10.1029/92wr00711.
- Pahud, D., and B. Matthey (2001), Comparison of the thermal performance of double U-pipe borehole heat exchangers measured in situ, *Energy and Buildings*, 33(5), 503-507, doi: 10.1016/S0378-7788(00)00106-7.
-

Palmer, C. D., D. W. Blowes, E. O. Frind, and J. W. Molson (1992), Thermal energy storage in an unconfined aquifer: 1. Field Injection Experiment, *Water Resources Research*, 28(10), 2845-2856, doi: 10.1029/92wr01471.

Pannike, S., M. Kölling, B. Panteleit, J. Reichling, V. Scheeps, and H. D. Schulz (2006), Auswirkung hydrogeologischer Kenngrößen auf die Kältefahren von Erdwärmesondenanlagen in Lockersedimenten, *Grundwasser*, 11, 6-18.

Parr, A. D., F. J. Molz, and J. G. Melville (1983), Field Determination of Aquifer Thermal Energy Storage Parameters, *Ground Water*, 21(1), 22-35, doi: 10.1111/j.1745-6584.1983.tb00701.x.

Pehme, P., B. L. Parker, J. A. Cherry, J. W. Molson, and J. P. Greenhouse (2013), Enhanced detection of hydraulically active fractures by temperature profiling in lined heated bedrock boreholes, *J Hydrol(0)*, doi: 10.1016/j.jhydrol.2012.12.048.

Pollack, H. N., S. J. Hurter, and J. R. Johnson (1993), Heat flow from the Earth's interior: Analysis of the global data set, *Reviews of Geophysics*, 31(3), 267-280, doi: 10.1029/93rg01249.

Popov, Y. A., D. F. C. Pribnow, J. H. Sass, C. F. Williams, and H. Burkhardt (1999), Characterization of rock thermal conductivity by high-resolution optical scanning, *Geothermics*, 28(2), 253-276, doi: 10.1016/s0375-6505(99)00007-3.

Rath, V., A. Wolf, and H. M. Bucker (2006), Joint three-dimensional inversion of coupled groundwater flow and heat transfer based on automatic differentiation: sensitivity calculation, verification, and synthetic examples, *Geophysical Journal International*, 167(1), 453-466, doi: 10.1111/j.1365-246X.2006.03074.x.

Rau, G. C., M. S. Andersen, and R. I. Acworth (2012), Experimental investigation of the thermal dispersivity term and its significance in the heat transport equation for flow in sediments, *Water Resources Research*, 48(3), 1-21, doi: 10.1029/2011wr011038.

Raymond, J., R. Therrien, and L. Gosselin (2011a), Borehole temperature evolution during thermal response tests, *Geothermics*, 40(1), 69-78, doi: 10.1016/j.geothermics.2010.12.002.

Raymond, J., R. Therrien, L. Gosselin, and R. Lefebvre (2011b), Numerical analysis of thermal response tests with a groundwater flow and heat transfer model, *Renewable Energy*, 36(1), 315-324, doi: 10.1016/j.renene.2010.06.044.

-
- Raymond, J., R. Therrien, L. Gosselin, and R. Lefebvre (2011c), A Review of Thermal Response Test Analysis Using Pumping Test Concepts, *Ground Water*, 10.1111/j.1745-6584.2010.00791.x, doi: 10.1111/j.1745-6584.2010.00791.x.
- Read, T., O. Bour, V. Bense, T. Le Borgne, P. Goderniaux, M. V. Klepikova, R. Hochreutener, N. Lavenant, and V. Boschero (2013), Characterizing groundwater flow and heat transport in fractured rock using fiber-optic distributed temperature sensing, *Geophysical Research Letters*, 40(-), 1-5, doi: 10.1002/grl.50397.
- Rein, A., R. Hoffmann, and P. Dietrich (2004), Influence of natural time-dependent variations of electrical conductivity on DC resistivity measurements, *J Hydrol*, 285(1-4), 215-232.
- Riva, M., L. Guadagnini, A. Guadagnini, T. Ptak, and E. Martac (2006), Probabilistic study of well capture zones distribution at the Lauswiesen field site, *J. Contam. Hydrol.*, 88(1-2), 92-118.
- Roth, P., A. Georgiev, A. Busso, and E. Barraza (2004), First in situ determination of ground and borehole thermal properties in Latin America, *Renewable Energy*, 29(12), 1947-1963.
- Rybach, L. (2010), Status and prospects of geothermal energy, paper presented at Proc. World Geothermal Congress 2010, Bali, Indonesia, 25-29 April.
- Rybach, L., and W. J. Eugster (2010), Sustainability aspects of geothermal heat pump operation, with experience from Switzerland, *Geothermics*, 39(4), 365-369.
- Saar, M. O. (2011), Review: Geothermal heat as a tracer of large-scale groundwater flow and as a means to determine permeability fields, *Hydrogeology Journal*, 19(1), 31-52, doi: 10.1007/s10040-010-0657-2.
- Sack-Kühner, B. (1996), Einrichtung des Naturmessfeldes "Lauswiesen Tübingen", Diploma thesis, University of Tübingen, Germany, Tübingen, Germany.
- Saner, D., R. Juraske, M. Kübert, P. Blum, S. Hellweg, and P. Bayer (2010), Is it only CO₂ that matters? A life cycle perspective on shallow geothermal systems, *Renewable and Sustainable Energy Reviews*, 14(7), 1798-1813, doi: 10.1016/j.rser.2010.04.002.
- Sanner, B., C. Karytsas, D. Mendrinou, and L. Rybach (2003), Current status of ground source heat pumps and underground thermal energy storage in Europe, *Geothermics*, 32(4-6), 579-588, doi: 10.1016/S0375-6505(03)00060-9.
-

Sanner, B., G. Hellström, J. Spitler, and S. Gehlin (2005), Thermal Response Test - Current Status and World Wide Application, in *World Geothermal Congress* edited, pp. 1436–1445, Antalya, Turkey.

Sass, I., and C. Lehr (2011), Improvements on the thermal response test evaluation applying the cylinder source theory, paper presented at Thirty-sixth Workshop on Geothermal Reservoir engineering 2011, Stanford, United States of America.

Sauty, J. P., A. C. Gringarten, H. Fabris, T. D., A. Menjoz, and P. A. Landel (1982a), Sensible energy storage in aquifers - 2. Field experiments and comparison with theoretical results, *Water Resources Research*, 18(2), 253-265.

Sauty, J. P., A. C. Gringarten, Menjoz, and P. A. Landel (1982b), Sensible energy storage in aquifers 1. Theoretical study, *Water Resources Research*, 18(2), 245-252.

Schmidt, C., M. Bayer-Raich, and M. Schirmer (2006), Characterization of spatial heterogeneity of groundwater-stream water interactions using multiple depth streambed temperature measurements at the reach scale, *Hydrology and earth system sciences.*, 10(6), 849-859.

Schneidewind, U. (2008), Determination of the hydraulic conductivity using Direct-Push Injection Logger, Master thesis, University of Tübingen, Germany, Tübingen, Germany.

Sharqawy, M. H., E. M. Mokheimer, and H. M. Badr (2009a), Effective pipe-to-borehole thermal resistance for vertical ground heat exchangers, *Geothermics*, 38(2), 271-277, doi: 10.1016/j.geothermics.2009.02.001.

Sharqawy, M. H., S. A. Said, E. M. Mokheimer, M. A. Habib, H. M. Badr, and N. A. Al-Shayea (2009b), First in situ determination of the ground thermal conductivity for borehole heat exchanger applications in Saudi Arabia, *Renewable Energy*, 34(10), 2218-2223, doi: 10.1016/j.renene.2009.03.003.

Sharqawy, M. H., H. M. Badr, and E. M. Mokheimer (2013), Investigation of buoyancy effects on heat transfer between a vertical borehole heat exchanger and the ground, *Geothermics*, 48(0), 52-59, doi: 10.1016/j.geothermics.2013.04.003.

Shonder, J., and J. Beck (1999), Determining effective soil formation thermal properties from field data using a parameter estimation technique, *ASHRAE Transactions: Symposia*, 105(1), 458-466.

Shook, G. M. (1999), Prediction of thermal breakthrough from tracer tests, paper presented at Twenty-Fourth Workshop on Geothermal Reservoir Engineering, Stanford, California.

Shook, G. M. (2001), Predicting thermal breakthrough in heterogeneous media from tracer tests, *Geothermics*, 30(6), 573-589, doi: 10.1016/S0375-6505(01)00015-3.

Signorelli, S., S. Bassetti, D. Pahud, and T. Kohl (2007), Numerical evaluation of thermal response tests, *Geothermics*, 36(2), 141-166, doi: 10.1016/j.geothermics.2006.10.006.

Slater, L. (2007), Near Surface Electrical Characterization of Hydraulic Conductivity: From Petrophysical Properties to Aquifer Geometries—A Review, *Surv Geophys*, 28(2-3), 169-197, doi: 10.1007/s10712-007-9022-y.

Stallman, R. W. (1963), Computation of groundwater velocity from temperature data, *USGS Water Supply Paper*, 1544, 36-46.

Stober, I., and K. Bucher (2012), *Geothermie*, Springer.

Sudicky, E. A. (1986), A natural gradient experiment on solute transport in a sand aquifer: Spatial variability of hydraulic conductivity and its role in the dispersion process, *Water Resour. Res.*, 22(13), 2069-2082, doi: 10.1029/WR022i013p02069.

Sutton, M. G., D. W. Nutter, and R. J. Couvillion (2002), A ground resistance for vertical bore heat exchangers with groundwater flow, *ASME Journal of Energy Resources Technology*, 125, 183-189.

Taniguchi, M., J. Shimada, T. Tanaka, I. Kayane, Y. Sakura, Y. Shimano, S. Dapaah-Siakwan, and S. Kawashima (1999), Disturbances of temperature-depth profiles due to surface climate change and subsurface water flow: 1. An effect of linear increase in surface temperature caused by global warming and urbanization in the Tokyo Metropolitan Area, Japan, *Water Resour. Res.*, 35(5), 1507-1517, doi: 10.1029/1999wr900009.

Taniguchi, M., J. V. Turner, and A. J. Smith (2003), Evaluations of groundwater discharge rates from subsurface temperature in Cockburn Sound, Western Australia, *Biogeochemistry*, 66(1-2), 111-124.

Taniguchi, M., and T. Uemura (2005), Effects of urbanization and groundwater flow on the subsurface temperature in Osaka, Japan, *Physics of the Earth and Planetary Interiors*, 152(4), 305-313, doi: 10.1016/j.pepi.2005.04.006.

Taylor, C. A., and H. G. Stefan (2009), Shallow groundwater temperature response to climate change and urbanization, *J Hydrol*, 375(3-4), 601-612, doi: 10.1016/j.jhydrol.2009.07.009.

Tholen, M., and S. Walker-Hertkorn (2008), *Arbeitshilfen Geothermie: Grundlagen für oberflächennahe Erdwärmesondenbohrungen*, Wirtschafts- und Verlag-Ges. Gas und Wasser.

Vandenbohede, A., A. Louwyck, and L. Lebbe (2008a), Identification and reliability of microbial aerobic respiration and denitrification kinetics using a single-well push-pull field test, *J. Contam. Hydrol.*, 95(1–2), 42-56, doi: 10.1016/j.jconhyd.2007.07.003.

Vandenbohede, A., E. Van Houtte, and L. U. C. Lebbe (2008b), Study of the feasibility of an aquifer storage and recovery system in a deep aquifer in Belgium, *Hydrological Sciences Journal*, 53(4), 844-856, doi: 10.1623/hysj.53.4.844.

Vandenbohede, A., A. Louwyck, and L. Lebbe (2009), Conservative solute versus heat transport in porous media during push-pull tests, *Transport Porous Media*, 76(2), 265-287.

Venkataraman, P. (2009), *Applied Optimization with MATLAB Programming*, Wiley.

Vogt, T., P. Schneider, L. Hahn-Woernle, and O. A. Cirpka (2010), Estimation of seepage rates in a losing stream by means of fiber-optic high-resolution vertical temperature profiling, *J Hydrol*, 380(1–2), 154-164, doi: 10.1016/j.jhydrol.2009.10.033.

Wagner, R., and C. Clauser (2005), Evaluating thermal response tests using parameter estimation for thermal conductivity and thermal capacity, *Journal of Geophysics and Engineering*, 2(4), 349.

Wagner, R., and E. Rohner (2008), Improvements of thermal response tests for geothermal heat pumps, in *IEA Heat Pump Conference* edited, Zürich, Switzerland.

Wagner, V. (2010), Analysis of thermal response tests using advanced analytical and high resolution numerical simulations, Diplom thesis, Eberhard-Karls Universität, Tübingen, Deutschland.

Wagner, V., P. Bayer, G. Bisch, J. Braun, N. Klaas, and P. Blum (2012a), Calibrating a High-resolution Numerical Model of a Borehole Heat Exchanger Using FEFLOW, in *3rd International FEFLOW User Conference*, edited, Berlin, Germany.

Wagner, V., P. Bayer, M. Kübert, and P. Blum (2012b), Numerical sensitivity study of thermal response tests, *Renewable Energy*, 41(0), 245-253, doi: 10.1016/j.renene.2011.11.001.

-
- Wagner, V., P. Blum, M. Kübert, and P. Bayer (2013), Analytical approach to groundwater-influenced thermal response tests of grouted borehole heat exchangers, *Geothermics*, 46(0), 22-31, doi: 10.1016/j.geothermics.2012.10.005.
- Wagner, V., P. Bayer, G. Bisch, M. Kübert, and P. Blum (2014a), Hydraulic characterization of aquifers by thermal response testing: validation by large scale tank and field experiments, *Water Resources Research*, 50(1), 71-85, doi: 10.1002/2013WR013939.
- Wagner, V., T. Li, P. Bayer, C. Leven, P. Dietrich, and P. Blum (2014b), Thermal tracer testing in a sedimentary aquifer: field experiment (Lauswiesen, Germany) and numerical simulation, *Hydrogeology Journal*, 22(1), 1-13, doi: 10.1007/s10040-013-1059-z.
- Witte, H. J. L. (2001), Geothermal Response Test with Heat Extraction and Heat Injection: Examples of Application in Research and Design of Geothermal Ground Heat Exchangers, in *Europäischer Workshop über Geothermische Response Tests*, edited, Lausanne, Switzerland.
- Witte, H. J. L., G. J. van Gelder, and J. D. Spitler (2002), In-situ measurements of ground thermal conductivity: The Dutch Perspective, *ASHRAE Transactions: Research*, 108(1), 263-272.
- Witte, H. J. L., and G. V. Gelder (2006), Geothermal response tests using controlled multi-power level heating and cooling pulses (MPL-HCP): quantifying ground water effects on heat transport around a borehole heat exchanger, paper presented at The Tenth International Conference on Thermal Energy Storage, New Jersey (USA).
- Witte, H. J. L. (2013), Error analysis of thermal response tests, *Applied Energy*, 109(0), 302-311, doi: 10.1016/j.apenergy.2012.11.060.
- Woodside, W., and J. H. Messmer (1961), Thermal Conductivity of Porous Media. I. Unconsolidated Sands, *Journal of Applied Physics*, 32(9), 1688-1699.
- Wu, X., G. A. Pope, G. M. Shook, and S. Srinivasan (2008), Prediction of enthalpy production from fractured geothermal reservoirs using partitioning tracers, *International Journal of Heat and Mass Transfer*, 51(5-6), 1453-1466, doi: 10.1016/j.ijheatmasstransfer.2007.06.023.
- Xue, Y., C. Xie, and Q. Li (1990), Aquifer thermal energy storage: A numerical simulation of field experiments in China, *Water Resources Research*, 26(10), 2365-2375, doi: 10.1029/WR026i010p02365.
-

Yavuzturk, C., J. Spitler, and S. Rees (1999), A transient two-dimensional finite volume model for the simulation of vertical U-tube ground heat exchangers, *ASHRAE Transactions*, 105(2), 465-474.

Zanchini, E., and T. Terlizzese (2008), Finite-element evaluation of thermal response tests performed on U-tube borehole heat exchangers, in *COMSOL Conference*, edited, Hanover, Germany.

Zeng, H., N. Diao, and Z. Fang (2003), Heat transfer analysis of boreholes in vertical ground heat exchangers, *International Journal of Heat and Mass Transfer*, 46(23), 4467-4481, doi: 10.1016/S0017-9310(03)00270-9.

Zeng, H. Y., N. R. Diao, and Z. H. Fang (2002), A finite line-source model for boreholes in geothermal heat exchangers, *Heat Transfer—Asian Research*, 31(7), 558-567, doi: 10.1002/htj.10057.

Zhu, K., P. Blum, G. Ferguson, K. D. Balke, and P. Bayer (2011), The geothermal potential of urban heat islands, *Environ Res Lett*, 5(044002).

Ziagos, J. P., and D. D. Blackwell (1986), A model for the transient temperature effects of horizontal fluid flow in geothermal systems, *Journal of Volcanology and Geothermal Research*, 27(3-4), 371-397, doi: 10.1016/0377-0273(86)90021-1.

Acknowledgments

This work was made possible by the help and support of many people. I would like to thank...

... Jun.-Prof. Dr. habil. Philipp Blum for giving me the opportunity to do a PhD, the mentoring beyond the research perspective and to be one part of an excellent supervision team.

... Dr. Peter Bayer for always having time for a discussion, several stays in Zurich, and to be the other part of an excellent supervision team.

... Prof. Dr. rer. nat. Thomas Kohl for his uncomplicated willingness to be the co-referent.

... Maike Schröder, Heidi Knierim, Mareile Horstmann, Thomas Schockmann, Vanessa Groß and Gabi Moser for language corrections of single parts enclosed in this thesis.

... the financial support of the state of Baden-Württemberg (BW-Plus: ZO4E 28003).

... the Herrenknecht AG for providing the data of the field experiment (chapter 4).

... Johannes Steger, Simone Walker-Hertkorn and André Voutta for their support to perform the tank experiment TRT (chapter 4).

... Gerhard Bisch for the collaboration during the tank experiment.

... Steffen Rehner, Jozsef Hecht Mendez, Nelson Molina Giraldo, Steffi Hähnlein, Tao Li and Ke Zhu for the joyful start in the life of a researcher.

... the Wagner “brothers”, Daniel Trumpp, Andreas Burger, Hagen Steger, Christoph Butscher and Thomas Mutschler for their company during the countless lunch breaks.

... Kathrin Menberg for the guidance through the maze of the regulation in the last month.

... all other colleagues of the Engineering and the Hydrogeology Group at the AGW for all the enjoyable years.

... my family for always believing in me and for their invaluable support.

... Miriam Kläsener for her infinite amount of faith.

Declaration of authorship

Study 1

Citation: Wagner, V., Bayer, P., Kübert, M., Blum, P. (2012a), Numerical sensitivity study of thermal response tests, *Renewable Energy*, 41(0), 245-253.

Declaration of authorship: Valentin Wagner (VW) developed the numerical model and obtained all results in consultation with Peter Bayer and Philipp Blum. VW wrote the manuscript. The final manuscript was reviewed by all authors.

Study 2

Citation: Wagner, V., Blum, P., Kübert, M., Bayer, P. (2013), Analytical approach to groundwater-influenced thermal response tests of grouted borehole heat exchangers, *Geothermics*, 46(0), 22-31.

Declaration of authorship: Valentin Wagner (VW) developed the numerical model, implemented a computer code to determine the correction term and obtained all results in consultation with Peter Bayer and Philipp Blum. VW wrote the manuscript. The final manuscript was reviewed by all authors.

Study 3

Citation: Wagner, V., Bayer, P., Bisch, G., Kübert, M., Blum, P. (2014), Hydraulic characterization of aquifers by thermal response testing: validation by large scale tank and field experiments, *Water Resources Research*, 50(1), 71-85.

Declaration of authorship: Valentin Wagner (VW) designed the tank experiment together with Gerhard Bisch (GB). GB supervised the tank experiment. Markus Kübert provided the TRT dataset from the field test. VW developed the parameter estimation procedure, implemented this procedure in a computer code and obtained all results in consultation with Peter Bayer and Philipp Blum. VW wrote the manuscript. The final manuscript was reviewed by all authors.

Study 4

Citation: Wagner, V., Li, T., Bayer, P., Leven, C., Dietrich, P., Blum, P. (2014), Thermal tracer testing in a heterogeneous sedimentary aquifer: Field experiment and numerical simulation, *Hydrogeology Journal*, 22(1), 175-187.

Declaration of authorship: Tao Li executed the thermal tracer test. Valentin Wagner developed the numerical model and obtained all results in consultation with Peter Bayer and Philipp Blum. VW wrote the manuscript in consultation with Peter Bayer. The final manuscript was reviewed by all authors.

Curriculum vitae

Personal Information

Name Valentin Kurt Wagner
Date of birth 27.07.1983
Place of birth Crailsheim
Nationality German

Education

07.2003 A-level, Schelztor Gymnasium, Esslingen, Germany.

Civilian service

09.2003 – 06.2004 Civil service at the welfare service for refugees AWO in Esslingen.

Academic studies

10.2004 – 04.2010 Dipl.-Mineralogist at the Center for Applied Geosciences (ZAG), University of Tübingen, Germany (Grade: 1.3).
Diploma thesis: „Analysis of thermal response Tests using advanced analytical and high resolution numerical simulations“.

Professional experience

07.2010 - presumably 12.2013 PhD position at the Karlsruhe Institute of Technology (KIT), Institute of Applied Geoscience.
Topic: „Thermal field methods of the shallow subsurface“.

Journal publications (peer-reviewed)

- Wagner, V., Bayer, P., Bisch, G., Kübert, M., Blum, P. (2014): Hydraulic characterization of aquifers by thermal response testing: validation by large scale tank and field experiments. *Water Resources Research*, 50, 71-85.
- Wagner, V., Li, T., Bayer, P., Leven, C., Dietrich, P., Blum, P. (2014): Thermal tracer testing in a heterogeneous sedimentary aquifer. *Hydrogeology Journal*, 22, 175-187.
- Wagner, V., Blum, P., Kübert, M., Bayer, P. (2013): Analytical approach to groundwater-influenced thermal response tests of grouted borehole heat exchangers. *Geothermics*, 46, 22-31.
- Wagner, V., Bayer, P., Kübert, M., Blum, P. (2012): Numerical sensitivity study of thermal response tests. *Renewable Energy*, 41, 245-253.

Conference contributions (presentation)

- Wagner, V., Blum, P., Kübert, M., Bayer, P. (2013) Determination of Aquifer Properties by the Thermal Response Test. 19. 8th IAHS International Groundwater Quality Conference, Gainesville, Florida, USA, April 2013.
- Wagner, V., Blum, P., Kübert, M., Bayer, P. (2013) Analytische und numerische Auswertung advektiv beeinflusster Thermal Response Tests. 19. Tagung für Ingenieurgeologie mit Forum für junge Ingenieurgeologen, München, Deutschland, März 2013.
- Wagner, V., Bayer, P., Kübert, M., Blum, P. (2012) Analytischer Ansatz zur Auswertung von Grundwasser beeinflussten Thermal Response Tests. Der Geothermiekongress 2012, Karlsruhe, Deutschland, 13.-16. November 2012, Kongressband (ISBN 978-3-932570-67-4).
- Wagner, V., Bayer, P., Bisch, G., Braun, J., Klaas, N., Blum, P. (2012): Calibrating a High-resolution Numerical Model of a Borehole Heat Exchanger Using FEFLOW. 3rd International FEFLOW User Conference, Berlin, Germany, 03.-05. September 2012.
- Wagner, V., Bayer, P., Bisch, G., Braun, J., Klaas, N., Blum, P. (2012): Bestimmung der thermischen Dispersivität im Kontext der oberflächennahen Geothermie. FH-DGG-Tagung 2012, Dresden, Deutschland, Mai 2012.

- Wagner, V., Bayer, P., Bisch, G., Braun, J., Klaas, N., Blum, P. (2012): Determination of thermal dispersivity using a borehole heat exchanger. EGU General Assembly Conference Abstracts. Vol. 14.
- Wagner, V., Bayer, P., Kübert, M., Blum, P. (2011): Numerische Sensitivitätsanalyse des Thermal Response Tests. Der Geothermiekongress 2011, Bochum, Deutschland, November 2011, Kongressband (ISBN 978-3-932570-66-7).
- Blum, P., Wagner, V., Hecht-Méndez, J., Bayer, P. (2011): Modellierung von Kälte- und Wärmefahnen in der oberflächennahen Geothermie. VEGAS-Kolloquium 2011 Flache Geothermie – Perspektiven und Risiken, Stuttgart, Deutschland, Oktober 2011, Kongressband (ISBN 978-3-942036-09-2).
- Walker-Hertkorn, S., Kübert, M., Kuntz D., Wagner, V., Urban, K. (2010): Konstruktion, Auslegung und Betrieb von Energiepfahlanlagen. 1. VDI Fachkonferenz Wärmepumpen - Umweltwärme effizient nutzen, Stuttgart, Deutschland, Juni 2010.

Conference contributions (scientific poster)

- Wagner, V., Bayer, P., Blum, P. (2013): Quantifying the contribution of advection in thermal response tests. EGU General Assembly Conference Abstracts. Vol. 15.
- Wagner, V., Bayer, P., Bisch, G., Braun, J., Klaas, N., Blum, P. (2013): Thermal dispersivity based calibration of a numerical borehole heat exchanger model. EGU General Assembly Conference Abstracts. Vol. 15.
- Wagner, V., Blum, P., Kübert, M., Bayer, P. (2010): Sensitivitätsanalyse von Thermal Response Tests anhand numerischer Simulationen. Der Geothermiekongress. Karlsruhe, Deutschland.
- Wagner, V., Blum, P., Kübert, M., Bayer, P. (2010): The dependency of the effective thermal conductivity on aquifer thickness and groundwater velocity. Geodarmstadt. Darmstadt, Germany, October 2010.
- Wagner, V., Blum, P., Kübert, M., Bayer, P. (2010): Influence of groundwater flow and aquifer thickness on thermal response test interpretation. International Groundwater Symposium 2010. Valencia, Spain, September 2010.
- Wagner, V., Blum, P., Kübert, M., Bayer, P. (2010): Analysis of thermal response tests (TRT) using high resolution numerical Simulations, EGU General Assembly Conference Abstracts. Vol. 12.